DEUTSCHES ELEKTRONEN-SYNCHROTRON DESY

DESY 71/50
September 1971

Photoproduction II: Compton Scattering, Vector Meson Production and Other Photon Induced Reactions

by

Günter Wolf

2 HAMBURG 52 · NOTKESTIEG 1

Photoproduction II: Compton Scattering, Vector Meson Production and Other Photon Induced Reactions

Rapporteur Talk at the 1971 International Symposium on Electron and Photon Interactions at High Energies at Cornell

by

Günter Wolf

Deutsches Elektronen-Synchrotron, DESY

Hamburg, Germany

I. Introduction

The subject of this talk are the recent experimental results on photoproduction of nucleons. The following topics will be covered:

Total γN Cross Sections

Compton Scattering

Vector Meson Production

Evidence for Other Resonance Channels,

e. g. $\gamma N \to A_2 N$, $\Delta\rho$, etc.

The field of pseudoscalar meson - baryon reactions has been discussed in the talk of Dr. Wiik at this conference.

Comparing the experimental results which are now available to what was known at the time of the last Electron-Photon Conference one finds that considerable progress has been made in several areas. To give a few examples:

Two years ago there were no data yet on high energy Compton scattering; now the measurements cover the region from 2 all the way up to 17 GeV.

Extensive studies have been made on vector meson production, $\gamma N \to VN$. The experiments with polarized photons have allowed to separate the contributions from natural ($P = (-1)^J$) and unnatural parity ($P = -(-1)^J$) exchange in the t-channel to a high degree of accuracy. They tell us, e. g., that ρ^o-production is completely dominated by natural parity exchange which gives corroborating evidence that the ρ^o-mesons are produced by a diffraction mechanism. The measurements of the rho spin density matrix showed that for moderate momentum transfers ρ^o production conserves s-channel helicity at the photon-rho vertex. The rho photoproduction data and in parallel, results on elastic πN scattering then led to the hypothesis that diffraction scattering in general conserves s-channel helicity a conjecture which subsequently stimulated new theoretical

and experimental work on diffractive like processes. Another result which comes out of the new data on vector meson production is that the vector dominance model in its present form is not exact. The values of the photon-rho coupling constant determined from photoproduction data and in e^+e^- annihilation differ by a factor of two. However, the obvious way out of the difficulty is not supported by experiment: no conclusive evidence has so far been found for the existence of further vector mesons which couple to the photon.

The written version presents more data than the talk, but of course, not all. Apart from the original papers, the reader is referred to recent review articles[1] and a compilation of photoproduction data[2].

II. Total Cross Section

1. On Protons

Direct measurements of the total hadronic γp cross section, $\sigma^T_{\gamma p}$, are now available from 0.275 GeV up to 18 GeV (Fig. 1a, b). The data were obtained using either a counter setup and a tagged photon beam (DESY[3], Santa Barbara-SLAC[4], NINA[5]) or a bubble chamber with a monochromatic photon beam (SLAC[6], SLAC-Berkeley-Tufts[7]). One observes good agreement between the various sets of measurements in the overlap regions. Total cross section values obtained from extrapolations of inelastic ep and μp data gave results consistent with the direct measurements to within 10 - 20 %[8,9]. The total cross section in the low energy region (Fig. 1a) shows the expected bumps in the region of the Δ(1236) and around 1520 MeV and 1690 MeV cms energy. Above 2 GeV $\sigma^T_{\gamma p}$ becomes rather constant and is of the order of 120 - 130 μb.

2. On Neutrons

Three experiments have been published measuring the total cross section on deuterons, $\sigma^T_{\gamma d}$ (NINA: 0.4 - 4.3 GeV [5], DESY: 1.4 - 6.5 GeV [4], Santa Barbara-SLAC 4 - 18 GeV [5]). The data are shown in Figs. 1b, c. From the $\sigma^T_{\gamma d}$ data, using

the values on $\sigma^T_{\gamma p}$ as measured in the same experiments, the total neutron cross section, $\sigma^T_{\gamma n}$, was determined by the DESY and the UCSB-SLAC groups according to the relation

$$\sigma^T_{\gamma n} = \frac{\sigma^T_{\gamma d}}{1 - x} - \sigma^T_{\gamma p} \qquad (1)$$

where x is the Glauber correction[10] to account for the shadow-effect. The correction term x as estimated by both groups is small, ranging from 0.01 to 0.02 for energies between 2 and 20 GeV. The resulting $\sigma^T_{\gamma n}$ values are given in Fig. 2. Also shown in Fig. 2 is the difference $\sigma^T_{\gamma p} - \sigma^T_{\gamma n}$; the total cross section for protons appears to be slightly larger than for neutrons.

At high energies the forward Compton scattering amplitude, $T_{\gamma N}$, and via the optical theorem, $\sigma^T_{\gamma N}$ are expected to be dominated by Pomeron (P), P' and A_2 exchange leading to an energy dependence of the form

$$\sigma^T_{\gamma N} = C_p + C_{p'} E_\gamma^{-1/2} + C_{A_2} E_\gamma^{-1/2} \quad . \qquad (2)$$

The isospin 0 and 1 t-channel exchanges contribute with different relative signs to proton and neutron Compton scattering:

$$\begin{aligned} T_{\gamma p} &= T_o + T_1 \\ T_{\gamma n} &= T_o - T_1 . \end{aligned} \qquad (3)$$

Because of this property the $T = 0$ and $T = 1$ contributions can be separated:

$$1/2(\sigma^T_{\gamma p} + \sigma^T_{\gamma n}) = \mathrm{Im}\, T_o ; \quad 1/2(\sigma^T_{\gamma p} - \sigma^T_{\gamma n}) = \mathrm{Im}\, T_1 \qquad (4)$$

leading to

$$1/2(\sigma^T_{\gamma p} + \sigma^T_{\gamma n}) = C_p + C_{p'} E_\gamma^{-1/2} ; \quad 1/2(\sigma^T_{\gamma p} - \sigma^T_{\gamma n}) = C_{A_2} E_\gamma^{-1/2} \qquad (5)$$

The data shown in Fig. 2 were fitted to Eq. (5) and gave the following results, using only cross section points above 2 GeV (fits with cut off energies ranging between 1.4 and 3.5 GeV yielded, within errors, the same results)[4b]:

$$\begin{aligned} C_p &= 97.4 \pm 1.9 \ \mu b \\ C_{p'} &= 55.0 \pm 5.1 \ \mu b \\ C_{A_2} &= 12.3 \pm 2.3 \ \mu b \end{aligned} \qquad (6)$$

(E_γ is measured in units of GeV.)

Two conclusions can be drawn from these numbers:

(i) The cross section decreases slowly with energy, e. g. $\sigma^T_{\gamma p}$ changing by $\sim$12 % between 5 and 20 GeV.

(ii) The total cross section on protons is larger than on neutrons implying a nonzero contribution from $T = 1$ exchange to Compton scattering.

From (6) one finds

$$\frac{\text{Im } T_1}{\text{Im } T_0} = \begin{cases} (4.5 \pm 0.8)\ \% & \\ (2.3 \pm 0.5)\ \% & \end{cases} \text{ at } \begin{matrix} 5 \text{ GeV} \\ 20 \text{ GeV} \end{matrix}$$

The errors do not include an additional 0.5 - 1 % part caused by the uncertainty in the Glauber correction term.

III. Compton Scattering

A measurement of Compton scattering in the GeV region has long been thought to be extremely difficult because of the π^o background. In the last two years several experiments on Compton scattering have been done yielding data over a wide energy and momentum transfer band: CEA (4 GeV)[11], DESY (2 - 7 GeV)[12] and

SLAC (5 - 17 GeV [13], 8 and 16 GeV [14]). Except for one experiment the π^o problem was solved by detecting the scattered γ in coincidence with the recoiling proton. Counting γ's in the production plane (defined by the proton) and outside allowed a clear discrimination against background photons.

1. Differential Cross Section

A compilation of the differential cross section measurements for protons is given in Fig. 3. Wherever several experiments have been done at the same energy there is good agreement between the data sets. One observes an exponential fall off with increasing momentum transfer, $|t|$, and approximately energy independence for $E_\gamma > 3$ GeV in close similarity to elastic hadron nucleon scattering. Table I summarizes the fits of the differential cross section to the forms

$$d\sigma/dt = \begin{cases} d\sigma^o/dt \exp(At) \\ d\sigma^o/dt \exp(At + Bt^2) \end{cases} \qquad (7)$$

As is evident from Table I for $E_\gamma \gtrsim 3$ GeV the variation of the magnitude and shape of the differential cross section with energy is small. If fitted over a wide t region (e. g., $|t| < 0.6$ GeV^2) the data definitely require a quadratic term in the exponential similar to, e. g., elastic πp scattering (for comparison: at 9 GeV the slope parameters for elastic πp scattering for $|t| < 1$ GeV^2 were found to be[15] $A = 9.0 \pm 0.2$ GeV^{-2}, $B = 2.5 \pm 0.3$ GeV^{-4}).

2. Forward Scattering Amplitude

The forward Compton scattering amplitude is conventionally expressed in terms of the amplitudes f_1 and f_2 for parallel and perpendicular polarization vectors $\vec{\varepsilon}_i$, $\vec{\varepsilon}_f$ respectively of the initial and final photons[16,17]:

$$f(E_\gamma) = f_1(E_\gamma)\, \vec{\varepsilon}_f \cdot \vec{\varepsilon}_i + i f_2(E_\gamma)\, \vec{\sigma} \cdot (\vec{\varepsilon}_f \times \vec{\varepsilon}_i) \qquad (8)$$

where $\vec{\sigma}$ is the spin matrix of the nucleon. The optical theorem connects the imaginary part of f_1 to the total γN cross section:

$$\text{Im } f_1(E_\gamma) = \frac{4\pi}{E_\gamma} \sigma^T_{\gamma N} \tag{9}$$

The forward differential cross section for Compton scattering is then given by

$$d\sigma^o/dt = \frac{1}{16\pi} |\sigma^T|^2 + \frac{\pi}{E_\gamma^2} |\text{Re } f_1|^2 + \frac{\pi}{E_\gamma^2} |f_2|^2 \tag{10}$$

The real part of $f_1(E_\gamma)$ can be determined from σ^T with the help of a dispersion relation,

$$\text{Re } f_1(E_\gamma) = -\frac{\alpha}{M} + \frac{E_\gamma^2}{2\pi^2} \cdot P\int_{E_o}^{\infty} \frac{dE' \, \sigma^T(E')}{E'^2 - E_\gamma^2} \tag{11}$$

Here M is the nucleon mass and E_o is the threshold for single pion production. Several evaluations of Eq. (11) have been done leading to consistent results for Re $f_1(E_\gamma)$ above 2 GeV. A recent analysis for $\text{Re}f_1/\text{Tm}f_1$ is shown in Fig. 4.*

Knowing $d\sigma^o/dt$, σ^T and Re f_1, and neglecting the f_2 term, a comparison of the right and left hand sides of Eq. (10) is possible. The result is shown in Fig. 5. Within errors agreement is found between both sides over the whole energy range ($2.5 < E_\gamma < 17$ GeV) which implies that f_2 is small. The data give an upper limit of 10 % (2 s.d) for the f_2 contribution to $d\sigma^o/dt$ [14].

3. Spin Dependence

Compton scattering with linearly polarized photons has been measured at DESY[18]. The experiment determined at 3.5 GeV the t dependence of the asymmetry Σ de-

---

* It is interesting to note that the ratio of real to imaginary part deduced from the analysis of $\sigma^T_{\gamma N}$ in terms of P, P' and A_2 and using the appropriate signature factors is approximately the same as the result from the dispersion theory calculation; the presence of a small fixed-pole contribution[17] cannot be ruled out, however.

fined as[19]

$$\Sigma = \frac{\sigma_\perp - \sigma_\parallel}{\sigma_\perp + \sigma_\parallel} \qquad (12)$$

with $\sigma_\parallel(\sigma_\perp)$ being the cross section for incoming photons polarized parallel (perpendicular) to the production plane. The result is shown in Fig. 6. Within errors Σ is found to be zero for $|t| < .6$ GeV^2. The measurements do not allow to decide between the following three models (see Fig. 6):

0^+ exchange: $\sigma_\parallel = \sigma_\perp/\cos^2\theta^*$

Spin independence in the CMS: $\sigma_\parallel = \sigma_\perp \cdot \cos^2\theta^*$

s-channel helicity conservation: $\sigma_\parallel = \sigma_\perp$

(θ^* = CMS scattering angle)

4. Isospin Dependence

Compton scattering on deuterons has been measured at SLAC for 8 and 16 GeV [14]. Combining the data with their results on protons the authors obtain for the isoscalar and isovector t-channel exchange amplitudes off nucleons T_o, T_1 the following relations:

$$\frac{\mathrm{Re}\,(T_o^+ T_1)}{|T_o + T_1|^2} = 0.030 \pm 0.015$$

and

$$\frac{|T_1|^2}{|T_o + T_1|^2} = -0.09 \pm 0.11$$

averaged over the $|t|$ interval 0.014 - 0.17 GeV^2.

From the comparison of $\sigma^T_{\gamma p}$ and $\sigma^T_{\gamma n}$ we saw that the ratio $\mathrm{Im}\,T_1/\mathrm{Im}\,T_o$ is small in the forward direction. The above data show that also the real part of T_1 is small for small values of $|t|$.

Summary of the data on Compton scattering:

- $d\sigma/dt$ falls off exponentially, with the shape and magnitude above $\sim$ 3 GeV being approximately energy independent,
- In the forward direction the amplitude f_2 for perpendicular polarization vectors of the initial and final photons is small.
- The isovector t-channel exchange amplitude is small near $|t| = 0$.
- The asymmetry Σ measured with linearly polarized photons is small; the average over $0.1 < |t| < 0.7$ GeV^2 is $\Sigma = -0.02 \pm 0.06$.

IV. Topological and Channel Cross Sections

Recent bubble chamber experiments have accumulated[20-25] data on the size and energy dependence of the cross sections of various topologies and channels of γp and γn interactions.

Fig. 7 shows the cross sections for the production of 1-, 3-, 5-, 7- and 9 charged particles in γp interactions together with the total cross section σ^T. The lion's share of σ^T comes from the production of 3 charged particles. The energy behavior of the various topologies looks similar to that observed for corresponding πN or kN interactions.

Fig. 8 summarizes the results for three body channels. The $p\pi^+\pi^-$ final state is dominated at low energies by $\pi^-\Delta^{++}$ production and at high energies by $\rho^o p$ production. Approximately one third of the pk^+k^- cross section comes from ϕ production, $\gamma p \to \phi p$.

In Fig. 9 cross sections for various other γp channels are given.

A compilation of γd cross sections is shown in Fig. 10.

V. Vector Meson Production

There are three major items we hope to learn from the study of vector meson production,

$$\gamma N \rightarrow V^{o}N, \quad V = \rho, \quad \omega, \quad \phi \tag{13}$$

(i) Diffraction Mechanism: We know from experiment that ρ^{o} and ϕ production look very much like diffractive scattering (approximately energy independent cross section, exponential fall off of the momentum transfer distribution). If we accept this hypothesis and produce the vector mesons with polarized photons the decay angular distribution of the vector mesons will tell us about the spin dependence of diffraction scattering. In this respect we are better off than with a study of, say elastic πp scattering.

(ii) Pomeron Properties: As Freund[26] pointed out photoproduction of mesons is best suited to study the properties of what is called the Pomeron since here all other exchange contributions (P', A_2, π etc.) should be negligible.

(iii) VDM: The vector meson dominance model (VDM) can be directly tested by comparing vector meson production in the forward direction with $\sigma^{T}_{\gamma N}$ and Compton scattering and with vector meson production through $e^{+}e^{-}$ annihilation.

1. Rhoproduction, $\gamma p \rightarrow \rho^{o} p$

The analysis of ρ^{o} photoproduction has both experimental and theoretical problems. Table II lists the various rho experiments and indicates the technique and the number of events observed. Track chamber experiments allow a clear isolation of the $p\pi^{+}\pi^{-}$-final state and measure the full ρ decay angular distribution but have problems with very forward ρ^{o} production due to scanning losses. Some of the high statistics counter experiments (Cornell[30], DESY-

MIT[31]) use a bremsstrahlung beam and detect only π^+ and π^-. This way inelastic ρ^o production ($\gamma p \to \rho^o N$ ..) cannot be excluded and will contaminate the data[35]. The size of the contamination will depend on the cross section for inelastic ρ^o production and on the running conditions (peak energy of the bremsstrahlung beam, momentum acceptance for $\pi^+\pi^-$ pairs, etc.). The Cornell group has measured the inelastic contributions at 8.5 GeV in a separate experiment[30]. They find for their running conditions that in the ρ mass region the contamination at small $|t|$ values is 5 - 10 % and increases to $\sim$ 25 % for $|t| = 0.4$ GeV^2 (see Fig. 11).

a. ρ^o Decay Angular Distribution and s-Channel Helicity Conservation

The ρ^o decay angular distribution for the case of linearly polarized photons has been analyzed in a bubble chamber experiment by the SLAC-Berkeley-Tufts collaboration using the Compton back-scattered Laser beam at SLAC. Data are now available at three energies: 2.8, 4.7 and 9.3 GeV[22]. The decay angles Θ, ϕ, Φ (and ψ) are defined in Fig. 12 for the case of the Gottfried-Jackson system (z-axis = γ direction in ρ rest frame); similar definitions hold for the helicity and the Adair system which differ in the choice of the quantization axis, namely

Gottfried-Jackson: $\hat{z}$ = γ direction in ρ rest frame

Helicity: $\hat{z}$ = ρ direction in total CMS

Adair: $\hat{z}$ = γ direction in total CMS

The full information of the decay angular distribution is contained in nine independent ρ density matrix elements[36],

$$
\begin{aligned}
W(\cos\Theta,\phi,\Phi) = 3/4\pi \Big\{ & 1/2(1 - \rho^o_{oo}) + 1/2(3\,\rho^o_{oo} - 1)\cos^2\Theta \\
& - \sqrt{2}\,\mathrm{Re}\,\rho^o_{1o}\sin 2\Theta\cos\phi - \rho^o_{1-1}\sin^2\Theta\cos 2\phi \\
& - P_\gamma\cos 2\Phi\big(\rho^1_{11}\sin^2\Theta + \rho^1_{oo}\cos^2\Theta - \sqrt{2}\,\mathrm{Re}\,\rho^1_{1o}\sin 2\Theta\cos\phi \\
& \qquad - \rho^1_{1-1}\sin^2\Theta\cos 2\phi\big) \\
& - P_\gamma\sin 2\Phi\,\big(\sqrt{2}\,\mathrm{Im}\,\rho^2_{1o}\sin 2\Theta\sin\phi + \mathrm{Im}\,\rho^2_{1-1}\sin^2\Theta\sin 2\phi\big)\Big\}
\end{aligned}
\qquad (14)
$$

where P_γ is the degree of linear polarization and the density matrix of the rho has been split into three parts:

$$\rho_{ik} = \rho^0_{ik} - P_\gamma \cos 2\Phi \cdot \rho^1_{ik} - P_\gamma \sin 2\Phi \cdot \rho^2_{ik} \qquad (15)$$

One of the interesting questions which a study of the ρ decay angular distribution can answer has to do with helicity flip: because of its zero mass, the photon can have only helicities $\lambda_\gamma = \pm 1$ whereas the ρ meson may have helicities $\lambda_\rho = \pm 1$ and 0; are there helicity flip transitions from $\lambda_\gamma = \pm 1$ to $\lambda_\rho = 0$? The decay angular distribution $W(\cos\Theta,\phi,\Phi)$ will have the form for:

$$\lambda_\rho = \pm 1 \qquad W \sim |Y^1_1|^2 \sim \sin^2\Theta$$
$$\lambda_\rho = 0 \qquad W \sim |Y^0_1|^2 \sim \cos^2\Theta \qquad \text{in the helicity system}$$

Another point is that for linearly polarized photons, t-channel exchanges of natural ($P = (-1)^J$, σ^N) and unnatural parity ($P = -(-1)^J$, σ^U) lead to different decay angular distributions and can therefore be separated[36]. For natural parity exchange the decay pions emerge preferentially in the plane of photon polarization ($\psi \simeq 0^\circ$) and for unnatural parity exchange perpendicular to it ($\psi \simeq 90^\circ$).

Fig. 13 shows the distribution of cosΘ versus ψ in the helicity system as measured by the SBT-collaboration at 4.7 GeV [22]. One observes a distribution $W \sim \sin^2\Theta \cos^2\psi$, consistent with zero helicity flip contributions and dominant natural parity exchange. Similar results have been obtained at 2.8 and 9.3 GeV [22].

In Fig. 14 the nine density matrix elements are given as a function of $|t|$ at 4.7 GeV [22] (the results at the other two energies are similar) for the Gottfried-Jackson (G.J.), the helicity (H) and the Adair (A) systems. In the Gottfried-Jackson system the t-channel helicity flip terms increase rapidly off

the forward direction (see e. g. ρ^0_{oo}; see also Fig. 15 where the results of the SLAC-streamerchamber-group on $\rho^0_{11} = \frac{1}{2}(1 - \rho^0_{oo})$ are shown for energies up to 18 GeV [27]). Therefore ρ production is not dominated by an elementary 0^+ exchange. In the Adair system one finds also significant spin flip contributions which exclude the hypothesis of spin independence[37]. In the helicity system the density matrix elements are consistent with no flip contributions, in other words they are consistent with the conservation of s-channel helicity at the $\gamma\rho$ vertex. This means that in the CMS the rho behaves like the photon with the spin along its direction of flight (see Fig. 16). We will come back to the question of limits on the size of the helicity flip amplitudes.

The relative contributions from natural parity (σ^N) and unnatural parity exchange (σ^U) in the t-channel is measured by the parity asymmetry[36],

$$P_\sigma = (\sigma^N - \sigma^U)/(\sigma^N + \sigma^U) \simeq 2\rho^1_{1-1} - \rho^1_{oo} \qquad (16)$$

In Fig. 17 P_σ is given at 2.8, 4.7 and 9.3 GeV [22] as a function of the momentum transfer; we see that rho production is completely dominated by natural parity exchange (namely $P_\sigma \simeq 1$) as expected for a diffraction mechanism. The fraction of unnatural parity exchange, $\sigma^U/\sigma = \frac{1}{2}(1 - P_\sigma)$, for $|t| < 1$ GeV^2 is found to be consistent with the contribution expected from one-pion exchange (OPE) as can be seen from Table III.

Rhoproduction with linearly polarized photons has also been studied in counter experiments at DESY[39] and Cornell[40]. These experiments roughly speaking measured the yields of pion paris emitted in the plane of polarization ($\sigma_{\parallel}$) and perpendicular to it ($\sigma_{\perp}$); the asymmetry Σ then determines the relative contributions from natural and unnatural parity exchange to the combination $(\rho^0_{11} + \rho^0_{1-1})$:

$$\Sigma \equiv \frac{\sigma_{\parallel} - \sigma_{\perp}}{\sigma_{\parallel} + \sigma_{\perp}} = \frac{\left(\rho^0_{11} + \rho^0_{1-1}\right)^N - \left(\rho^0_{11} + \rho^0_{1-1}\right)^U}{\rho^0_{11} + \rho^0_{1-1}} = \frac{\rho^1_{11} + \rho^1_{1-1}}{\rho^0_{11} + \rho^0_{1-1}} \qquad (17)$$

Figure 18 shows the energy dependence of Σ for small momentum transfers; it is remarkable that even down to 1.4 GeV Σ is close to one (the ρ threshold is at 1.1 GeV).

Size of the s-channel CMS helicity flip amplitudes: With $P_\sigma = 1$ there are six independent helicity amplitudes, $T_{\lambda_\rho \lambda_N, \lambda_\gamma N}$, or 12 real quantities (phases and magnitudes):

$$T_{1\frac{1}{2}\,1\frac{1}{2}},\ T_{0\frac{1}{2}\,1\frac{1}{2}},\ T_{1\frac{1}{2}\,1-\frac{1}{2}},\ T_{0\frac{1}{2}\,1-\frac{1}{2}},\ T_{1\frac{1}{2}\,-1\frac{1}{2}},\ T_{1\frac{1}{2}\,-1-\frac{1}{2}}$$

but besides the cross section only five independent density matrix elements which can be measured with linearly polarized photons and $P_\sigma = 1$:

$$\rho^0_{oo},\quad \mathrm{Re}\,\rho^0_{1o},\quad \rho^0_{1-1},\quad \mathrm{Im}\,\rho^2_{1o},\quad \mathrm{Im}\,\rho^2_{1-1}$$

The present experiments therefore do not allow a complete determination (phase and magnitude) of the helicity amplitudes. The magnitude of the following flip terms can be obtained from the data:

$$|t_{o1}|^2 \equiv \frac{|T_{0\frac{1}{2}\,1\frac{1}{2}}|^2 + |T_{0\frac{1}{2}\,1-\frac{1}{2}}|^2}{\Sigma\,|T|^2} = \rho^0_{oo}$$

$$|t_{1-1}|^2 \equiv \frac{|T_{1\frac{1}{2}\,-1\frac{1}{2}}|^2 + |T_{1\frac{1}{2}\,-1-\frac{1}{2}}|^2}{\Sigma\,|T|^2} = 1/2(1 - \rho^0_{oo}) + \mathrm{Im}\,\rho^2_{1-1}$$

In Fig. 19 $|t_{o1}|^2$ and $|t_{1-1}|^2$ and their sum, $|t_{o1}|^2 + |t_{1-1}|^2$, are shown versus t as determined from the SBT data[22]. The $|\lambda_\gamma| = 1 \rightarrow \lambda_\rho = 0$

contributions to the cross section are seen to be less than 5 % and consistent with zero for $|t| < 0.4$ GeV^2 and of the order of 10 - 20 % between $|t| = 0.4$ and $|t| = 1$ GeV^2. The data points for the double flip terms $\lambda_\gamma = \pm 1 \to \lambda_\rho = \mp 1$ have larger errors; $|t_{1-1}|^2$ is smaller than 10 % for $|t| < 0.4$ GeV^2 and of the order of 10 - 20 % above. The same is true for the sum $|t_{o1}|^2 + |t_{1-1}|^2$. We conclude that the amplitudes for helicity flip at the γ-ρ vertex contribute less than 10 % of the cross section for $|t| < 0.4$ GeV^2. This statement holds also for the nucleon vertex except for the flip term $T_{1\frac{1}{2}\,1-\frac{1}{2}}$ which at present cannot be separated from the non flip amplitude $T_{1\frac{1}{2}\,1\frac{1}{2}}$. Note, however, that $T_{1\frac{1}{2}\,1-\frac{1}{2}}$ has to vanish in the forward direction because of angular momentum conservation*.

b. Models of ρ production and the measured ρ cross sections

Fig. 20 shows as an example the $\pi^+\pi^-$ mass spectrum for the reaction

$$\gamma p \to p\pi^+\pi^-$$

as measured by the SLAC-Weizmann-Tel Aviv collaboration between 2 and 8 GeV [23]. The dominant feature is ρ^o production; other processes, mainly $\Delta^{++}\pi^-$ production (shaded areas) become less and less important with increasing photon energy. The skewing of the ρ^o mass shape is clearly visible: relative to a p-wave Breit-Wigner the low mass side is enhanced whereas there are too few events above the ρ mass. The skewing or ρ-mass shift depends on the momentum transfer and is most pronounced near $|t| = 0$ (see Fig. 21).

---

*Assuming SCHC at the $\gamma\rho$ vertex the Munich[41] group has fitted a Regge pole model to the SBT data in order to study the t-dependence of the real and imaginary parts of the helicity amplitudes. Eremian and others[42] have made an attempt to determine the helicity amplitudes for vector meson production fitting simultaneously the data for ρ^o, ω and ϕ production with P, P', A_2, π and cut contributions.

Since the cause of the skewing is not yet fully understood it is necessary to determine the ρ cross section in a model dependent way. As we shall see the resulting uncertainties are of the order of 10 - 30 %.

A quantity which is related to the ρ cross section and which can be determined model independently is the intensity Π for p-wave pion pairs produced through s-channel helicity conservation (SCHC)[22] at the photon vertex; obviously Π constitutes an upper limit for ρ production through SCHC. In the case of SCHC the decay angular distribution is given by

$$\begin{aligned} W(\cos\Theta,\psi) &= 3/4\pi \sin^2\Theta \cos^2\psi \\ &= 3/8\pi \{\sin^2\Theta + \sin^2\Theta \cos 2\psi\} \end{aligned} \tag{19}$$

where Θ and ψ are the polar and polarization angles in the helicity system. The second term is proportional to the spherical harmonic $\mathrm{Re}\, Y_2^2(\Theta,\psi)$ and can be measured through moment analysis leading directly to the intensity:

$$\Pi = \sqrt{40\,\pi/3} \sum_i \mathrm{Re}\, Y_2^2\,(\Theta_i,\psi_i) \tag{20}$$

The summation is to be done over all events. Fig. 22 shows the $\pi^+\pi^-$ mass spectra as measured by SBT at 2.8 and 4.7 GeV[22] for different regions of t. The dots give the values of Π. Except for $|t| > 1$ GeV^2 Π is close to the total $\pi^+\pi^-$ mass distributions which implies that nearly all $\pi^+\pi^-$ pairs are produced through SCHC at the photon vertex. It is interesting to note that Π shows the same mass skewing as the distribution for all events.

We shall now discuss various models for ρ production. According to Ross and Stodolsky[43] the ρ mass shift is of kinematical origin. They suggest that near $t = 0$ the Breit-Wigner for the rho should be multiplied by a factor $(M_\rho/M_{+-})^4$ where M_{+-} is the $\pi^+\pi^-$ effective mass. This factor was tested by SBT[22] and

others[28] by allowing for a variable exponent n, vis. $(M_\rho/M_{+-})^{n(t)}$. Good fits to the mass distributions were obtained (see e. g., Fig. 22). The exponent n was found to vary with t from $n = 5$ near $t = 0$ to $n = 0$ for $|t| \geq 0.5$ GeV^2 (see Fig. 23) - i. e., the ρ mass shift disappears above $|t| \geq 0.5$ GeV^2, in agreement with what we have seen qualitatively from the Chew-Low-plot of Fig. 21. The conclusion is that the Ross-Stodolsky factor does not fit the data at small or large $|t|$ values; it gives, however, a reasonable approximation to the mass spectrum averaged over all t.

The SBT collaboration has made a detailed comparison of their data with the Söding model[44]. The Söding model illustrated in Fig. 24 describes the ρ mass shift as due to the interference of ρ production (diagram a) with the production of pion pairs through a Drell mechanism (diagrams b, c). Rescattering terms proposed by Bauer and Yennie[45] and by Pumplin[46] to avoid problems with double counting were included in the analysis. The model was found to agree well with most of the features of the $p\pi^+\pi^-$ final state; see for example the M_{+-} distributions given in Fig. 22 (the solid lines were obtained with the Söding model) and the M_{+-} dependence of certain moments $Y_\ell^m(\Theta,\psi)$ shown in Fig. 25. The magnitude of the background amplitudes (diagrams b - e) which was treated as a fit parameter in the comparison is correctly predicted by the model if Benecke-Dürr[38] form factors for the πN vertex are used (see Fig. 26)*.

Fig. 27 illustrates how in the Söding model the various terms add up to the total $\pi^+\pi^-$ mass distribution. The contribution from the Drell terms (including the rescattering corrections) vanishes at $M = M_\rho$. In addition the other background terms are found to be small near $M = M_\rho$. Based on this fact, Yennie[48]

* Gutbrod[47] has argued that the ρ amplitude should be defined as the sum of all terms which vary rapidly with M_{+-} in the ρ region; in the Söding model this is the sum of diagrams a, d and e. This leaves the predictions of the Söding model for the $\pi^+\pi^-$ mass distributions etc. unchanged. The values of the forward and total ρ cross sections are found to increase by 5 - 10 %.

has proposed a simple recipe to determine σ_ρ free of the problem of the mass shape: measure the $\pi^+\pi^-$ yield at $M = M_\rho$ to obtain

$$\frac{d\sigma_\rho}{dt} = \frac{\pi}{2} \Gamma_\rho \frac{d^2\sigma}{dt\, dM} \qquad (21)$$

$$\text{at } M = M_\rho$$

where Γ_ρ is the width of the rho. There is, however, a fly in the ointment: the result depends critically on the values of M_ρ and Γ_ρ which are not well known yet. For the range of M_ρ and Γ_ρ values allowed by the Orsay storage ring data[49] (M_ρ = 774 - 786 MeV, Γ_ρ = 138 - 168 MeV) the SBT forward cross sections vary by $\sim$ 30 % from 120 to 170 (80 - 115) $\mu b/GeV^2$ at 2.8 (4.7) GeV. Furthermore in this, what might be called the pole method, the ω-ρ interference cannot be ignored; it increases the cross section at $M = M_\rho$ by $\sim$ 10 % (see below).

Results very similar to those from the model of Söding are predicted by the Kramer model[50] which has just the opposite view of rho production. In this model the $\pi^+\pi^-$ pairs are produced by the Drell-mechanism and through strong final state interaction generates the ρ, i. e., the model is represented by diagrams d, and e of Fig. 24. All p-wave $\pi\pi$ production is called ρ production and therefore Π gives the cross section for s-channels helicity conserving (at the $\gamma\rho$ vertex) ρ production. The model makes an interesting prediction, namely for forward produced $\pi^+\pi^-$ pairs there should be a dip in the $\pi^+\pi^-$ mass distribution around 1.0 - 1.2 GeV. While the available data are consistent with this prediction, they are statistically not sufficient to provide a real test. For further models on ρ production see Ref. 41 and 51.

Let us now look at the measured differential ρ cross sections.

(i) Consistency of the data: In Fig. 28 $d\sigma/dt$ values in the energy range 4.5 - 6 GeV and 9 - 11 GeV from different experiments are compiled. (The ABBHHM and the SBT data were obtained with the factor $(M_\rho/M_{+-})^4$ and $(M_\rho/M_{+-})^{n(t)}$ respectively, Cornell used the Söding model, Anderson et al. a p-wave Breit-Wigner.) At 4.5 - 6 GeV one finds all data points lie within a ±10 % wide band*. At 9 - 11 GeV the width of the band is approximately ±15 %.**

(ii) Model dependence of $d\sigma_\rho/dt$: Table IV summarizes the values of the forward cross section, $d\sigma/dt$ and the slope as obtained with different methods and in different experiment. According to the SBT data the $d\sigma^o/dt$ values determined with the Söding model are considerably smaller (∿30 % at 2.8 GeV, ∿ 20 % at 4.7 GeV) than those for Π or those obtained with the factor $(M_\rho/M_{+-})^{n(t)}$. The smaller $d\sigma^o/dt$ values are correlated with a shallower $|t|$ distribution found with the Söding model ($A \simeq 6$ GeV^2 as compared to $A \simeq 7$ GeV^2). The SBT forward cross section at 9.3 GeV which is obtained by extrapolation is smaller by ∿2 s.d. than the values of Bulos et al. and of the Cornell group. In addition, Bulos et al. find a steeper slope. This might

---

* Preliminary data from Gladding et al.[52], however, show consistently smaller cross sections.

** Note that the Cornell[30] experiment which detects only pion pairs near decay angles $\theta = \phi = 90^o$ in the helicity system is not measuring the cross section but rather the combination (see Eq. (14)).

$$d\sigma/dt_{Cornell} = 2(\rho^o_{11} + \rho^o_{1-1})\, d\sigma/dt = (1 - \rho_{oo} + 2\,\rho_{1-1})\, d\sigma/dt$$

where the density matrix elements are those of the helicity system. Whereas the correction is negligible near $|t| = 0$, $d\sigma/dt_{Cornell}$ may be smaller than the ρ cross section by 5 - 10 % for $0.05 < |t| < 0.25$ GeV^2 and by 15 - 30 % above: The SBT data[22] give for $\rho_{oo} - 2\,\rho_{1-1}$ the following values:

$\|t\|$ (GeV^2)	E_γ = 4.7 GeV	9.3 GeV
.02 - .05	- .01 ±.07	
.05 - .25	.05 ±.04	.10 ±.06
.25 - .4	.17 ±.09	.19 ±.12
.4 - 1.0	.30 ±.12	.28 ±.20

indicate that at small $|t|$ values (say below $|t| < 0.1$ GeV^2) the slope increases, leading to a forward cross section which is larger than that predicted by a linear extrapolation over $0.02 < |t| < 0.4$ GeV^2. (Fits to the SBT data with a quadratic form, $d\sigma^o/dt \exp(At + Bt^2)$, did not give evidence for the presence of the B-term, however.)

The forward cross sections are plotted in Fig. 29 as a function of the photon energy. There is a rather large spread of the data points which reflects at least partly the theoretical uncertainty of how to extract the ρ^o cross sections, and the difference between measured and extrapolated forward cross sections. Despite the spread, the data show that the forward cross section decreases with energy, approaching at 10 GeV a value of 95 μb/GeV^2 with an estimated uncertainty of ∿ 15 %.

In Fig. 30 the total cross sections for ρ production, σ_ρ, have been compiled. There is good agreement among the various experiments. The energy dependence of σ_ρ is the same as that of the average of the elastic $\pi^\pm p$ cross sections. From the quark model plus VDM one expects[53]

$$\sigma_\rho = \frac{\alpha}{\gamma_\rho^2} \frac{1}{2} (\sigma^{el}_{\pi^+ p} + \sigma^{el}_{\pi^- p}) \qquad (22)$$

This relation is consistent with the data[54] for a value of $\gamma_\rho^2/4\pi = 0.7$.

c. Rho meson production on the deuteron

Data on ρ^o production off deuterons, and on ρ^- production from neutrons ($\gamma n \to \rho^- p$) together with the $\rho^o p$ measurements provide information on the relative size of the $T = 0$ and $T = 1$ t-channel exchange contributions to $\gamma N \to \rho^o N$.

$\gamma d \to \rho^o d$: The $\rho^o d/\rho^o p$ ratios for forward production measured at Cornell[30] and SLAC[32] showed that for $t = 0$ the isovector exchange is small. Averaged over

photon energies between 4 and 9 GeV, the result for the amplitudes T_o, T_1 was[30]:

$$\frac{\mathrm{Re}\,(T_o^{+}\,T_1)}{|T_o + T_1|^2} = -0.02 \pm 0.02$$

$$\left|\frac{T_1}{T_1 + T_o}\right| = 0.14 \pm 0.06$$

New results from a deuterium bubble chamber experiment at DESY[55] indicate that $|T_1| \ll |T_o|$ also for larger momentum transfers. Fig. 31 shows the measurements of $d\sigma/dt$ for $\gamma d \to \rho^o d$ for $|t|$ values between 0.04 and 0.2 GeV^2. Over that t range the deuteron could be identified with certainty thus excluding a contamination from break-up processes ($\gamma d \to \rho^o np$). The data points at larger $|t|$ values match quite well with those obtained by Anderson et al.[56] for $|t| > 0.15$ GeV^2 (the latter data will be discussed in the talk of Prof. Gottfried). The exponential slope for the $d\sigma/dt$ values of Fig. 31 is $A \simeq 25$ GeV^{-2} which is an indication that single scattering dominates here. In order to test on the size of the T_1 amplitude, the authors calculated $d\sigma/dt(\gamma d \to \rho^o d)$ from the single scattering diagrams under the assumption that the differential cross sections for $\gamma p \to \rho^o p$ and $\gamma n \to \rho^o n$ are equal. Furthermore, T_o which can only contribute to single scattering was assumed to be given by $|T_o| = \sqrt{d\sigma/dt(\gamma p \to \rho^o p)}$ (i. e., $T_1 = 0$). The calculation makes absolute cross section predictions shown by the curves in Fig. 31. From the good agreement with the measured points it follows that $T = 1$ exchange is small also off the forward direction. The actual numbers for $0.04 < |t| < 0.2$ GeV^2 are[55]:

$$\left|\frac{T_o + T_1}{T_o}\right| = \begin{array}{ll} 0.96 \pm 0.09 & \text{at } E_\gamma = 1.8 - 2.5 \text{ GeV} \\ 1.02 \pm 0.11 & 2.5 - 3.5 \text{ GeV} \\ 1.03 \pm 0.10 & 3.5 - 5.3 \text{ GeV} \end{array}$$

$\gamma n \to \rho^- p$: Fig. 32 shows the latest cross section data for ρ^- production on neutrons from the same experiment[55]. The large errors are mainly caused by the difficulties with a deuteron target. At energies above 3.5 GeV one finds $\sigma(\rho^- p) = 1.0 \pm 0.4$ μb. Possible t-channel exchange candidates are π, ρ, A_2. Provided that ρ and A_2 do not interfere destructively the size of $\sigma(\rho^- p)$ and $\sigma(\rho^o p)$ leads to $|T_1|^2/|T_o|^2 < 0.05$.

The ρ^- cross section peaks around 1.9 GeV. The cross section in the peak is approximately half of that observed for ρ^o production (see Fig. 32) which is consistent with the s-channel excitation of a T = 3/2 isobar ($\Delta(1950)$?); for the formation of a T = 1/2 isobar the ratio would be the reciprocal, namely $\sigma(p\rho^-) : \sigma(p\rho^o) = 2 : 1$.

d. Omega-rho interference

Clear evidence for ω-ρ interference for the case of ρ production off protons has been observed by the DESY-MIT group[57] (see Fig. 33). This subject will be covered by Prof. Gottfried.

e. Summary of rho photoproduction

The differential cross sections measured in different experiments agree to within ±15 % outside the forward direction ($|t| > 0.05$ GeV^2). They disagree in the size of the forward cross section. Part of the discrepancy is connected with the lack of theoretical understanding of ρ production; another part could be due to an increase of the slope at small $|t|$ values.

The forward cross section decreases with energy and reaches a value of 95 μb/GeV^2 at 10 GeV with an estimated uncertainty of ±15 %.

The total ρ cross section has the same energy dependence as $\sigma^{el}_{\pi p}$ in accordance with the quark model plus VDM.

The data are consistent with s-channel helicity conservation at the γρ vertex up to $|t| < 0.4$ GeV^2.

Rho production proceeds almost completely through natural parity exchange. Candidates for t-channel exchange are P, P' and A_2.

The T = 1 t-channel exchange contributions are small compared to those with T = 0. This is consistent with the observed difference $\sigma^T_{\gamma p} - \sigma^T_{\gamma n}$.

The summary can be summarized by saying that ρ^o production is consistent with a diffraction mechanism.

2. ω Production via $\gamma p \to \omega p$

a. Cross sections

The available data (∿ 1700 events) on this reaction have all been obtained in trackchamber experiments[21,23,27,58,59*]. The ω is detected in the $p\pi^+\pi^-\pi^o$ final state. As an example in Fig. 34 the $\pi^+\pi^-\pi^o$ mass distribution is shown from the SBT experiment at 9.3 GeV. Because of the narrow ω width the determination of the cross section is straightforward. The energy dependence of $\sigma_{\omega p}$ is displayed in Fig. 35. The ω cross section rises steeply above threshold, goes through a maximum around 2 GeV and drops off. The new data at 7.5 [23] and 9.3 [59] GeV show that the cross section does not go to zero between 5 and 10 GeV but rather approaches a finite value.

---

* Preliminary data on ω production from a counter experiment have been reported by Gladding et al.[52].

The energy dependence of $\sigma_{\omega p}$ was always understood as the consequence of two production mechanisms: one-pion exchange (OPE) and diffraction scattering, with OPE dominating the low energy region and the latter taking over at high energies. The data obtained by SBT[59] with linearly polarized photons confirm this picture. As in the case of ρ^o production the ω decay angular distribution allows a separation of the contributions σ^N, σ^U from natural and unnatural parity exchange in the t-channel. In Fig. 36 the distribution of the polarization angle ψ is shown. It gives a clear demonstration for the changing importance of σ^N, σ^U: At 2.8 GeV the ψ distribution is flat, hence, $\sigma^N \simeq \sigma^U$; at 9.3 GeV $W(\psi)$ looks much like the ψ distribution for ρ events: it peaks at 0^o, 180^o, therefore $\sigma^N >> \sigma^U$ *. The energy behavior of σ^N and σ^U can be read off from Fig. 35 and Table V. Whereas σ^N stays approximately constant σ^U drops from $\sim$5 µb at 2.8 GeV to zero at 9.3 GeV. Results on the t dependence of the total cross section and of σ^N are also given in Table V. The values of $d\sigma^N/dt$ agree with the forward cross sections obtained for $\gamma N \to \omega N$ from coherent ω production:

$$d\sigma/dt^{coh}(\gamma N \to \omega N)\Big|_{t=0} = 14.9 \pm 3.1 \text{ µb/GeV}^2 \text{ at 5.7 GeV (Bonn-Pisa)}^{60}$$
$$= 11.4 \pm 1.9 \text{ µb/GeV}^2 \text{ at 6.8 GeV (Rochester)}^{61}$$

Whereas σ^N may have contributions from T = 1 exchange, they should be negligible for σ^{coh}.

b. Decay angular distribution

Fig. 36 shows besides $W(\psi)$ the distributions of the polar angle in the helicity system at 2.8, 4.7 and 9.3 GeV[59]. The cosθ distribution is not a pure $\sin^2\theta$ distribution, i. e. $\rho_{oo}^{oH} \neq 0$. A nonzero ρ_{oo}^{oH} indicates the presence of heli-

* Note, the degree of linear polarization is 94 % at 2.8, 4.7 GeV and 77 % at 9.3 GeV.

city flip terms. A closer inspection of the density matrix elements shows that flip contributions are probably present even in the natural parity part:

$$\sigma_{oo}^{oN} = \frac{1}{2}(\rho_{oo}^{o} - \rho_{oo}^{1}) = 0.15 \pm 0.06,\ 0.11 \pm 0.06,\ 0.14 \pm 0.06$$

at 2.8, 4.7 and 9.3 GeV for $|t| < 0.5\ \mathrm{GeV}^2$.

c. Production mechanism

σ^U: The energy dependence and the magnitude of σ^U agree with the predictions from OPE (using Benecke-Dürr-form factors[38] the partial width $\Gamma_{\omega\pi\gamma}$ is found to be 0.8 ±0.1 MeV which is to compared with the directly measured value[62] of 1.06 ±0.15 MeV).

σ^N: The interesting question here is whether σ^N is completely due to diffraction production or whether there is in addition a T = 1 t-channel exchange contribution (A_2 exchange). Sufficiently accurate data for ω production on neutrons could answer this; so far we don't have such data. Harari[63], from the observed difference between $\sigma_{\gamma p}^T$ and $\sigma_{\gamma n}^T$ predicted a large contribution from A_2 exchange and from the interference of A_2 with P and P' exchange. Starting from the relation

$$\mathrm{Im}\ T^1_{\gamma p\to\omega p} = \frac{1}{2}\,\frac{\gamma_\omega}{\gamma_\rho}\,\frac{\mathrm{Im}\ T^1_{\gamma p\to\gamma p}}{\mathrm{Im}\ T^o_{\gamma p\to\gamma p}}\,\mathrm{Im}\ T^o_{\gamma p\to\rho^o p} \qquad (23)$$

T^o, T^1 forward amplitudes for isoscalar and isovector exchange respectively;

$\gamma_\rho, \gamma_\omega$ measure the γ-ρ and γ-ω coupling strengths;

and combining the data for $\sigma_{\gamma p}^T - \sigma_{\gamma n}^T$, $d\sigma^o/dt(\gamma p\to p\rho)$ and $\sigma_{\omega p}^N$ one estimates the P + P' contribution to $\sigma_{\omega p}^N$ to be 1.4 μb and those from A_2 plus interference 0.8 μb, 0.6 μb and 0.4 μb at 2.8, 4.7 and 9.3 GeV respectively. For the forward cross section from P + P' exchange one finds a value of 10 $\mu b/\mathrm{GeV}^2$. In

other words, A_2 plus interference terms are expected to contribute at 9.3 GeV about 25 % of the cross section. This contribution may also be responsible for the presence of s-channel helicity flip terms.

3. ϕ production

New data on ϕ production via

$$\gamma p \rightarrow \phi p$$

have been obtained by the Cornell group at 8.5 GeV[30]. Contamination from inelastic ϕ production has been measured in a separate experiment and was found to be $\sim$15 %. The corrected cross section data together with those from previous experiments[21,33] are shown in Fig. 37. There is consistency between the different data sets. An exponential fit to the Cornell points alone gives[30]

$$d\sigma/dt = (2.85 \pm 0.2)\, e^{(5.4 \pm 0.3)\, t} \quad (\mu b/GeV^2).$$

The Cornell group[64] and a group from SLAC-Wisconsin[65] (in a triple coincidence experiment at SLAC) have studied ϕ production with linearly polarized photons. The results for the asymmetry, $\Sigma = (\sigma_{\parallel} - \sigma_{\perp})/(\sigma_{\parallel} + \sigma_{\perp})$, are:

$E_\gamma = 5.7$ GeV, $\theta = 0^\circ$ (Cornell)[64]: $\Sigma = 0.53 \pm 0.15$

$E_\gamma = 8$ GeV, $|t| = 0.2$ GeV^2 (SLAC-Wisconsin)[65]: $\Sigma = 1.05 \pm 0.12$

The Cornell value is not corrected for a possible contamination by inelastic ϕ events. Since ϕ production is rather energy independent, the two measurements seem to be inconsistent. An asymmetry of 0.5 would indicate a sizeable contribution from unnatural parity exchange, contrary to the belief that this reaction preceeds only via pomeron exchange. The only likely cadidates for

unnatural parity exchange seem to be π and η. From an estimate of the contribution from π and η exchange* it is found that π and η exchange reduce Σ from unity to 0.92 at $E_\gamma = 5.7$ GeV and $\theta = 0^\circ$.

4. Comparison with the vector dominance model

The vector dominance model (VDM) relates the photoproduction of vector mesons, $\gamma p \to Vp$, $(V = \rho^\circ, \omega, \phi)$ to the total hadronic photon proton cross section, $\sigma_T(\gamma p)$, and to vector meson production through electron-positron annihilation, $e^+e^- \to V$. The starting point for all VDM relations is the conjecture that the electromagnetic current, j_μ, can be written as a sum of the vector meson fields[67]:

$$j_\mu(x) = -\left\{ \frac{M_\rho^2}{2\gamma_\rho} \rho_\mu(x) + \frac{M_\omega^2}{2\gamma_\rho} \omega_\mu(k) + \frac{M_\phi^2}{2\gamma_\phi} \phi_\mu(x) \right\} \tag{24}$$

where M_V is the mass of the vector meson and γ_V measures the strength of the photon-vector meson coupling. For the ratio of the γ-V coupling constants SU_6 predicts:**

$$1/\gamma_\rho : 1/\gamma_\omega : 1/\gamma_\phi = 3 : 1 : -\sqrt{2} \tag{25}$$

We shall consider the following VDM relations:

$$\text{a)} \quad d\sigma^\circ/dt(\gamma p \to Vp) = \frac{\alpha/4}{\gamma_V^2/4\pi} \frac{d\sigma^\circ}{dt}(Vp \to Vp) \tag{26}$$

$$= \frac{(1 + \eta_V^2)\,\alpha/64}{\gamma_V^2/4\pi} \sigma_T(Vp)$$

---

* The calculation had the following ingredients: for $\Gamma_{\phi\pi\gamma}$ and $\Gamma_{\eta\pi\gamma}$ the recent Orsay measurements were used[49]; the ηNN coupling constant was taken from relativistic SU_6[66]; the π and η exchange amplitudes were assumed to interfere constructively as predicted by theory; the form factors of Ref.38 were used.

** Modifications due to symmetry breaking change these ratios either to $1/\gamma_\rho^2 : 1/\gamma_\omega^2 : 1/\gamma_\phi^2 = 9 : 0.65 : 1.33$ [68] or to $9 : 1.2 : 1$ [69].

where $d\sigma^o/dt$ denotes the forward cross section and η_V the ratio of the real to imaginary part. With the help of the quark model [53,70] the total Vp cross sections can be related to $\sigma^T(\pi^{\pm}p)$ and $\sigma^T(K^{\pm}p)$:

$$\begin{aligned} \sigma_T(\rho^o p) &= \sigma_T(\omega p) = \tfrac{1}{2}(\sigma_T(\pi^+ p) + \sigma_T(\pi^- p)) = 28 \text{ mb at 5 GeV} \\ \sigma_T(\phi p) &= \sigma_T(K^+ p) + \sigma_T(K^- n) - \sigma_T(\pi^+ p) = 13 \text{ mb at 5 GeV.} \end{aligned} \tag{27}$$

From Eqs. (26,27) one can calculate the forward cross sections for vector meson photoproduction and compare the predictions with the data. This is done in Table VI. The ratio $\rho : \omega$ predicted from Eqs. (25) - (27) is consistent with measurements. The measured ϕ cross section relative to that for ρ and ω is smaller than the predicted one.

b) We can use Eq. (26) together with the quark model relations (27) and determine $\gamma_V^2/4\pi$ from the measured forward cross sections:

$$\frac{\gamma_V^2}{4\pi} = \frac{\alpha}{64\,\pi} \frac{(1 + \eta_V^2)\,\sigma_T^2(Vp)}{d\sigma^o/dt(\gamma p \to Vp)} \tag{28}$$

The forward ρ^o cross section data are best described with a value of $\gamma_\rho^2/4\pi = 0.65 \pm 0.1$ (see Fig. 29). For γ_ω and γ_ϕ the results are given in Table VII.

c) A direct test of VDM is provided by the following relation:

$$\sigma_T(\gamma p) = \sum_{V=\rho,\omega,\phi} \sqrt{\frac{4\pi\alpha}{\gamma_V^2/4\pi} \frac{1}{1 + \eta_V^2} \frac{d\sigma^o}{dt}(\gamma p \to Vp)} \tag{29}$$

The by far largest contribution to the sum comes from ρ production. We will therefore use Eq. (29) to determine $\gamma_\rho^2/4\pi$ inserting the total γp cross

section and the forward cross section data for ρ, ω, ϕ. (η_ρ and η_ω are put equal to the ratio of the real to imaginary parts for Compton scattering, and $\eta_\phi = 0$; for $\gamma_\omega^2/4\pi$ and $\gamma_\phi^2/4\pi$ the Orsay storage ring values, Table VII, are used). The considerable uncertainties in the ω and ϕ quantities have only a minor effect on the determination of γ_ρ.*

The analysis yields $\gamma_\rho^2/4\pi = 0.35 \pm 0.05$ and gives, within a few percent, the same curve as the quark model result for $\gamma_\rho^2/4\pi = 0.65$ (see Fig. 29).

d) Finally, the differential cross sections for vector meson production and Compton scattering can be compared as a function of t (at $|t| = 0$ Compton scattering and $\sigma_T(\gamma p)$ are related through the optical theorem and the present test is equivalent to the previous one):

$$d\sigma/dt\ (\gamma p \to \gamma p) \simeq \alpha/4 \left| \sum_{\rho,\,\omega,\,\phi} \sqrt{\frac{1}{\gamma_V^2/4\pi} \frac{d\sigma}{dt}(\gamma p \to V p)} \right|^2 \qquad (30)$$

The approximation here is that the ratio of real to imaginary part is assumed to be the same for the three vector meson reactions. The analysis in terms of the P, P' and A_2 trajectories supports this assumption for ρ and ω. The error made for the ϕ term is negligible. In Fig. 38 the ratio of the Compton cross sections predicted by VDM (defined by the r.h.s. of Eq. (30) with $\gamma_\rho^2/4\pi = 0.5$) to the experimentally measured ones is shown as obtained by Buschhorn et al.[12]. The ratio is of the order of 0.4 - 0.6 independent of E_γ

* Actually, a more refined analysis was done to determine γ_ρ: the results on the P, P' and A_2 contributions to Compton scattering (see Eq. (6)) were used to construct the $\gamma p \to Vp$ amplitudes; the phases of the amplitudes were calculated from the signature factors of the P, P' and A_2 trajectories (the ratio of real to imaginary part for forward Compton scattering calculated this way agrees with the dispersion theoretical result, Fig. 4). The curve shown in Fig. 29 has been obtained in that manner. The difference between this curve and the result from Eq. (29) is less than 10 % in the energy region considered.

and t. Translated into a value for $\gamma_\rho^2/4\pi$ the data give $\gamma_\rho^2/4\pi = 0.2 - 0.3$, consistent with the γ_ρ determination from $\sigma_T(\gamma p)$ (previous section). A comparison of Compton scattering and rho production off deuterons has given similar results[14,72].

Conclusion: In Table VII the various results on the γ-V coupling constants are collected. The value of $\gamma_\rho^2/4\pi$ obtained through Eqs.(29) or (30) from photoproduction data alone is smaller by a factor of two than the result from e^+e^- annihilation. Since the relations (29) and (30) are based on VDM alone the disagreement must be due to a failure of VDM.

Possible reasons for the discrepancy are (a) the value of γ_ρ depends on the photon mass: The photoproduction data determine γ_ρ at $m_\gamma = 0$, the e^+e^- annihilation experiments at $m_\gamma = m_\rho$; (b) there exist further vector mesons which couple to the photon. The first explanation appears to be unlikely because the ρ^o forward cross section (here also $m_\gamma = 0$) plus the quark model as well as the analysis of ρ^o production off deuterons in terms of single and double scattering give the same $\gamma_\rho^2/4\pi$ value as the storage ring experiment, namely ~ 0.65. As to the second possibility: if we assume the existence of a $J^P = 1^-$, $T^G = 1^+$ state, ρ' (resonance or continuum) and take the process $\rho' N \to \rho N$ to be small as compared to elastic $\rho' N$ scattering then consistency between the photoproduction and the e^+e^- data can be obtained for

$$\frac{1}{\gamma_{\rho'}^2/4\pi} \frac{d\sigma}{dt}(\gamma p \to \rho' p) \simeq 30\ \mu b/GeV^2.$$

The experimental situation concerning this question is discussed in the following paragraph.

5. Are there higher mass vector mesons?

The existence of higher mass vector mesons is predicted, e. g., by the Veneziano Model[73]. Examples are the ρ' and ρ'' with masses of $\sim$1.3 and $\sim$1.7 GeV. A recent analysis of the nucleon from factor data[74] predicts the existence of several new isovector and isoscalar vector mesons with masses above 1.5 GeV. Extensive searches for these objects in photoproduction and in μ pair production by γA and pp interactions[75,76] so far have been unsuccessful. As an example, Fig. 39 shows the mass spectrum of $\pi^+\pi^-$ pairs produced off carbon at E_γ = 6 GeV, $\theta = 0^\circ$ as measured by the DESY-MIT group[77]. Results similar to those of Fig.39 have been obtained at higher energies ($\sim$ 15 GeV) by Bulos et al.[78]. Apart from the ρ the spectrum shows no narrow (say $\sim$ 200 MeV wide) structure. The broad shoulder from 1.2 to 1.8 GeV above a certain ρ tail could perhaps be explained by the Söding interference mechanism. The cross section in this bump is approximately hundred times smaller than that for ρ° production. On the other hand, the mass spectrum seems to be roughly consistent with the multiperipheral dual model which includes ρ and ρ' [79].

Evidence for the existence of a vector meson with M = 1968 MeV, Γ = 35 MeV has been claimed in an experiment measuring $\bar{p}p \to K_S^\circ K_L^\circ$ as a function of the $\bar{p}$ momentum[80].

There exists the possibility that some of the threshold phenomena observed in photoproduction (see section VI, 4) are connected with the production of a high mass photon-like state.

VI. Other Photoproduction Reactions

1. $\gamma N \to A_2 N$

Fig. 40a shows a compilation[23,59,81] of three charged pion mass spectra obtained for the reactions

$$\gamma p \rightarrow n\pi^+\pi^+\pi^-$$

and

$$\gamma n \rightarrow p\pi^+\pi^-\pi^- \ .$$

A peak in the A_2 mass region is clearly seen. If this peak is attributed to A_2 production one finds an A_2 cross section of the order of 0.5 - 1 μb (see Fig. 40b). The data are consistent with the predictions for one pion exchange[38] if $\Gamma_{A_2\rho\gamma} = 0.5$ MeV is used.

2. $\gamma p \rightarrow B^o p$

There exists evidence for the photoproduction of a meson with mass around 1.23 GeV. Anderson et al.[33] in a missing mass experiment

$$\gamma p \rightarrow pX$$

were the first to observe a bump around 1.2 GeV in the mass spectrum of X. The SBT bubble chamber[59] and the DESY streamer chamber[82] experiments have found an enhancement around that mass value, studying the reaction

$$\gamma p \rightarrow p\pi^+\pi^- + (m\pi^o), \ m \geq 2 \ .$$

The enhancement is more pronounced if events with $0.33 < M_{\pi^+\pi^-} < 0.60$ GeV are selected. This suggests that the bump is due to B production:

$$\gamma p \rightarrow B^o p$$
$$\downarrow$$
$$\pi^o \omega$$
$$\downarrow$$
$$\pi^+\pi^-\pi^o$$

Fig. 41 shows the combined SBT and DESY data. Assuming that one really deals with B production the cross section for $|t| < 0.5$ GeV^2 is found to be[59]:

$$\sigma(\gamma p \rightarrow B^o p) = 0.9 \pm 0.5 \ \mu b \quad \text{at 2.8 GeV}$$
$$= 1.1 \pm 0.4 \ \mu b \quad \text{at 4.7 GeV}$$

An intriguing aspect of B^o photoproduction is that although the B has $J^P = 1^+$ it can be produced by pomeron exchange if γ and pomeron couple in a relative p-wave. This would violate the Gribov-Morrison rule[83]. Clearly more data covering a large energy range are needed to decide upon this question.

3. $\gamma p \to \rho^- \Delta^{++}$ and $\gamma n \to \omega \Delta^o$

The cross section data for these two reactions are somewhat puzzling. Previously, when only $\rho^- \Delta^{++}$ data have been available it has been assumed that the $\rho^- \Delta^{++}$ events are produced mainly via one-pion exchange (OPE) and the $\rho^- \Delta^{++}$ cross section was used[21] to determine an upper limit for $\Gamma_{\rho^\pm \pi\gamma}$. If both reactions proceed through OPE and if the prediction $\Gamma_{\rho\pi\gamma} = 1/9\ \Gamma_{\omega\pi\gamma}$ from SU_3 + mixing holds then

$$\sigma(\rho^- \Delta^{++}):\ \sigma(\omega\Delta^o, \Delta^o \to \rho\pi^-) = 1 : 2\ . \qquad (31)$$

In Fig. 42 the distribution of $M_{p\pi^+}$ versus $M_{\pi^-\pi^o}$ is shown giving clear evidence for $\rho^- \Delta^{++}$ production[59]. The $\rho^- \Delta^{++}$ cross section data from the SBT[59] and SWT[23] experiments are plotted in Fig. 43. Data on $\omega\Delta^o$ production come from a deuterium bubble chamber experiment of the Weizmann group[84] at 4.3 GeV. Fig. 44 displays the relevant mass distributions. From relation (31) and the data on $\sigma(\rho^- \Delta^{++})$ one expects $\sigma(\omega\Delta^o, \Delta^o \to \rho\pi^-) \simeq 2.5$ μb and ≃70 $\omega\Delta^o$ events to be seen in Fig. 44, whereas an upper limit of 3 events is observed leading to $\sigma(\omega\Delta^o, \Delta^o \to \rho\pi^-) < 0.5$ μb. A further discrepancy is found when the cross sections are compared separately to the OPE predictions. With $\Gamma_{\omega\pi\gamma} = 1.06$ MeV [62] one finds at 4.3 GeV $\sigma^{OPE}(\omega\Delta^o, \Delta^o \to \rho\pi^-)$[38] = 1.2 μb which is more than a factor of two larger than the measured upper limit; on the other hand the OPE cross section predicted[38] for $\rho^- \Delta^{++}$ with $\Gamma_{\rho\pi\gamma} = 1/9\ \Gamma_{\omega\pi\gamma} = 0.12$ MeV is smaller by a factor of 2 - 3 than the experimental data (see Fig. 43). Therefore, OPE

is not the only mechanism for $\rho^- \Delta^{++}$ and $\omega\Delta^o$ production. The fact that for $\omega\Delta^o$ production $\sigma^{exp} < \sigma^{OPE}$ points to the presence of an unnatural parity exchange contribution with $T^G = 1^-$ interferring destructively with pion-exchange.

4. Threshold Bumps

Photoproduction now too has entered the era of A bumps and threshold enhancements, which puzzle those studying purely hadronic interactions since many years (A_1, A_3, Q and L bumps etc.). The SLAC Streamerchamber group[85] investigating the reaction

$$\gamma p \rightarrow p\pi^+\pi^+\pi^-\pi^-$$

observes for the $\rho^o\pi^\pm$ system a strong enhancement in the A region (1.0-1.3 GeV, see Fig. 45). In addition the $\rho^o\pi^+\pi^-$ mass distribution shows a broad bump around 1.6 GeV near the low mass end of phase space with an approximate energy independent cross section of $\sim$ 0.9 μb. In hadronic interactions these threshold phenomena are not understood (e. g., resonance or kinematical reflections); experiments with polarized photons and analyzing the ρ^o decay distribution could give further clues on their nature.

Finally, I want to mention two highly speculative subjects which might stimulate new experiments.

5. $\gamma p \rightarrow \Delta^{++}\rho^o\pi^-$ and $\gamma p \rightarrow \Delta^{++}\omega\pi^-$

The five and six pion final states

$$\gamma p \rightarrow p\, 2\pi^+\, 2\pi^-$$
$$\rightarrow p\, 2\pi^+\, 2\pi^-\pi^o$$

show strong ρ^o and ω production[59,86,87] (see e. g. Fig. 46). The larger fraction of the ρ^o and ω events comes from associate production with the $\Delta^{++}(1236)$,

$$\gamma p \rightarrow \Delta^{++}\rho^{\circ}\pi^{-}$$

$$\rightarrow \Delta^{++}\omega\pi^{-} \ .$$

From a preliminary analysis of the SBT data[59] one finds that those events where the $\rho^{\circ}(\omega)$ is peripherally produced the momentum transfer from the photon to the $\rho^{\circ}\pi^{-}(\omega\pi^{-})$ system is smaller than from the photon to the $\rho^{\circ}(\omega)$. The bachelor π^{-} therefore appears to be associated with the $\rho(\omega)$ vertex:

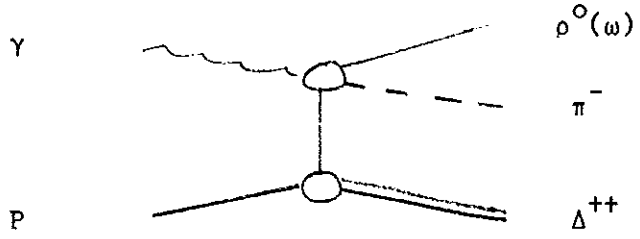

Suppose one-pion exchange mediates these reactions, then events of this type will tell us about the $\gamma\rho \rightarrow \rho^{\circ}\pi$ and $\gamma\rho \rightarrow \omega\pi$ interactions[88]. Unfortunately we need at least an order of magnitude more events than presently available. For example, the SBT experiment at 4.7 GeV from an exposure of $\sim 0.5 \cdot 10^{6}$ pictures yields $\sim$100 events each of the type depicted by the above diagram.

6. Inelastic Diffractive Vector Meson Production

By analogy with the diffractive like production of $T = 1/2$ isobars observed in πp and pp collisions[89] (e. g., $\pi^{-}p \rightarrow \pi^{-}N^{*}(1500)$) one expects at high energies the presence of inelastic diffractive vector meson photoproduction[90]. The dominant contributions supposedly come from the diagrams shown in Fig. 47 with X being a pion. Fig. 48 shows the differential and total cross sections estimated from these diagrams for the case of ρ° production. At 20 GeV the total inelastic diffractive ρ° cross section should be of the order of 3 μb or about one third of the cross section for elastic ρ° production. Similar predictions hold for ω and ϕ.

Evidence for strong inelastic ρ^o production at small angles has first been seen in the SLAC streamerchamber experiment[91].

Inelastic diffractive vector meson production is studied best at high, say NAL, energies where the nondiffractive part has become negligible for small momentum transfers.

One of the interesting questions in connection with this type of process is whether here too the s-channel helicity (at least at the $\gamma\rho$ vertex) is conserved. Similar studies of hadronic reactions ($\pi p \to A_1 p$, $Kp \to Qp$) so far have given negative results[92].

Acknowledgements

That this report got ready in time was only possible because of the assistance from Dr. Chris Berger, who acted as the scientific secretary. Thanks go to Miss Hell, Mrs. S. Pratt and Miss Schöning for typing the manuscript. Discussions with Dr. C. Berger, Profs. W. Busza, E. Lohrmann, Drs. W.J. Podolsky, P. Söding and Prof. Yennie are gratefully acknowledged. I want to thank Prof. B.D. McDaniel and the staff of the Laboratory of Nuclear Studies at Cornell University for the hospitality extended to me.

References

1. See e. g., A. Silverman, Proc. 4th Int. Symp. on Electron and Photon Interactions at High Energies, Liverpool, England, 1969, (ed. by D.W. Braben), p. 71; E. Lohrmann, Proc. of the Lund International Conference on Elementary Particles, held at Lund, Sweden, 1969, (Berlingska Bortryskeriet, Lund, Sweden, 1970), p. 13; K. Lübelsmeyer, Rapporteur's talk at the Kiev Conference, 1970 ; P. Söding, and D. Lüke, Symposium on Meson Photo- and Electroproduction at Low and Intermediate Energies, University of Bonn, 1970, Springer Tracts in Modern Physics, Vol. 59, (1971), in press.

2. P. Joos, DESY report DESY-HERA 70-1 (1970).

3a. H. Meyer et al., Physics Letters B33, 189 (1970).

b. B. Naroska, Thesis, University of Hamburg, DESY report DESY-F1-70/3 (1970).

4a. D.O. Caldwell et al., Phys. Rev. Letters 23, 1256 (1969), (E) 24, 796 (1970); IBID 25, 609 (1970), (E) 25, 902 (1970).

b. W.P. Hesse, Thesis, University of California, Santa Barbara (1971).

5. T.A. Armstrong et al., Phys. Letters B34, 535 (1971); PAPER 195 submitted to this conference and private communication.

6. J. Ballam et al., Phys. Rev. Letters 21, 1544 (1968).

7. SLAC-Berkeley-Tufts Collaboration, Phys. Rev. Letters 23, 498 (1969).

8. E.D. Bloom et al., SLAC-PUB-653 (1969).

9. W.L. Lakin et al., Phys. Rev. Letters 26, 34 (1971).

10. V. Franco, R.J. Glauber, Phys. Rev. 142, 1195 (1966).

11. M. Deutsch, Contribution to the Kiev Conference, 1970.

12. G. Buschhorn et al., Phys. Letters 33B, 241 (1970);
and PAPER 16 submitted to this conference.

13. R.L. Anderson et al., Phys. Rev. Letters 25, 1218 (1970).

14. A.M. Boyarski et al., Phys. Rev. Letters 26, 1600 (1971).

15. K.J. Foley et al., Phys. Rev. Letters 11, 425 (1963).

16. M. Gell-Mann, M.L. Goldberger and W.E. Thirring, Phys. Rev. 95, 1612 (1954).

17. M. Damashek and F.J. Gilman, Phys. Rev. D1, 1319 (1970).

18. G. Buschhorn et al., PAPER 16A submitted to this conference.

19. An expression of Σ in terms of helicity amplitudes can be found in B. Otto, DESY report DESY 67/8 (1967), unpublished.

20. CEA-Bubble-Chamber Collaboration, Phys. Rev. 146, 994 (1966).

21. Aachen-Berlin-Bonn-Hamburg-Heidelberg-München Collaboration, Phys. Rev. 175, 1669 (1968); and 188, 2060 (1969).

22. SLAC-Berkeley-Tufts Collaboration, Phys. Rev. Letters 24, 955 (1970); 24, 960 (1970); and PAPERS 20-23 submitted to this conference; K.C. Moffeit, thesis, University of California, Berkeley, UCRL 19890 (1970).

23. SLAC-Weizmann-Tel Aviv Collaboration, PAPER 245 submitted to this conference.

24. Aachen-Bonn-Hamburg-Heidelberg-München Collaboration, submitted to Nuclear Physics B: the quark model predictions have been computed according to H. Satz, Phys. Letters 25 B, 27 (1967).

25. G. Alexander et al., Phys. Rev. Letters 26, 340 (1971).

26. P.G.O. Freund, Nuovo Cimento 48, 541 (1967); see also V. Barger and D. Cline, Phys. Rev. Letters 24, 1313 (1970).

27. M. Davier et al., Phys. Rev. D1, 790 (1970); and PAPERS 99, 220 and 232 submitted to this conference.

28. Aachen-Hamburg-Heidelberg-München Collaboration, PAPER 283 submitted to this conference.

29. H. Blechschmidt et al., Nuovo Cimento 52A, 1348 (1967).

30. G. McClellan et al., Phys. Rev. Letters 22, 374 (1969),and Cornell Preprints CLNS-154 (1971) and CLNS-168 (1971).

31. H. Alvensleben et al., Phys. Rev. Letters 23, 1058 (1969).

32. F. Bulos et al., see data quoted by D.W.G.S. Leith in lectures presented to the Scottish Universities Summer School in Physics (1970), (unpublished).

33. R. Anderson et al., Phys. Rev. D1, 27 (1970).

34. G.E. Gladding, J.J. Russell, M.J. Tannenbaum, J.M. Weiss and G.B. Thomson, PAPER submitted to this conference.

35. G. Wolf, DESY report 70/64 and Springer Tracts in Modern Physics, Vol. 59, (1971), in press; see also Ref. 22.

36. See e. g., K. Schilling, P. Seyboth and G. Wolf, Nucl. Phys. B15, 397 (1970); (E) B18, 332 (1970), and references given therein.

37. This assumption was made in the strong absorption model, Y. Eisenberg, E.E. Ronat, A. Brandstetter, A. Levy, Phys. Letters 22, 217 (1966); 22, 223 (1966); see also G. Kramer, DESY report 67/32 (1967).

38. The OPE calculation is of the type described in G. Wolf, Phys. Rev. 182, 1538 (1969); Benecke-Dürr form factors (J. Benecke and H.P. Dürr, Nuovo Cimento 56, 269 (1968)) have been used.

39. L. Criegee et al., Phys. Rev. Letters 25, 1306 (1970).

40. G. Diambrini-Palazzi et al., Phys. Rev. Letters 25, 478 (1970).

41. I. Derado, G. Kronseder, P. Schlamp and P. Schacht, PAPER 122 submitted to this conference.

42. S.S. Eremian et al., PAPER submitted to this conference.

43. M. Ross and L. Stodolsky, Phys. Rev. 149, 1172 (1966)

44. P. Söding, Phys. Letters 19, 702 (1966); see also A. Krass, Phys. Rev. 159, 1496 (1967).

45. D.R. Yennie, private communication and T. Bauer, Phys. Rev. Letters 25, 485 (19670).

46. J. Pumplin, Phys. Rev. D2, 1859 (1970) .

47. F. Gutbrod, private communication.

48. D.R. Yennie, private communication.

49. See results quoted by J. Lefrancois at this conference.

50. G. Kramer and J.L. Uretsky, Phys. Rev. 181, 1918 (1969);
G. Kramer and H.R. Quinn, DESY report DESY 70/23 (1970);
G. Kramer, DESY report DESY 71/40 (1971).

51. H. Satz and K. Schilling, Nuovo Cimento 67A, 511 (1970);
P.D. Mannheim and U. Maor, Phys. Rev. D2, 2105 (1970).

52. G.E. Gladding, J.J. Russell, M.J. Tannenbaum, J.M. Weiss, G.B. Thomson, PAPER submitted to this conference.

53. See e. g., H. Joos, Proceedings of the Int. Conf. on Elementary Particles, Heidelberg, Germany (1967), (ed. by H. Filthuth) p. 349.

54. The elastic $\pi^{\pm}p$ cross sections were taken from the compilation of G. Giacomelli, CERN report, CERN-HERA-69-3 (1969).

55. Aachen-Bonn-Hamburg-Heidelberg-München Collaboration, PAPER submitted to this conference.

56. R. Anderson et al., SLAC report, SLAC-PUB-916 (1971).

57. H. Alvensleben et al., DESY report, DESY-71/37 (1971).

58. CEA Bubble Chamber Collaboration, Phys. Rev. 155, 1468 (1967).

59. SLAC-Berkeley-Tufts Collaboration, Phys. Rev. Letters 24, 1364 (1970); W.J. Podolsky, thesis, University of California, Lawrence Rad. Lab., UCRL-20128 (1971);and PAPER 21 submitted to this conference.

60. Bonn-Pisa Collaboration, Nucl. Phys. B24, 173 (1970).

61. H.J. Behrend et al., Phys. Rev. Letters 24, 1246 (1970).

62. Particle Data Group, Rev. Mod. Phys. 43, (1971), in press.

63. H. Harari, Proc. 4th Int. Symp. on Electron and Photon Interactions at High Energies, Liverpool, England 1969, (ed. by D.W. Braben), p. 107.

64. G. McClellan et al., Phys. Rev. Letters 26, 1597 (1971).

65. R. Anderson et al., private communication by B. Wiik.

66. B. Sakita and K.C. Wali, Phys. Rev. 139, B1355 (1965).

67. J.J. Sakurai, Ann. Phys. 11, 1 (1960); M. Gell-Mann and F. Zachariasen, Phys. Rev. 124, 953 (1961); Y. Nambu and J.J. Sakurai, Phys. Rev. Letters 8, 79 (1962); M. Gell-Mann, D. Sharp and W.G. Wagner, Phys. Rev. Letters 8, 261 (1962).

68. R.J. Oakes and J.J. Sakurai, Phys. Rev. Letters 19, 1266 (1967).

69. T. Das, V.S. Mathur and S. Okubo, Phys. Rev. Letters 19, 470 (1967).

70. M. Krammer, DESY report DESY 70/53 (1970).

71. See rapporteur talk by Prof. Gottfried at this conference.

72. Y. Eisenberg et al., PAPER 214 submitted to this conference.

73. J.A. Shapiro, Phys. Rev. 179, 1345 (1969).

74. C.R. Schumacher, I.M. Engle, Argonne report ANL/HEP 7032 (1971), and PAPER 281 submitted to this conference.

75. D.R. Earles et al., Phys. Rev. Letters 25, 1312 (1970).

76. J.H. Christenson et al., Phys. Rev. 25, 1523 (1970).

77. H. Alvensleben et al., Phys. Rev. Letters 26, 273 (1971).

78. F. Bulos, W. Busza, R. Giese and E.E. Kluge, Phys. Rev. Letters 26, 149 (1971).

79. P.H. Frampton, K. Schilling and C. Schmidt, CERN report CERN-TH 1347 (1971).

80. A. Benvenuti et al., Phys. Rev. Letters 27, 283 (1971).

81. Aachen-Bonn-Hamburg-Heidelberg-München Collaboration, private communication.

82. E. Rabe, Diplomarbeit, University of Hamburg.

83. U.N. Gribov, Yadernaya Fizika 5, 197 (1967); D.R.O. Morrison, Phys. Rev. 165, 1699 (1968).

84. Y. Eisenberg et al., Phys. Rev. Letters 25, 764 (1970).

85. M. Davier et al., PAPER 232 submitted to this conference.

86. Aachen-Berlin-Bonn-Hamburg-Heidelberg-München Collaboration, Phys. Letters 27B, 54 (1968).

87. Y. Eisenberg et al., Phys. Rev. Letters 22, 669 (1969).

88. A. Levy et al., PAPER 130 submitted to this conference.

89. See e. g. E.W. Anderson et al., Phys. Rev. Letters 25, 699 (1970) and references given therein.

90. G. Wolf, Nucl. Phys. B26, 317 (1971).

91. D. Fries, private communication.

92. See e. g., G. Ascoli et al., Phys. Rev. Letters 26, 929 (1971).

Table I Results on $\gamma p \to \gamma p$: The forward differential cross sections, $d\sigma^o/dt$, and the slope parameter A,B from a fit of $d\sigma/dt$ to the forms $d\sigma^o/dt \exp(At)$ and $d\sigma^o/dt \exp(At+Bt^2)$, respectively.

Experiment	E (GeV)	t Range (GeV^2)	$d\sigma^o/dt$ ($\mu b/GeV^2$)	A (GeV^{-2})	B (GeV^{-4})
DESY	2.2 - 2.7	0.1 - 0.4	1.26 ±0.13	5.2 ±0.5	-
Ref. 12	2.7 - 3.2	-	1.14 ±0.11	5.7 ±0.4	-
	3.2 - 3.7	-	1.24 ±0.11	6.2 ±0.4	-
	3.7 - 4.2	-	1.02 ±0.14	5.3 ±0.5	-
	4.0 - 5.2	0.06 - 0.4	0.92 ±0.09	6.0 ±0.4	-
	5.0 - 6.2	-	0.76 ±0.06	5.5 ±0.3	-
	6.0 - 7.0	-	0.76 ±0.07	5.9 ±0.4	-
SLAC	8	0.014 - 0.17	0.82 ±0.04	7.7 ±0.5	-
		0.014 - 0.8	0.79 ±0.03	7.6 ±0.4	2.3 ±0.5
Refs. 13,14	16	0.014 - 0.17	0.69 ±0.03	7.9 ±0.5	-
		0.014 - 1.1	0.64 ±0.02	7.3 ±0.3	1.7 ±0.3

Table II Experiments on ρ^o photoproduction, $\gamma p \to \rho^o p$

Experiment	Technique	Beam	Photon Energy (GeV)	Particles Detected	Number of Rho Events Above 2 GeV	Remarks
CEA[20] Collaboration	HBC	bremsstrahlung	< 6	p, π^+, π^-	500	
DESY[21] (ABBHHM)	HBC	bremsstrahlung	<6	p, π^+, π^-	2000	
SLAC-Weizmann-Tel Aviv[23]	HBC	quasi monochromatic	2-8	p, π^+, π^-	3000	final state $p\pi^+\pi^-$ is 3 (or 4) constrained; background from other reactions is negligible; no data below $\|t\| = 0.02$ GeV^2
SLAC-Berkeley-Tufts[22]	HBC	Laser beam, lin.pol. approx.monochromatic	2.8;4.7 9.3	p, π^+, π^-	6000	
SLAC[27]	streamer-chamber	bremsstrahlung	2-16	p, π^+, π^-	1700	
DESY (AHHM)[28]	streamer-chamber	tagged γ beam	3-6	p, π^+, π^-	2000	
DESY[29] (Blech-schmidt et al.)	counter set up	tagged γ beam	3-5	π^+, π^-	350	1 constraint, $\sin^2\Theta$ assumed
Cornell[30]	counter set up	bremsstrahlung	4-8.5	π^+, π^-	many	inelast.BG subtracted at 8.5 GeV; 0 constraint, $\sin^2\Theta$ assumed
DESY-MIT[31]	counter set up	bremsstrahlung	3-7	π^+, π^-	10^5	inelast.BG not excluded; $\sin^2\Theta$ assumed
SLAC[32] (Bulos et al.)	counter set up	quasi monochromatic	9	π^+, π^-	1400	1 constraint
SLAC[33] (Anderson et al.)	counter set up	bremsstrahlung	6-18	p and missing mass	many	1 constraint, missing mass technique; resolution not good enough to separate ρ and ω production
CEA[34] (Gladding et al.)	counter set up	tagged γ beam	3-4.7	p and missing mass		ρ and ω separated

Table III $\gamma p \to \rho^{o} p$: Contribution from unnatural parity exchange. (Data from Ref. 22).

Photon energy	2.8 GeV	4.7 GeV	9.3 GeV
t-range	$0.02 < \|t\| < 1$ GeV^2	$0.02 < \|t\| < 1$ GeV^2	$0.05 < \|t\| < 0.8$ GeV^2
P_σ	0.94 ±0.06	1.02 ±0.05	1.01 ±0.09
σ^U/σ^{tot}: measured	3.1 ±3.1 %	- 1.1 ±2.8 %	- 0.5 ±4.5 %
OPE prediction[38] with $\Gamma_{\rho\pi\gamma}$ = 0.13 MeV	2 %	0.8 %	0.2 %

Table IV Results on $\gamma p \to \rho^o p$: The forward differential cross section, $d\sigma^o/dt$ and the slope parameter A from a fit of $d\sigma/dt$ to $d\sigma^o/dt \exp(At)$.

Experiment	E_γ (GeV)	t Range	Fit Method	$d\sigma^o/dt$ ($\mu b/GeV^2$)	A (GeV^{-2})
ABBHHM (DESY-HBC) Ref. 21	2.5 - 3.5	0.05 - 0.5	$(M_\rho/M_{+-})^4$	147 ±13	6.9 ±0.4
	3.5 - 4.5			149 ±19	8.1 ±0.7
	4.5 - 5.8			130 ±16	7.9 ±0.7
SLAC Bulos et al. Ref. 32	9.0	0.0 - 0.15	equiv. to $(M_\rho/M_{+-})^4$ Söding	122 ±12	
				104 ±11	9.5
SBT Ref. 22	2.8	0.02 - 0.4	$\Pi(t)$ $(M_\rho/M_{+-})^{n(t)}$ Söding	144 ±12	7.5 ±0.6
				138 ± 8	6.6 ±0.3
				104 ± 6	5.4 ±0.3
			Pole method, Γ_ρ=153 MeV	135 ±13	6.3 ±0.4
	4.7	0.02 - 0.4	$\Pi(t)$ $(M_\rho/M_{+-})^{n(t)}$ Söding	109 ± 8	7.6 ±0.5
				114 ± 6	7.2 ±0.3
				94 ± 6	5.9 ±0.3
			Pole method, Γ_ρ=153 MeV	102 ±10	6.0 ±0.3
	9.3	0.02 - 0.5	$\Pi(t)$ $(M_\rho/M_{+-})^{n(t)}$ Söding	79 ± 8	7.1 ±0.6
				90 ± 5	7.1 ±0.3
				79 ± 4	6.6 ±0.3
			Pole method, Γ_ρ=153 MeV	82 ± 8	6.3 ±0.5
Cornell* Ref. 30	3.9		Söding	169 ±14	
	4.1			150 ±14	
	4.6			140 ±13	
	5.6			134 ± 6	
	5.9			126 ± 9	
	6.5			109 ± 9	
	6.9			113 ±10	
	7.4			108 ± 4.5	
	8.5	0.0 - 0.5		103 ± 6	8.1 ±0.4
DESY-MIT** Ref. 31	3.0		$(M_\rho/M_{+-})^4$	156.5±11.5	
	3.6			132 $^{+22}_{-26}$	
	4.2			127 ± 8	
	4.8			138 ± 5	
	5.4			125 ± 5	
	6.0			117 ± 3	
	6.4		$(M_\rho/M_{+-})^4$ Söding	113 ± 5	
				119 ± 6	
	6.5		$(M_\rho/M_{+-})^4$	117 $^{+4}_{-5}$	

* In this experiment not the full ρ cross section, $d\sigma/dt$, but the quantity $2(\rho^o_{11} + \rho^o_{1-1})\, d\sigma/dt$ is measured (see text) and the numbers given here apply to this quantity.

** The data have not been corrected for contamination by inelastic ρ^o production.

Experiment	E_γ (GeV)	t Range	Fit Method	$d\sigma^o/dt$ ($\mu b/GeV^2$)	A (GeV^{-2})
SLAC-Weizmann-Tel-Aviv Ref. 23	2.0 - 2.5	0.06 - 0.4	Central rho, Söding	134 ±20	6.4 ±0.8
	2.5 - 3.0			177 ±26	8.8 ±1.1
	3.0 - 3.7			124 ±20	7.5 ±1.2
	3.7 - 4.7			101 ±12	6.5 ±0.5
	4.7 - 5.8			132 ±17	7.7 ±0.6
	6.8 - 8.2			98 ±15	7.1 ±0.6

Table V $\gamma p \rightarrow \omega p$: Cross sections and momentum transfer dependence for $0.02 < |t| < 0.4$ GeV^2 (2.8, 4.7 GeV) and $0.02 < |t| < 0.5$ GeV^2 (9.3 GeV) assuming $d\sigma/dt = d\sigma^o/dt \exp(At)$ for all events, and for the contributions from natural parity exchange in the t-channel. (Data from Ref. 59).

E_γ (GeV)	σ_{total} (μb)	$d\sigma^o/dt$ (μb/GeV^2)	A (GeV^{-2})	$\sigma^N(\|t\| < 1$ GeV$^2)$ (μb)	$\sigma^U(\|t\| < 1$ GeV$^2)$ (μb)	$d\sigma^{N^o}/dt$ (μb/GeV^2)	A_N (GeV^{-2})
2.8	5.3 ±0.5	31.7 ±4.3	6.4 ±0.7	2.3 ±0.4	2.6 ±0.4	12.4 ±4.2	5.9 ±2.1
4.7	3.0 ±0.3	23.4 ±3.9	8.2 ±0.9	1.7 ±0.3	1.2 ±0.25	13.9 ±3.8	7.9 ±1.7
9.3	1.8 ±0.2	12.7 ±2.4	7.3 ±1.2	1.7 ±0.3	0.1 ±0.3	12.0 ±2.7	7.2 ±1.3

Table VI VDM predictions for the ratio of the forward cross sections for vector meson photoproduction and comparison with experiment, according to Eqs. (25,26); η_ρ and η_ω are assumed to be the same as for Compton scattering (see Fig. 4); $\eta_\phi = 0$. For $d\sigma^o/dt(\rho^o p)$ averages of the data of Fig. 29 are used.

E_γ (GeV)	$d\sigma^o/dt(\rho^o p) : d\sigma^o/dt(\omega\rho) : d\sigma^o/dt(\phi\rho)$	
	Experiment	Theory
2.8	9 : (0.78 ±0.28) [59]	9 : 1 : 0.27
4.7	9 : (1.0 ±0.28) [59]	9 : 1 : 0.35
5.7	9 : (1.1 ±0.25) [60]	9 : 1 : 0.38
6.8	9 : (0.93 ±0.15) [61]	9 : 1 : 0.40
9.3	9 : (1.14 ±0.3)[59] : (0.27 ±0.04)[30]	9 : 1 : 0.44

Table VII γ-V Coupling constants

	$d\sigma^o/dt(\gamma p \to Vp)$ + Quark Model	$d\sigma^o/dt(\gamma p \to Vp)$ + $\sigma_T(\gamma p)$	$d\sigma/dt(\gamma p \to Vp)$ + $d\sigma/dt(\gamma p \to \gamma p)$	$\gamma d \to Vd$ [56]	Orsay[49] Storage Ring
$\gamma_\rho^2/4\pi$	0.65 ±0.1	0.35 ±0.05	0.2 - 0.3	0.6 - 0.7	0.64 ±0.05
$\gamma_\omega^2/4\pi$	6 ±1.5				4.8 ±0.5
$\gamma_\phi^2/4\pi$	5.1 ±0.6				2.8 ±0.2

Figure Captions

Fig. 1 a) Total γp cross section below 4 GeV; data from Ref. 5.

b) Total γp and γd cross sections above 1 GeV; data from Refs. 3(ϕ), 4(ϕ), 6(ϕ) and 7(ϕ).

c) Total γd cross section below 4 GeV; data from Ref. 5.

Fig. 2 The total γn cross section and the sum and difference of $\sigma_T(\gamma p)$ and $\sigma_T(\gamma n)$; data from Refs. 3, 4; Fig. taken from Ref. 4.

Fig. 3 Differential cross sections, $d\sigma/dt$, for Compton scattering for energies between 2.45 and 17 GeV. Data from Refs. 12(ϕ), 13(ϕ) and 14(ϕ).

Fig. 4 Ratio of the real to imaginary part for the amplitude f_1 for Compton scattering on protons. Fig. taken from Ref. 3b.

Fig. 5 Extrapolated forward cross section of proton Compton scattering as a function of the photon energy E_γ. The curves correspond to the optical point with/without Re f_1 taken into account. Fig. taken from Ref. 12.

Fig. 6 Asymmetry Σ of Compton scattering on protons, vs. four momentum transfer. Solid lines are the predictions of the spin independent model (SIM), s-channel helicity conservation (SHC, Σ = 0) and 0^+ exchange in the t-channel. Fig. taken from Ref. 18.

Fig. 7 Total and topological γp cross sections versus the square of the center of mass energy, s. Fig. taken from Ref. 22.

Fig. 8 Cross sections for $\gamma p \to p\pi^+\pi^-$, pk^+k^- and $p\bar{p}p$. Data taken from Refs. 21, 22 and 23. Fig. taken from Ref. 22.

Fig. 9 Cross sections for various γp reactions. Data taken from Refs. 21 and 23. Fig. taken from Ref. 23.

Fig. 10 Cross sections for various γd reactions. Data taken from Refs. 24, 25. Fig. taken from Ref. 24. Also shown are the predictions of the quark model of Satz.

Fig. 11 The fraction of inelastically produced $\pi^+\pi^-$ pairs for an average $\pi^+\pi^-$ momentum of 8.3 GeV, shown as a function of t for various $\pi^+\pi^-$ masses. Fig. taken from Ref. 30.

Fig. 12 The Gottfried-Jackson coordinate system for the analysis of the ρ^o decay angular distribution.

Fig. 13 Reaction $\gamma p \to \rho^o p$ at 4.7 GeV. Rho decay angular distribution in the helicity system without background subtraction. The curves are proportional to $\sin^2\theta_H$ and $(1 + P_\gamma \cos 2\psi_H)$. Fig. taken from Ref. 22.

Fig. 14 Reaction $\gamma p \to \rho^o p$ at 4.7 GeV. The spin density matrix elements in the Gottfried-Jackson, helicity and Adair systems. Fig. taken from Ref. 22.

Fig. 15 The density matrix element $\rho^o_{11} = \frac{1}{2}(1 - \rho^o_{oo})$ in the helicity and Gottfried-Jackson systems versus t for different photon energies. Fig. taken from Ref. 27.

Fig. 16 Illustration of the spin dependence of some production mechanisms for $\gamma p \to \rho^o p$ (namely 0^+ exchange, s-channel helicity conservation, spin independence in the CMS) which lead to a simple behaviour of the rho density matrix in either the Gottfried-Jackson (G-J), the helicity (H) or the Adair (A) frame; the photon is assumed to be circularly polarized; σ_z^γ, σ_z^γ indicate the directions along which the spins of γ and ρ have components equal to one.

Fig. 17 Reaction $\gamma p \to \rho^o p$. The parity asymmetry, P_σ, as a function of t at 2.8, 4.7 and 9.3 GeV. Data taken from Ref. 22.

Fig. 18 Reaction $\gamma p \to \rho^o p$. Energy dependence of the asymmetry Σ for $|t| < 0.4$ GeV^2. Data taken from Refs. 22, 39 and 40.

Fig. 19 Reaction $\gamma p \to \rho^o p$. The size of the s-channel helicity flip terms calculated from the data of Ref. 22 as a function of t for 2.8, 4.7 and 9.3 GeV.

Fig. 20 Reaction $\gamma p \to p\pi^+\pi^-$. The $\pi^+\pi^-$ mass spectra for different photon energy intervals. Fig. taken from Ref. 23.

Fig. 21 Chew-low plots for the reaction $\gamma p \to p\pi^+\pi^-$ at 2.8 and 4.7 GeV. Fig. taken from Ref. 22.

Fig. 22 $\pi^+\pi^-$ mass distributions for events of the reaction $\gamma p \to p\pi^+\pi^-$. The s-channel photon-helicity conserving p-wave intensity Π (see text) is shown by the points $\blacklozenge$. The curves give the results of a maximum likelihood fit using for the ρ^o the parametrization $(M_\rho/M_{+-})^{n(t)}$(---) and the Söding model (——). Fig. taken from Ref. 22.

Fig. 23 Reaction $\gamma p \to p\pi^+\pi^-$. Fitted values for n(t) using the parametrization $(M_\rho/M_{+-})^{n(t)}$. Data taken from Ref. 22($\blacklozenge$) and Ref. 28($\downarrow$).

Fig. 24 Diagrams for the production of $\pi^+\pi^-$ pairs in the reaction $\gamma p \to p\pi^+\pi^-$:

(a) ρ^o production

(b), (c) Drell processes

(d), (e) Rescattering terms

Fig. 25 Reaction $\gamma p \to p\pi^+\pi^-$. The dipion moments $Y_1^0(\theta)$, $Y_2^0(\theta)$, Re $Y_2^2(\theta,\psi)$, $Y_3^0(\theta)$, $Y_4^0(\theta)$, $Y_6^0(\theta)$ in the helicity frame as a function of $M_{\pi^+\pi^-}$ for $0.02 < |t| < 0.4$ GeV^2 at 2.8 and 4.7 GeV. The curves are obtained from the Söding model. Fig. taken from Ref. 22.

Fig. 26 The fitted ratio of the ρ^0 to Drell cross sections, $\sigma_\rho(t)/\sigma_{Drell}(t)$. The solid (dashed) curves show the predictions of the Söding model with the Ferrari-Selleri (Benecke-Dürr) form factor. Fig. taken from Ref. 22.

Fig. 27 The contributions of rho, Drell, interference terms, phase space and Δ^{++} to the $\pi^+\pi^-$ mass spectrum from a Söding-model fit to the channel $\gamma p \to p\pi^+\pi^-$. Fig. taken from Ref. 22.

Fig. 28 Comparison of differential cross sections for ρ^0 production from different experiments. Data taken from Refs. 21, 22, 30, 32 and 33.

Fig. 29 Energy dependence of the forward ρ^0 cross section. The data are those listed in Table IV. The curve shows the results of two VDM calculations:

(i) Using the measured total γp cross sections as input together with $\gamma_\rho^2/4\pi = 0.35$ (Eq.(29)).

(ii) Starting from the total $\rho^0 p$ cross section predicted by the quark model and using a value of $\gamma_\rho^2/4\pi = 0.65$ in Eq. (28).

Fig. 30 Energy dependence of the total cross section for $\gamma p \to \rho^0 p$. The curve is based on VDM and on the quark model prediction for $\sigma(\rho^0 p \to \rho^0 p)$, Eq. (22). For $\gamma_\rho^2/4\pi$ a value of 0.7 has been used. The data come from Refs. 21, 22, 23 and 27.

Fig. 31 Differential cross sections for the reaction $\gamma d \to \rho^o d$. The open (full) points were obtained with the Söding model (with the factor $(M_{+-}/M_\rho)^{n(t)}$). The curves are explained in the text. Fig. taken from Ref. 55.

Fig. 32 Total cross section for $\gamma n \to \rho^- p$ for $|t| < 1.1$ GeV^2. No corrections for deuteron effects are included. The curve shows the prediction for pion exchange (Ref. 38) with $\Gamma_{\rho^-\pi\gamma} = 0.13$ MeV. Fig. taken from Ref. 55.

Fig. 33 The mass spectrum of $\pi^+\pi^-$ pairs of 6.4 GeV momentum produced with a 7.4 GeV bremsstrahlung beam on hydrogen. The square of the $\pi^+\pi^-$ transverse momentum is $p_T^2 = 0.001$ GeV^2. The solid curve includes the ω-ρ interference term, the dashed curve does not. Fig. taken from Ref. 57.

Fig. 34 Reaction $\gamma p \to p\pi^+\pi^-\pi^o$ at 9.3 GeV. The $\pi^+\pi^-\pi^o$ mass spectrum. Fig. taken from Ref. 59.

Fig. 35 The total cross section for $\gamma p \to \omega p$. Data taken from Refs. 21, 23 and 59. Fig. taken from Ref. 59. Also shown are the cross sections (Ref. 59) for natural (σ^N) and unnatural parity exchange (σ^U).

Fig. 36 Decay angular distributions and P_σ for ω events at 2.8, 4.7 and 9.3 GeV in the helicity system. The curves give the decay distributions as calculated from the fitted density matrix elements. Fig. taken from Ref. 59.

Fig. 37 Differential cross sections for $\gamma p \to \phi p$. Data taken from Refs. 21, 30, 31 and 33.

Fig. 38 $\gamma p \to \gamma p$: Ratio of the VDM prediction to the measured Compton cross sections. Curves correspond to different analysis methods used to obtain the ρ^o contribution. Typical errors of the ratio are shown. Fig. taken from Ref. 12.

Fig. 39 Mass spectrum for $\pi^+\pi^-$ pairs of 6.2 GeV momentum produced with a 7.4 GeV bremsstrahlung beam at small transverse momenta. Fig. taken from Ref. 77.

Fig. 40 a) Compilation of $\pi^+\pi^\pm\pi^-$ mass spectra from the reactions $\gamma p \to n\pi^+\pi^+\pi^-$ and $\gamma n \to p\pi^+\pi^-\pi^-$. Data taken from Refs. 23, 59 and 81.

b) Cross sections for A_2 production. Curve shows OPE prediction for $\Gamma_{A_2\pi\gamma} = 0.5$ MeV [38].

Fig. 41 Reaction $\gamma p \to p\pi^+\pi^- + (m\pi^o)$, $m \geq 2$. Compilation of $\pi^+\pi^-$ $(m\pi^o)$ mass spectra for the cuts indicated in the Fig. Data taken from Refs. 59 and 82.

Fig. 42 Reaction $\gamma p \to p\pi^+\pi^-\pi^o$ at 2.8 and 4.7 GeV; $M_{p\pi^+}$ versus $M_{\pi^-\pi^o}$ distribution. Fig. taken from Ref. 59.

Fig. 43 Cross section for $\gamma p \to \rho^-\Delta^{++}$. Data taken from Ref. 23 and 59. The curve shows the one-pion exchange prediction (Ref. 38) for $\Gamma_{\rho^-\pi\gamma} = 0.12$ MeV.

Fig. 44 Reaction $\gamma n \to p\pi^+\pi^-\pi^-\pi^o$: at 4.3 GeV.

a) $\pi^+\pi^-\pi^o$ mass distribution.

b) $p\pi^-$ mass distribution. The shaded histogram is for $p\pi_2^-$ combinations with $M_{\pi^+\pi_1^-\pi^o}$ being in the ω mass region (0.75 - 0.85 GeV).

Reaction $\gamma n \to p\pi^+\pi^-\pi^-$:

c) $\pi^+\pi^-$ mass distribution.

d) $p\pi^-$ mass distribution.

Fig. taken from Ref. 84.

Fig. 45 Reaction $\gamma p \to p\pi^+\pi^+\pi^-\pi^-$ between 8.5 and 18 GeV. The $\rho^0\pi^\pm$ mass distribution. Fig. taken from Ref. 85.

Fig. 46 Reaction $\gamma p \to p\pi^+\pi^+\pi^-\pi^-\pi^0$ at 2.8 and 4.7 GeV. The $\pi^+\pi^-\pi^0$ mass distributions. Fig. taken from Ref. 59.

Fig. 47 Diagrams considered for inelastic diffractive ρ^0 production:
(a) diffractive isobar production.
(b), (c) double peripheral scattering.
Fig. taken from Ref. 90.

Fig. 48 Cross sections for inelastic diffractive ρ^0 production on protons via isobar production (diagram (a) of Fig. 47); and double peripheral scattering (diagrams (b) and (c) of Fig. 47). The curves labeled "total" show the incoherent sum of all contributions: (a) and (b) differential cross sections at E_γ = 5 and 10 GeV; (c) integrated cross sections as a function of the photon energy E_γ. Fig. taken from Ref. 90.

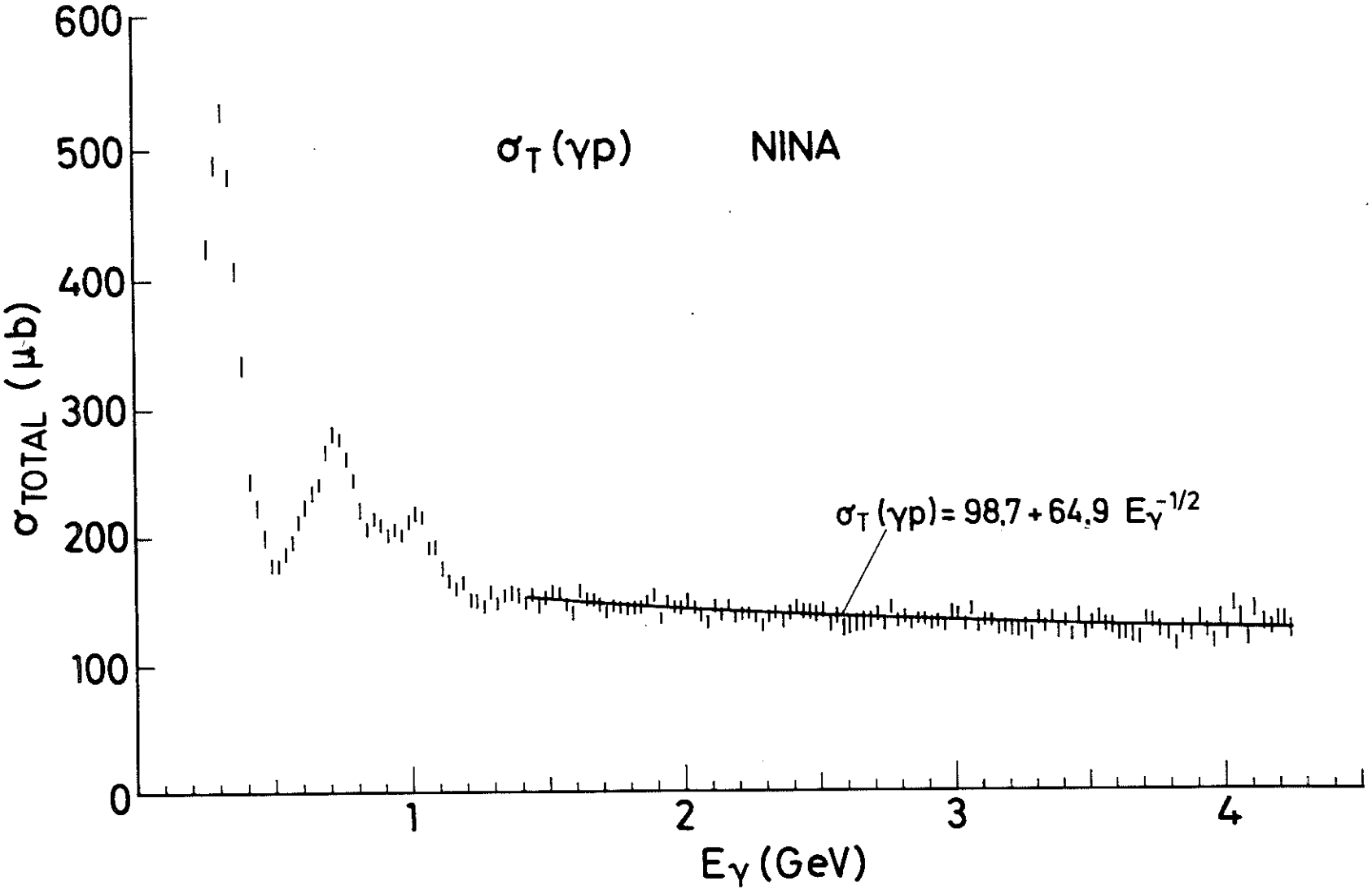
600
500
400
300
200
100
0
σ_{TOTAL} (μb)
σ_T (γp)
NINA
σ_T (γp) = 98,7 + 64,9 $E_\gamma^{-1/2}$
1
2
3
4
E_γ (GeV)

Fig. 1a

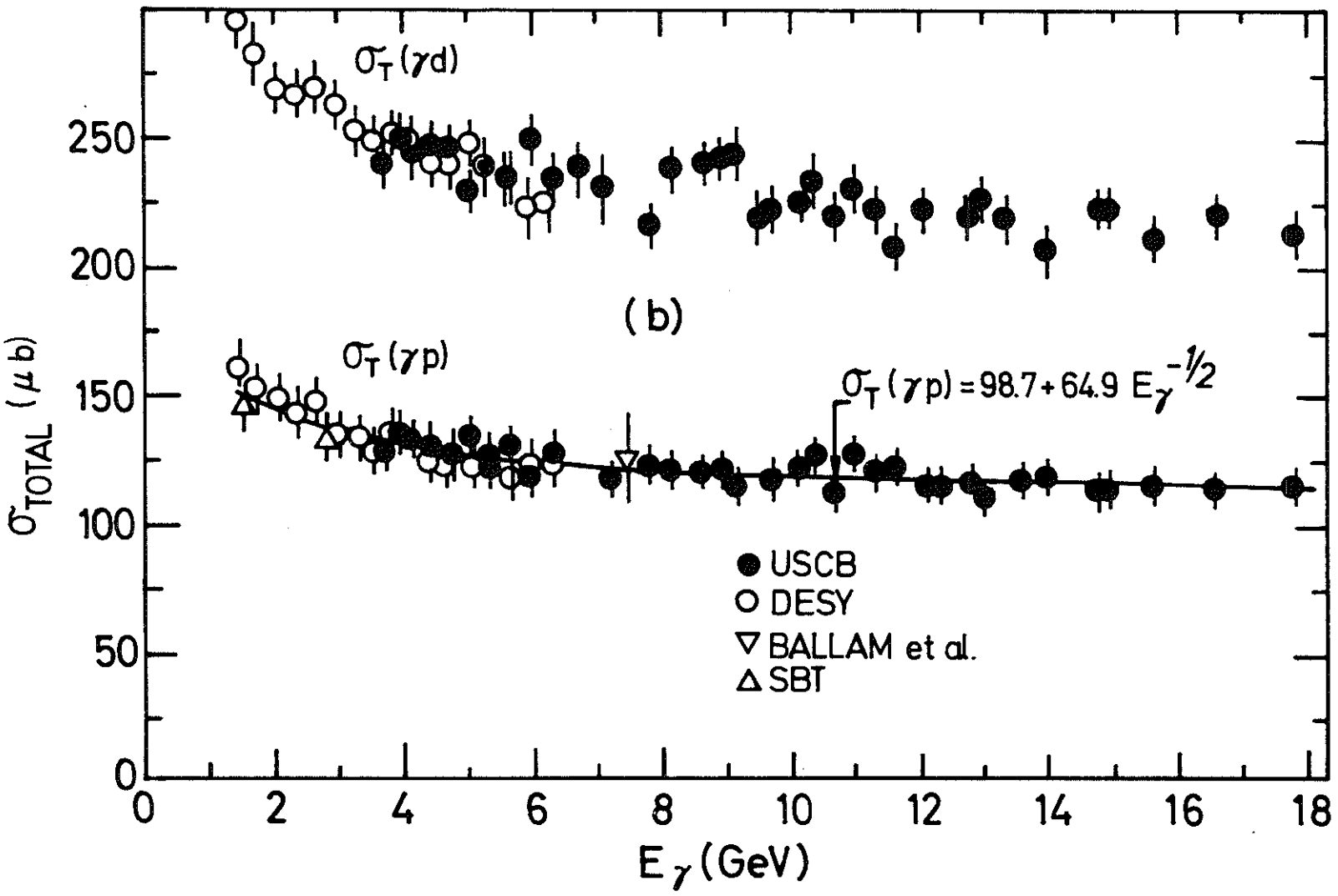
$\sigma_T(\gamma d)$
(b)
$\sigma_T(\gamma p)$
$\sigma_T(\gamma p) = 98.7 + 64.9\ E_\gamma^{-1/2}$
● USCB
○ DESY
▽ BALLAM et al.
△ SBT
σ_{TOTAL} (μb)
E_γ (GeV)
0
50
100
150
200
250
0
2
4
6
8
10
12
14
16
18

Fig. 1b

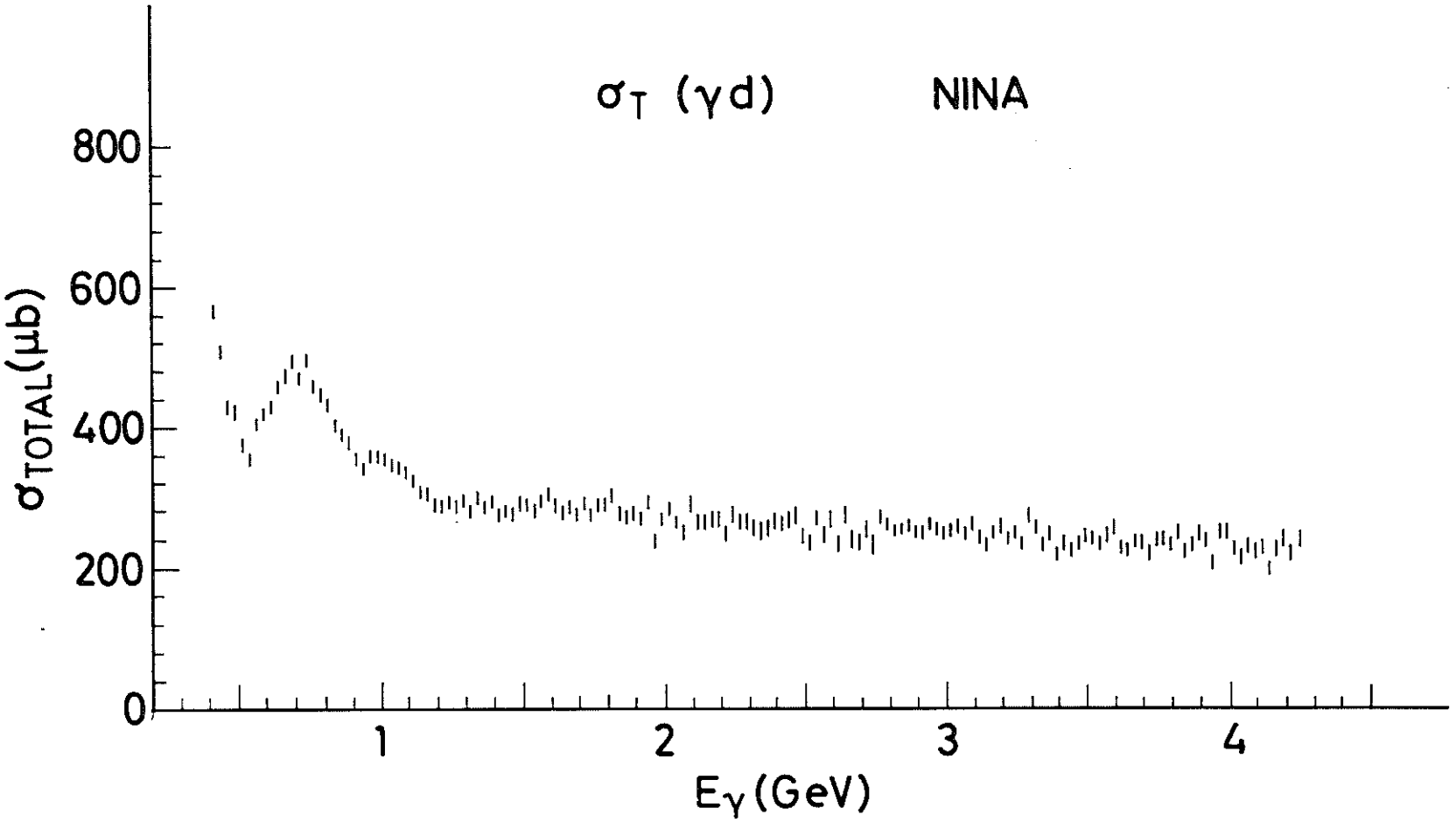
σ_T (γ d)
NINA
800
600
400
200
0
σ_{TOTAL}(μb)
1
2
3
4
E_γ (GeV)

Fig. 1c

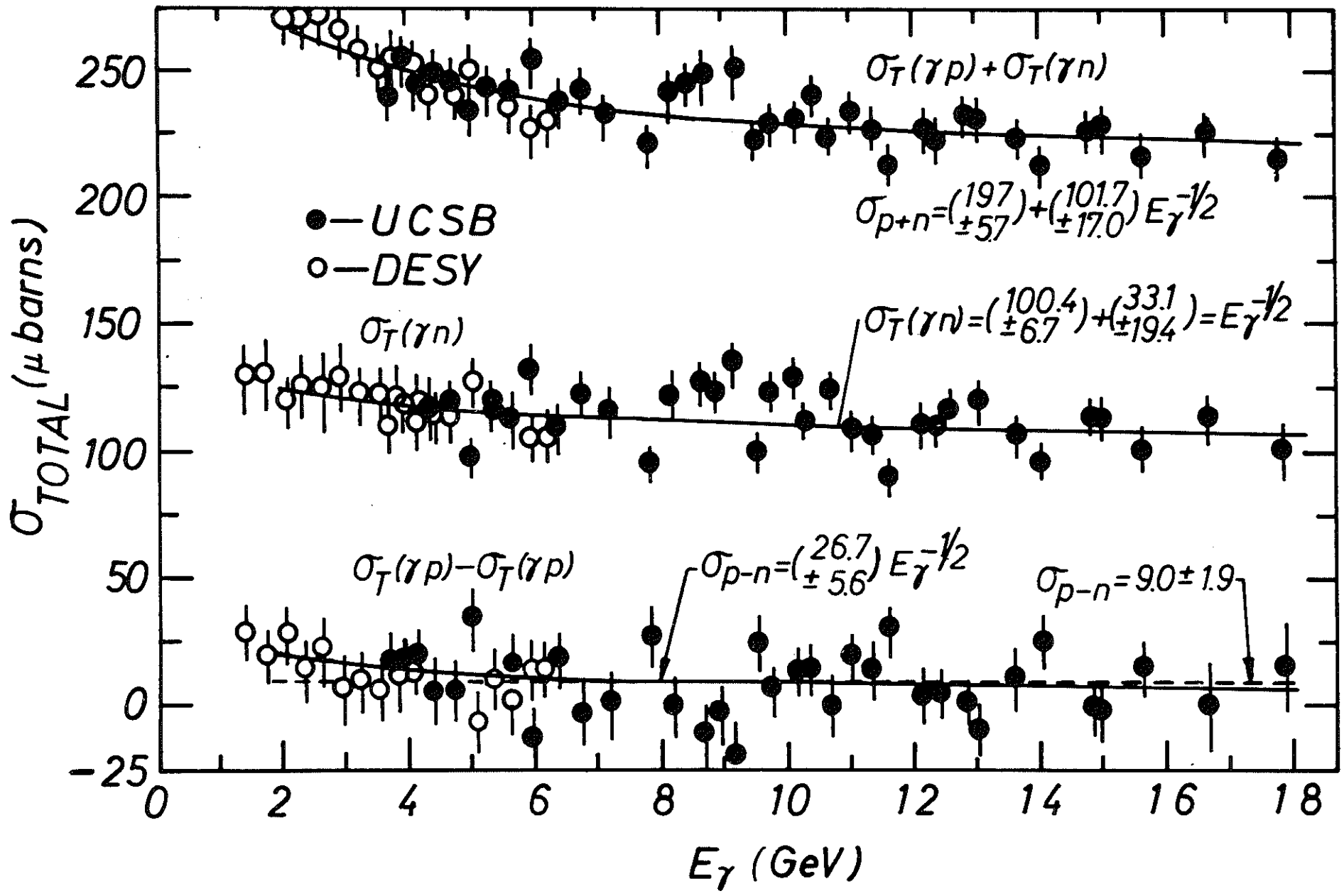
250
200
150
100
50
0
−25
0
2
4
6
8
10
12
14
16
18
σ_{TOTAL} (μ barns)
E_γ (GeV)
●—UCSB
○—DESY
$\sigma_T(\gamma p)+\sigma_T(\gamma n)$
$\sigma_{p+n}=(^{197}_{\pm 5.7})+(^{101.7}_{\pm 17.0})E_\gamma^{-1/2}$
$\sigma_T(\gamma n)$
$\sigma_T(\gamma n)=(^{100.4}_{\pm 6.7})+(^{33.1}_{\pm 19.4})=E_\gamma^{-1/2}$
$\sigma_T(\gamma p)-\sigma_T(\gamma p)$
$\sigma_{p-n}=(^{26.7}_{\pm 5.6})E_\gamma^{-1/2}$
$\sigma_{p-n}=9.0\pm 1.9$

Fig. 2

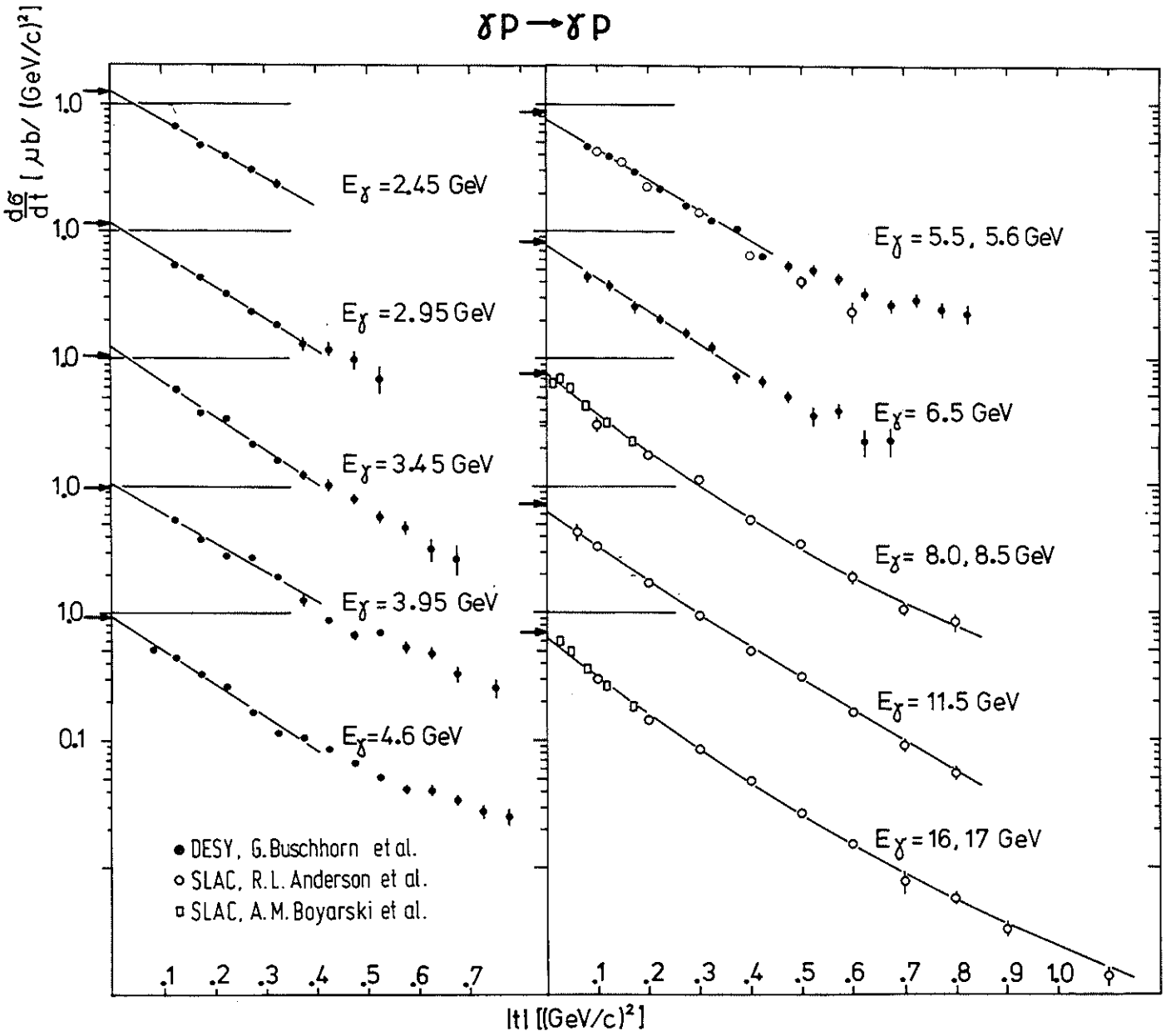
γp→γp
dσ/dt [μb/(GeV/c)²]
1.0
1.0
1.0
1.0
0.1
Eγ =2.45 GeV
Eγ =2.95 GeV
Eγ =3.45 GeV
Eγ =3.95 GeV
Eγ=4.6 GeV
Eγ = 5.5, 5.6 GeV
Eγ= 6.5 GeV
Eγ= 8.0, 8.5 GeV
Eγ= 11.5 GeV
Eγ = 16, 17 GeV
● DESY, G.Buschhorn et al.
○ SLAC, R.L. Anderson et al.
▫ SLAC, A.M. Boyarski et al.
.1 .2 .3 .4 .5 .6 .7
.1 .2 .3 .4 .5 .6 .7 .8 .9 1.0
|t| [(GeV/c)²]

Fig. 3

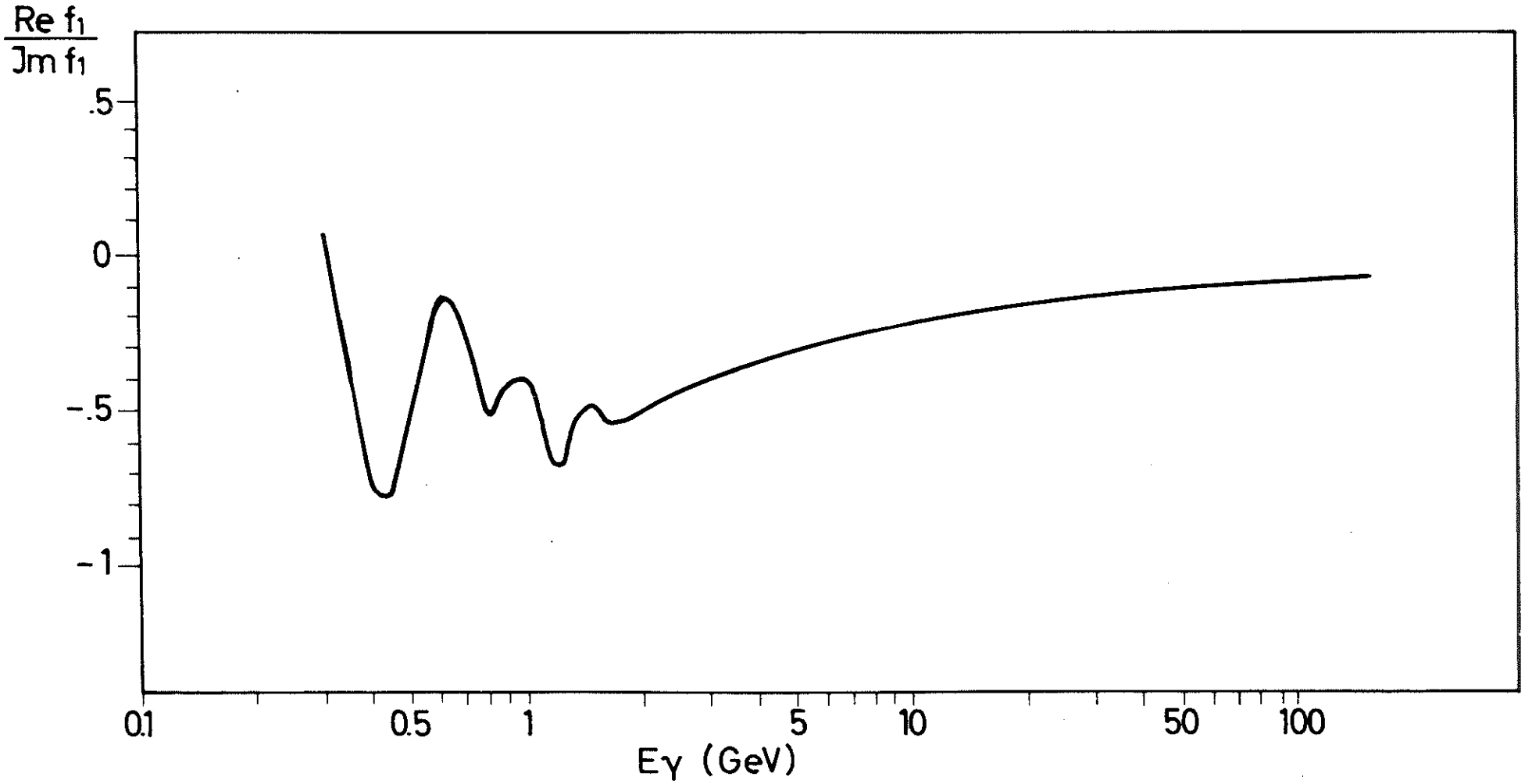

Fig. 4

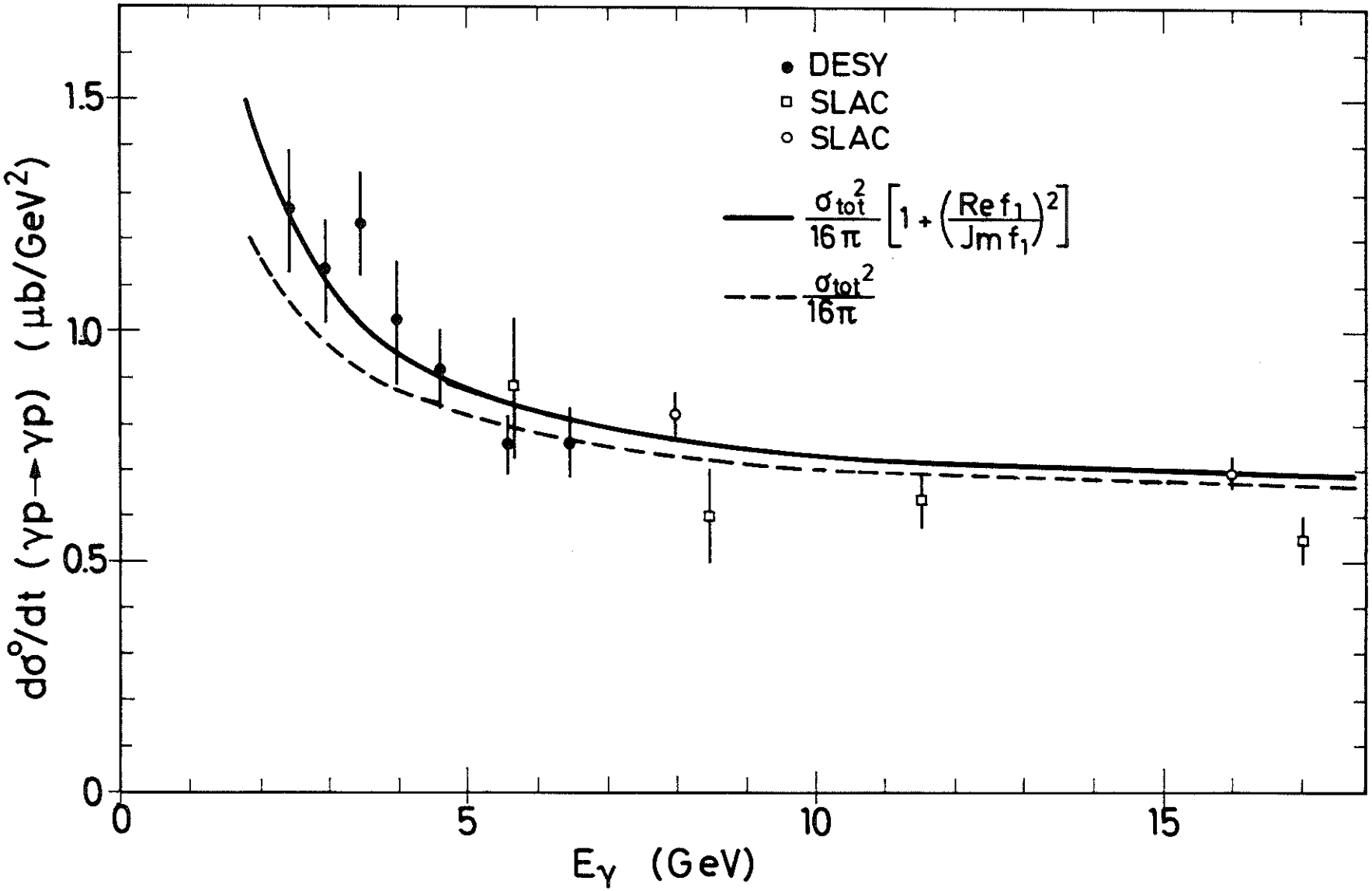
DESY
SLAC
SLAC
$\frac{\sigma_{tot}^2}{16\pi}\left[1+\left(\frac{Re\,f_1}{Im\,f_1}\right)^2\right]$
$\frac{\sigma_{tot}^2}{16\pi}$
$d\sigma^0/dt\ (\gamma p \to \gamma p)\ (\mu b/GeV^2)$
E_γ (GeV)
0
0.5
1.0
1.5
5
10
15

Fig. 5

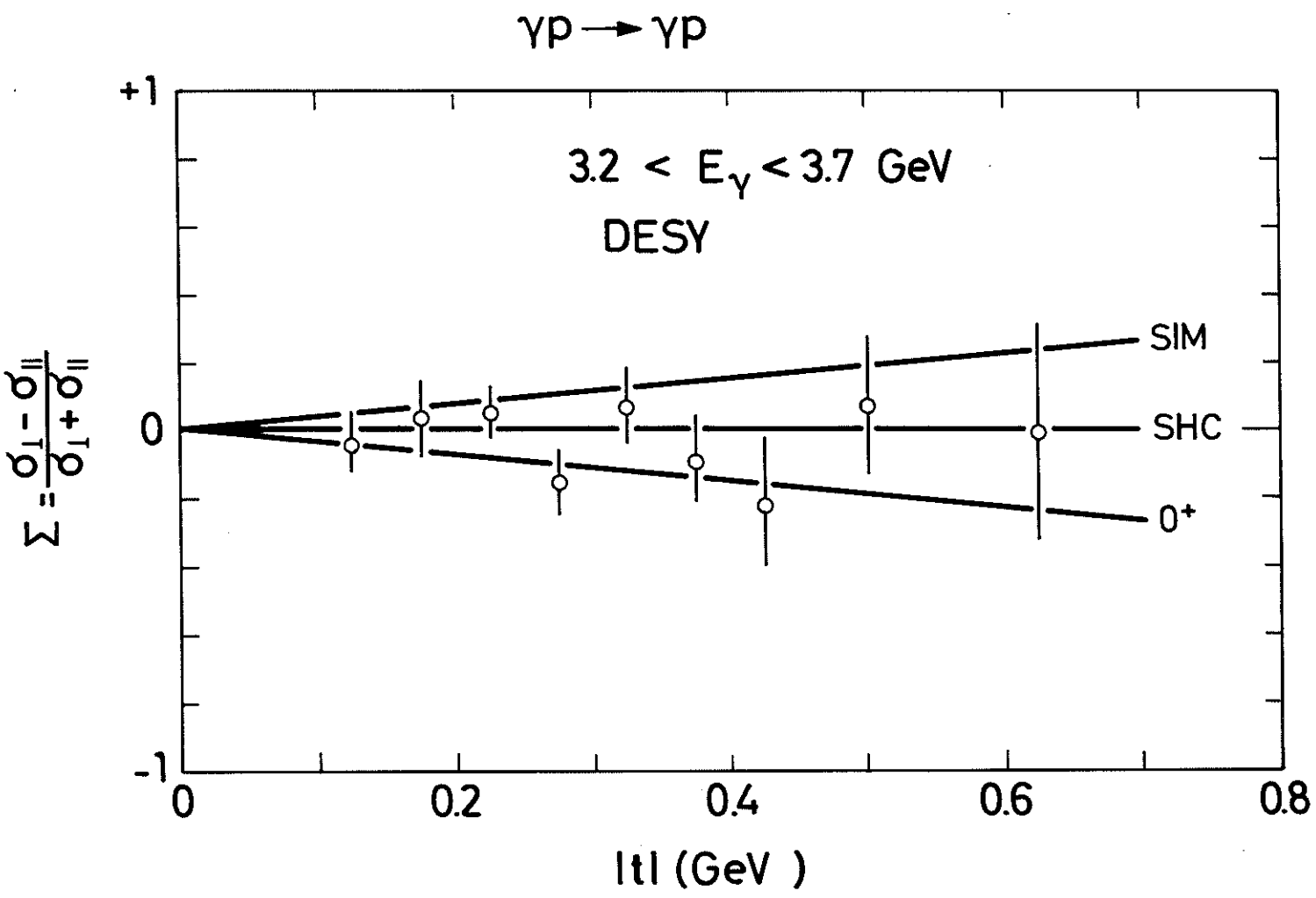

Fig. 6

SBT-Collaboration

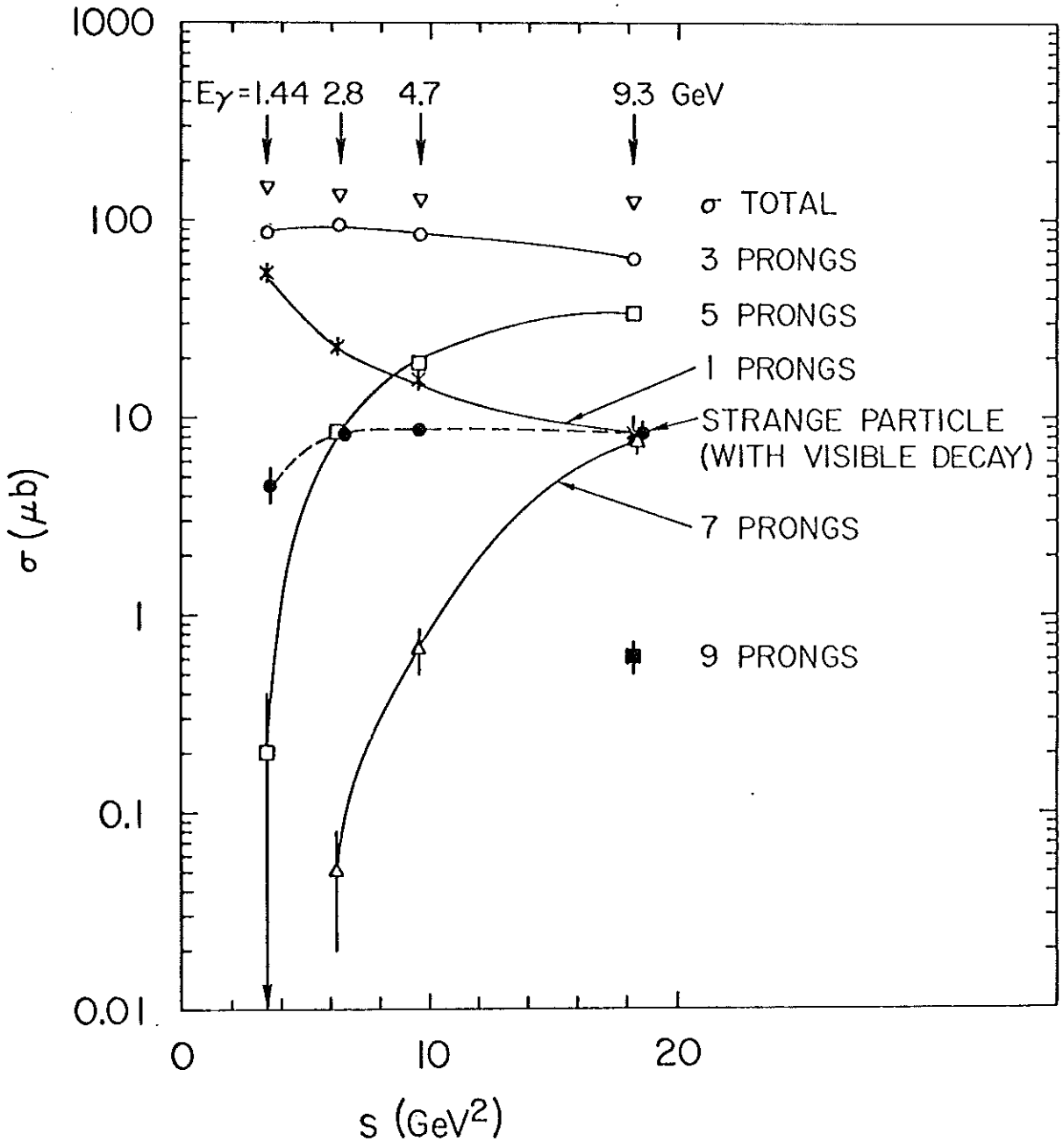

Fig. 7

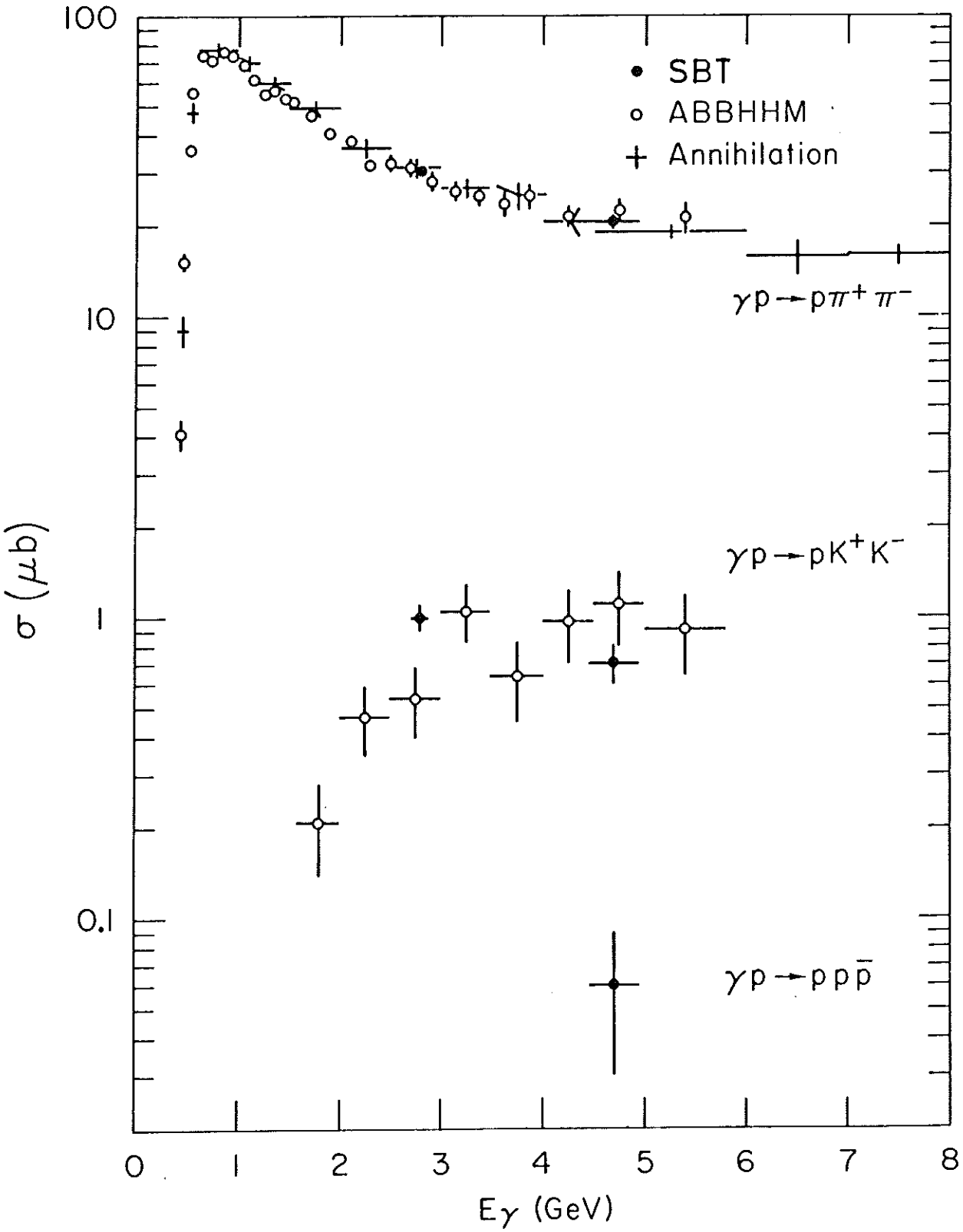
100
10
1
0.1
σ (μb)
SBT
ABBHHM
Annihilation
γp → pπ+ π−
γp → pK+K−
γp → pp p̄
0
1
2
3
4
5
6
7
8
Eγ (GeV)

Fig.8

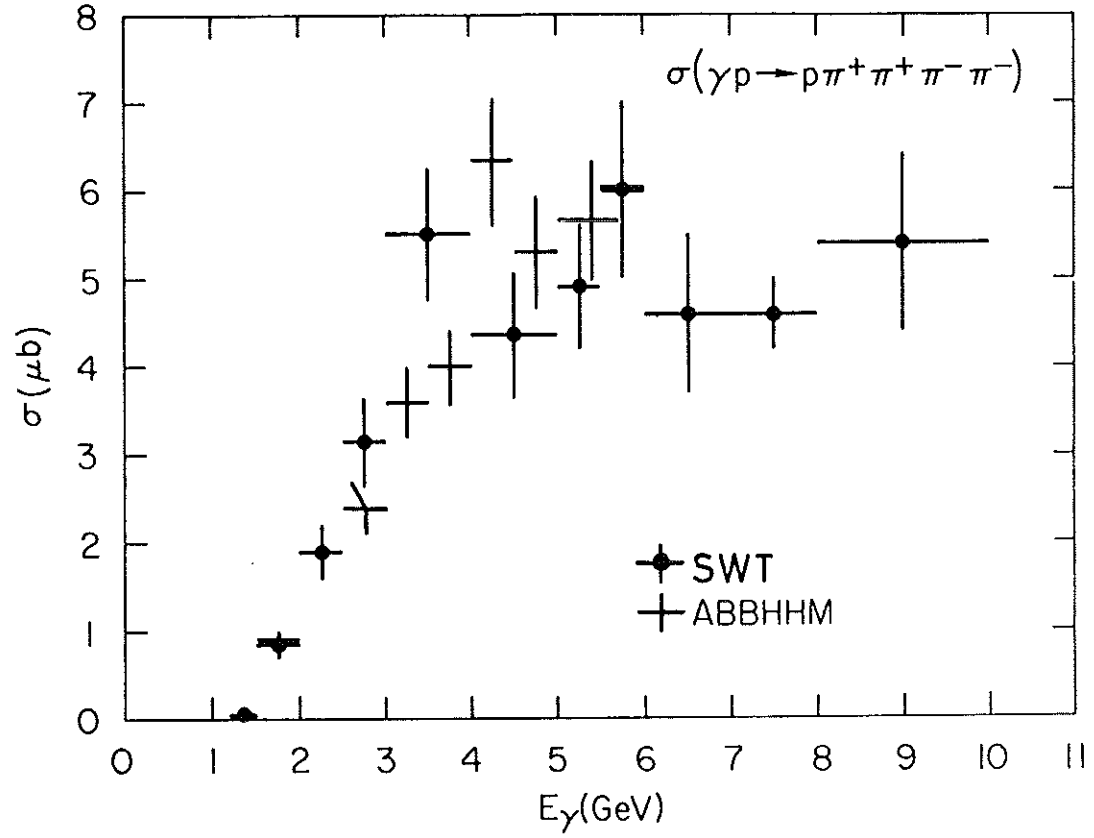
σ(γp→pπ⁺π⁺π⁻π⁻)
SWT
ABBHHM
σ(μb)
Eγ(GeV)

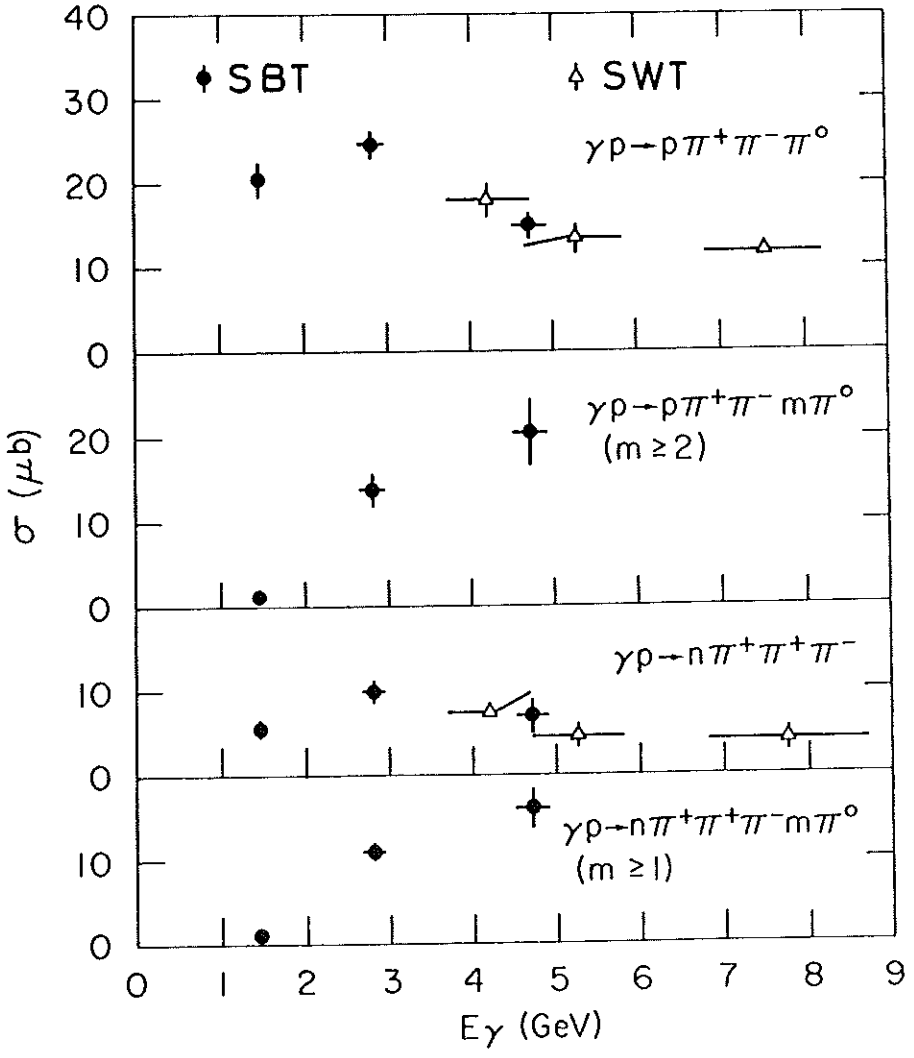
SBT
SWT
γp→pπ⁺π⁻π°
γp→pπ⁺π⁻mπ°
(m≥2)
γp→nπ⁺π⁺π⁻
γp→nπ⁺π⁺π⁻mπ°
(m≥1)
σ (μb)
Eγ (GeV)

Fig. 9

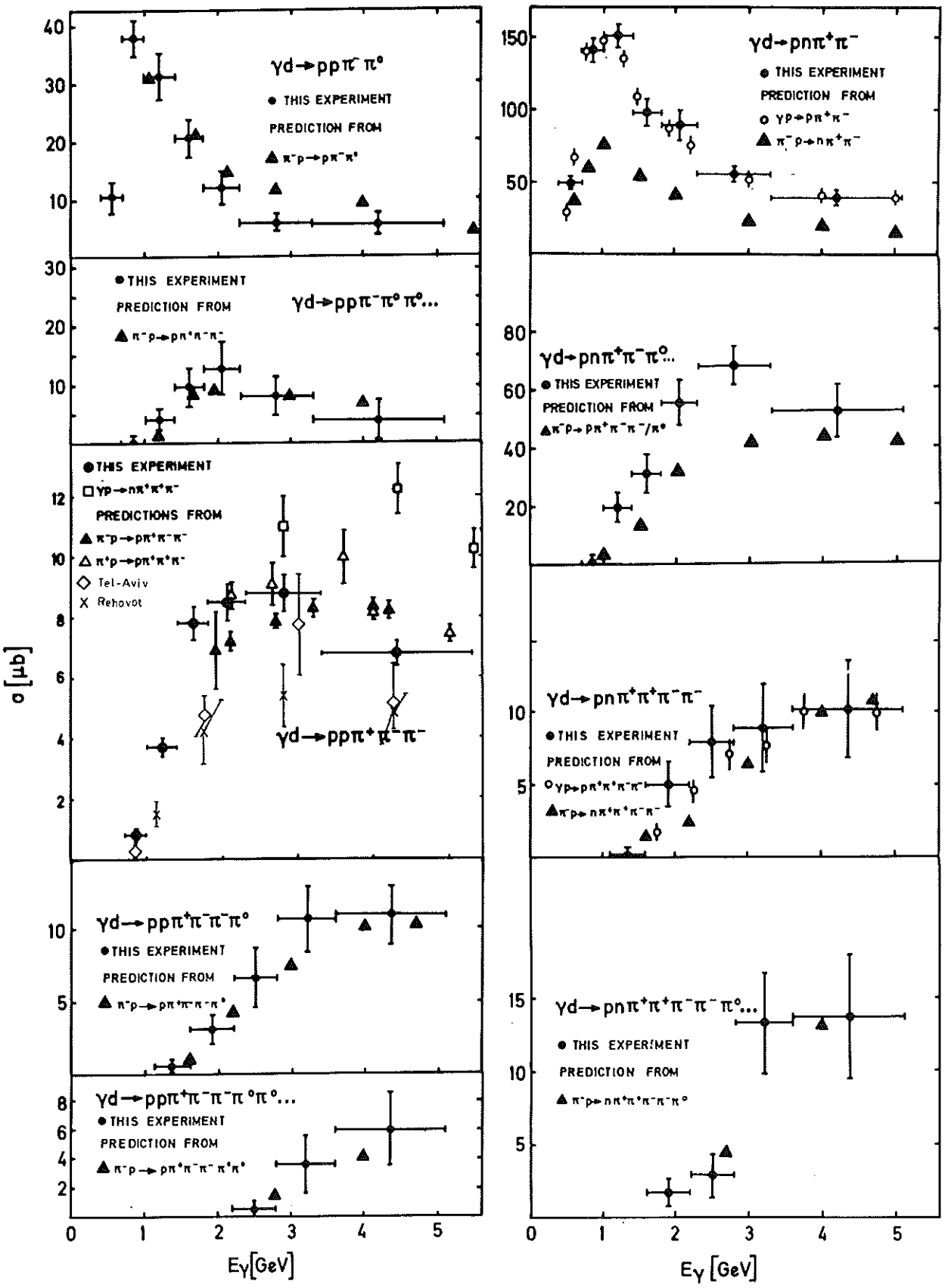
γd→ppπ⁻π°
THIS EXPERIMENT
PREDICTION FROM
π⁻p→pπ⁻π°
γd→ppπ⁻π°π°...
THIS EXPERIMENT
PREDICTION FROM
π⁻p→pπ⁺π⁻π⁻
γd→ppπ⁺π⁻π⁻
THIS EXPERIMENT
γp→nπ⁺π⁺π⁻
PREDICTIONS FROM
π⁻p→pπ⁺π⁻π⁻
π⁺p→pπ⁺π⁺π⁻
Tel-Aviv
Rehovot
γd→ppπ⁺π⁻π⁻
γd→ppπ⁺π⁻π⁻π°
THIS EXPERIMENT
PREDICTION FROM
π⁻p→pπ⁺π⁻π⁻π°
γd→ppπ⁺π⁻π⁻π°π°...
THIS EXPERIMENT
PREDICTION FROM
π⁻p→pπ⁺π⁻π⁻π⁺π°
σ [μb]
Eγ[GeV]
γd→pnπ⁺π⁻
THIS EXPERIMENT
PREDICTION FROM
γp→pπ⁺π⁻
π⁻p→nπ⁺π⁻
γd→pnπ⁺π⁻π°...
THIS EXPERIMENT
PREDICTION FROM
π⁻p→pπ⁺π⁻π⁻/π°
γd→pnπ⁺π⁺π⁻π⁻
THIS EXPERIMENT
PREDICTION FROM
γp→pπ⁺π⁺π⁻π⁻
π⁻p→nπ⁺π⁺π⁻π⁻
γd→pnπ⁺π⁺π⁻π⁻π°...
THIS EXPERIMENT
PREDICTION FROM
π⁻p→nπ⁺π⁺π⁻π⁻π°
Eγ [GeV]

Fig. 10

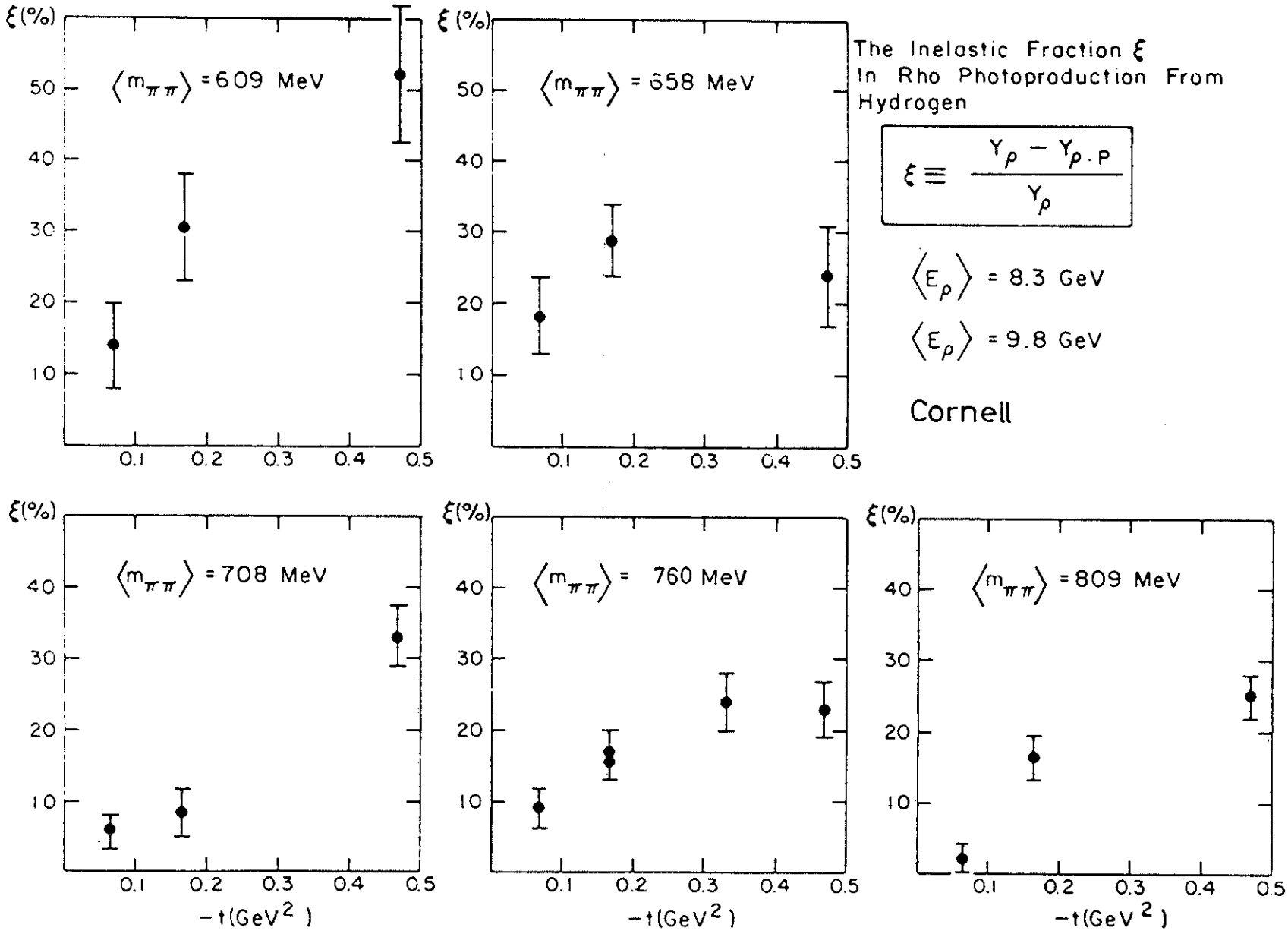
ξ(%)
⟨m_ππ⟩ = 609 MeV
⟨m_ππ⟩ = 658 MeV
⟨m_ππ⟩ = 708 MeV
⟨m_ππ⟩ = 760 MeV
⟨m_ππ⟩ = 809 MeV
−t(GeV²)
The Inelastic Fraction ξ In Rho Photoproduction From Hydrogen
ξ ≡ (Y_ρ − Y_ρ.P) / Y_ρ
⟨E_ρ⟩ = 8.3 GeV
⟨E_ρ⟩ = 9.8 GeV
Cornell

Fig. 11

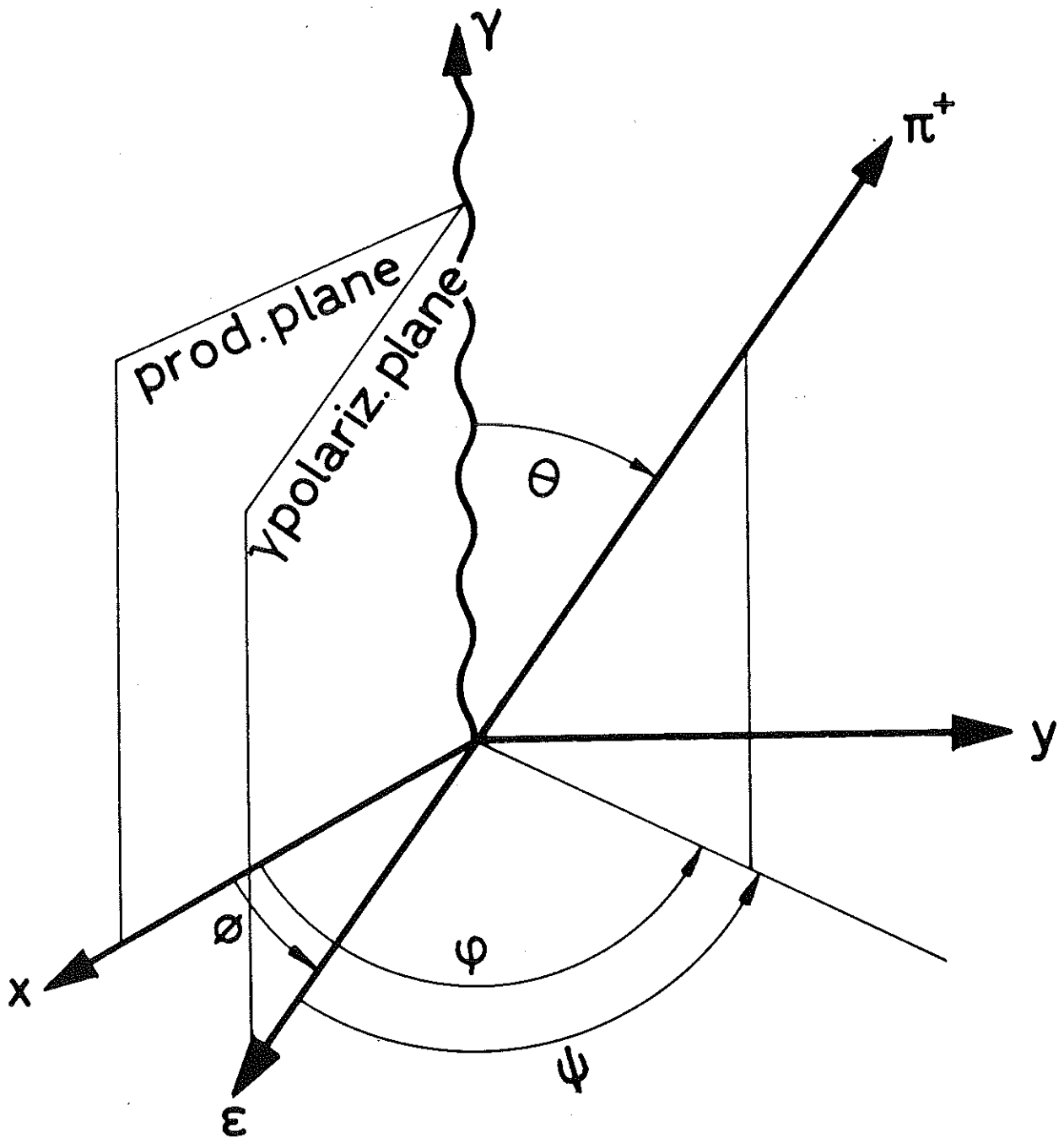

Fig.12

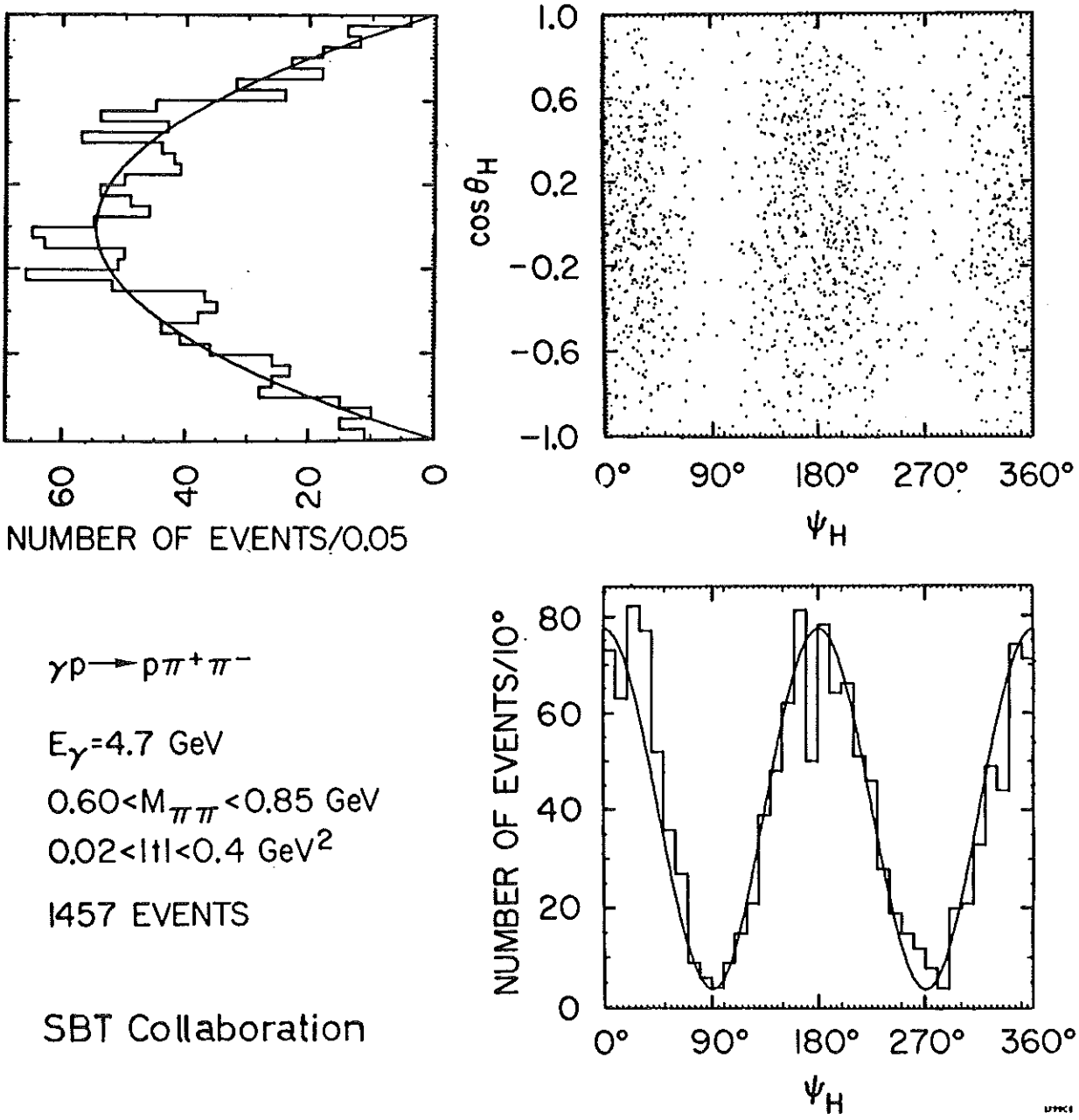
60
40
20
0
NUMBER OF EVENTS/0.05
1.0
0.6
0.2
−0.2
−0.6
−1.0
cos θH
0°
90°
180°
270°
360°
ΨH
γp → pπ+π−
Eγ=4.7 GeV
0.60<Mππ<0.85 GeV
0.02<|t|<0.4 GeV2
1457 EVENTS
SBT Collaboration
NUMBER OF EVENTS/10°
80
60
40
20
0
0°
90°
180°
270°
360°
ΨH

Fig. 13

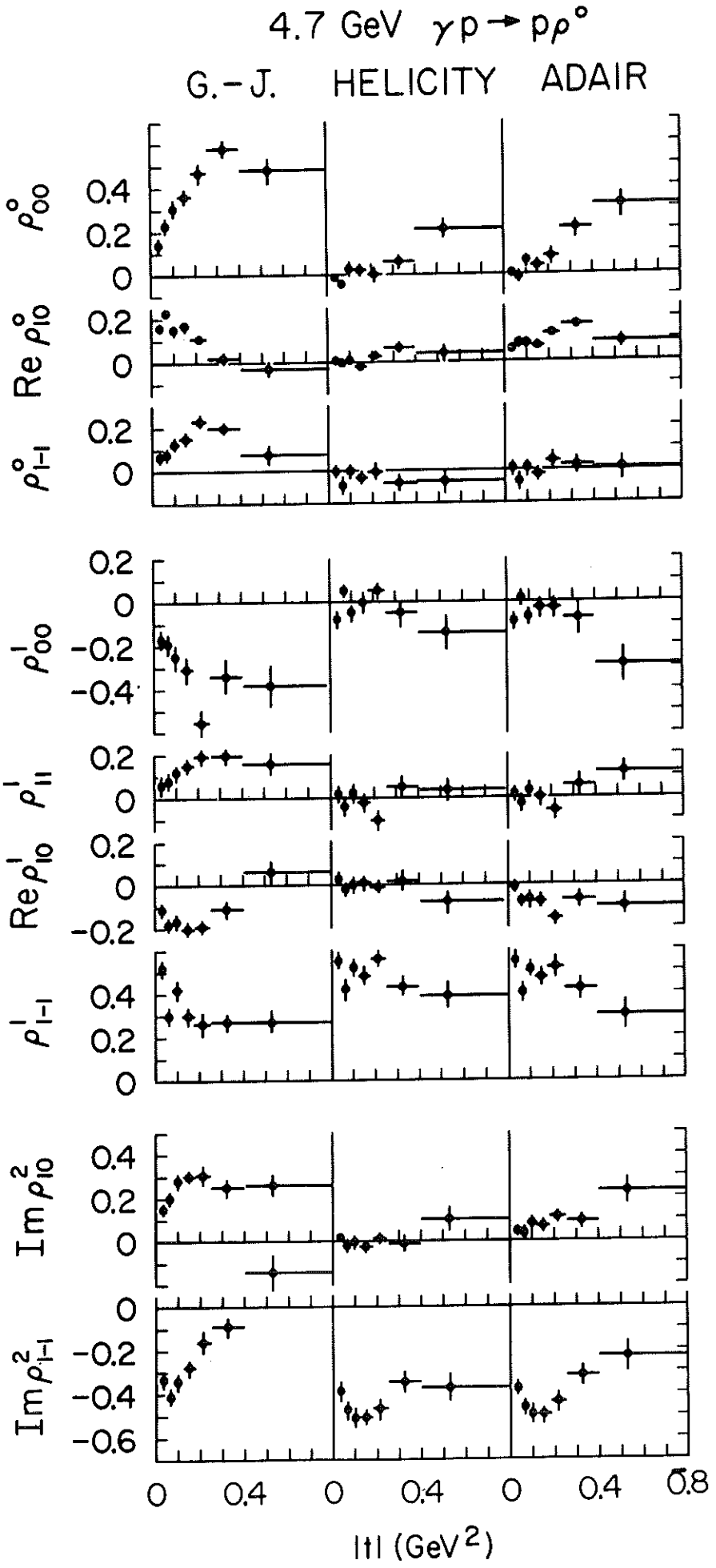
4.7 GeV γp → pρ°
G.-J. HELICITY ADAIR
ρ°00
Re ρ°10
ρ°1-1
ρ¹00
ρ¹11
Re ρ¹10
ρ¹1-1
Im ρ²10
Im ρ²1-1
0.4
0.2
0
-0.2
-0.4
-0.6
0.8
|t| (GeV²)

Fig.14

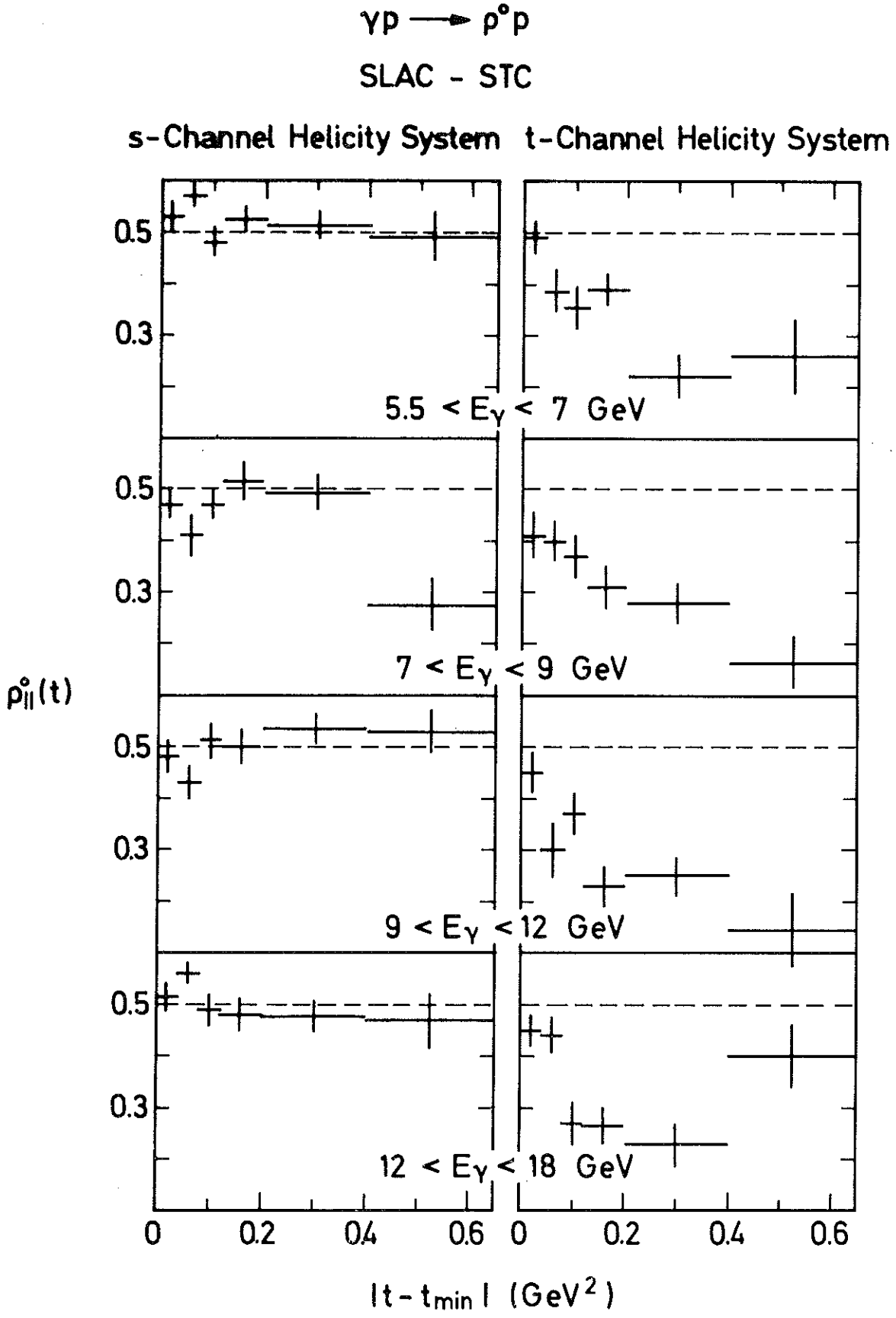
γp ⟶ ρ°p
SLAC - STC
s-Channel Helicity System
t-Channel Helicity System
5.5 < Eγ < 7 GeV
7 < Eγ < 9 GeV
9 < Eγ < 12 GeV
12 < Eγ < 18 GeV
ρ°11(t)
0.5
0.3
0
0.2
0.4
0.6
|t - tmin| (GeV²)

Fig. 15

G.-J.

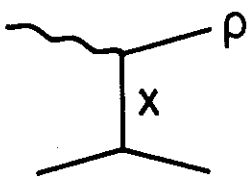

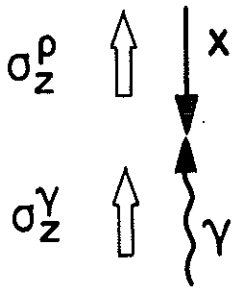

(ρ° rest frame)

H.

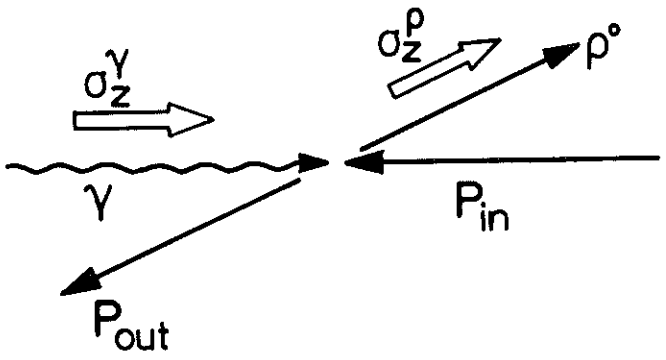

(total c.m.s.)

A.

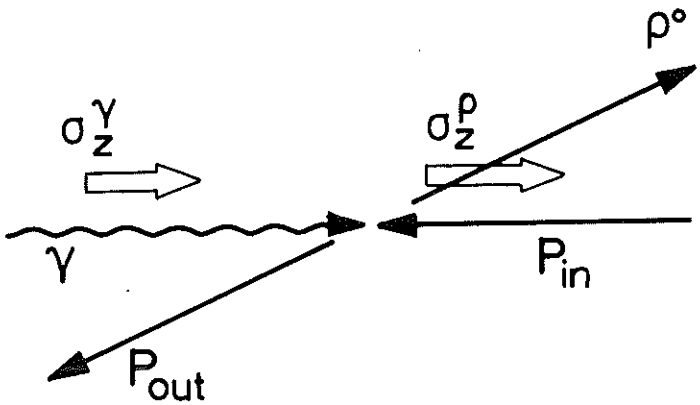

(total c.m.s.)

Fig. 16

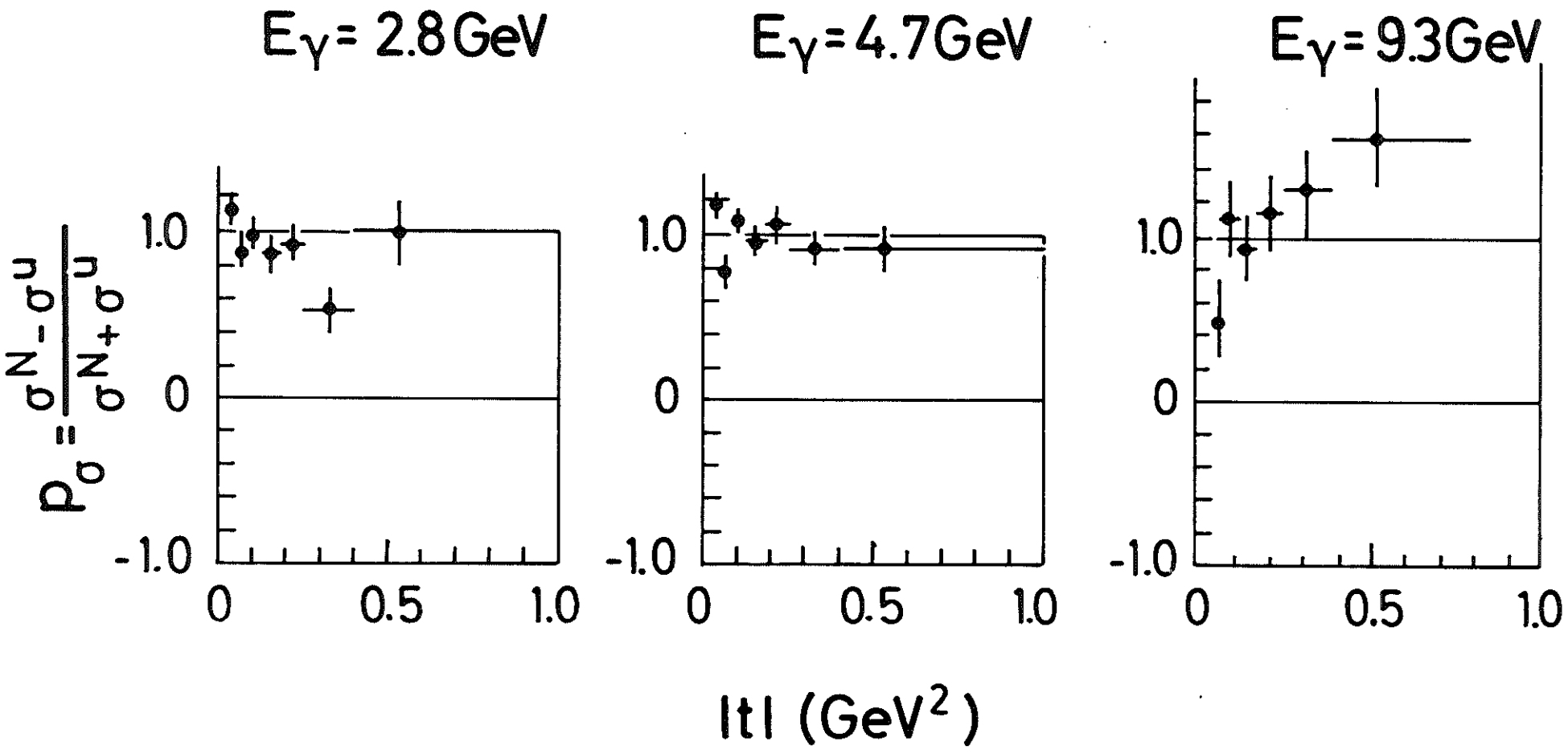
γp ⟶ ρ°p
SBT collaboration
Eγ= 2.8GeV
Eγ=4.7GeV
Eγ=9.3GeV
$P_D = \frac{\sigma^{N^-} - \sigma^{N^+}}{\sigma^{N^-} + \sigma^{N^+}}$
1.0
0
-1.0
0
0.5
1.0
|t| (GeV²)

Fig.17

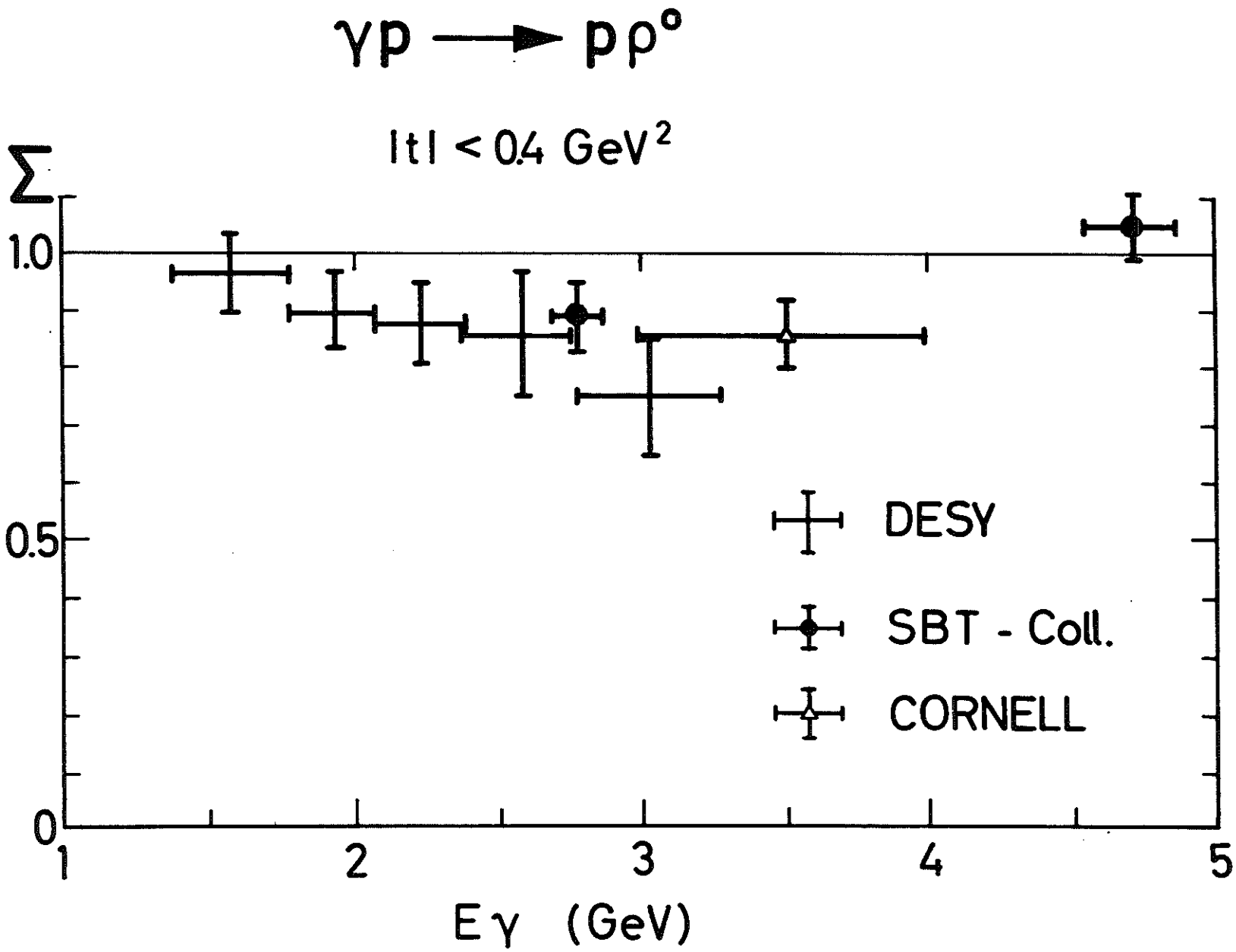

Fig.18

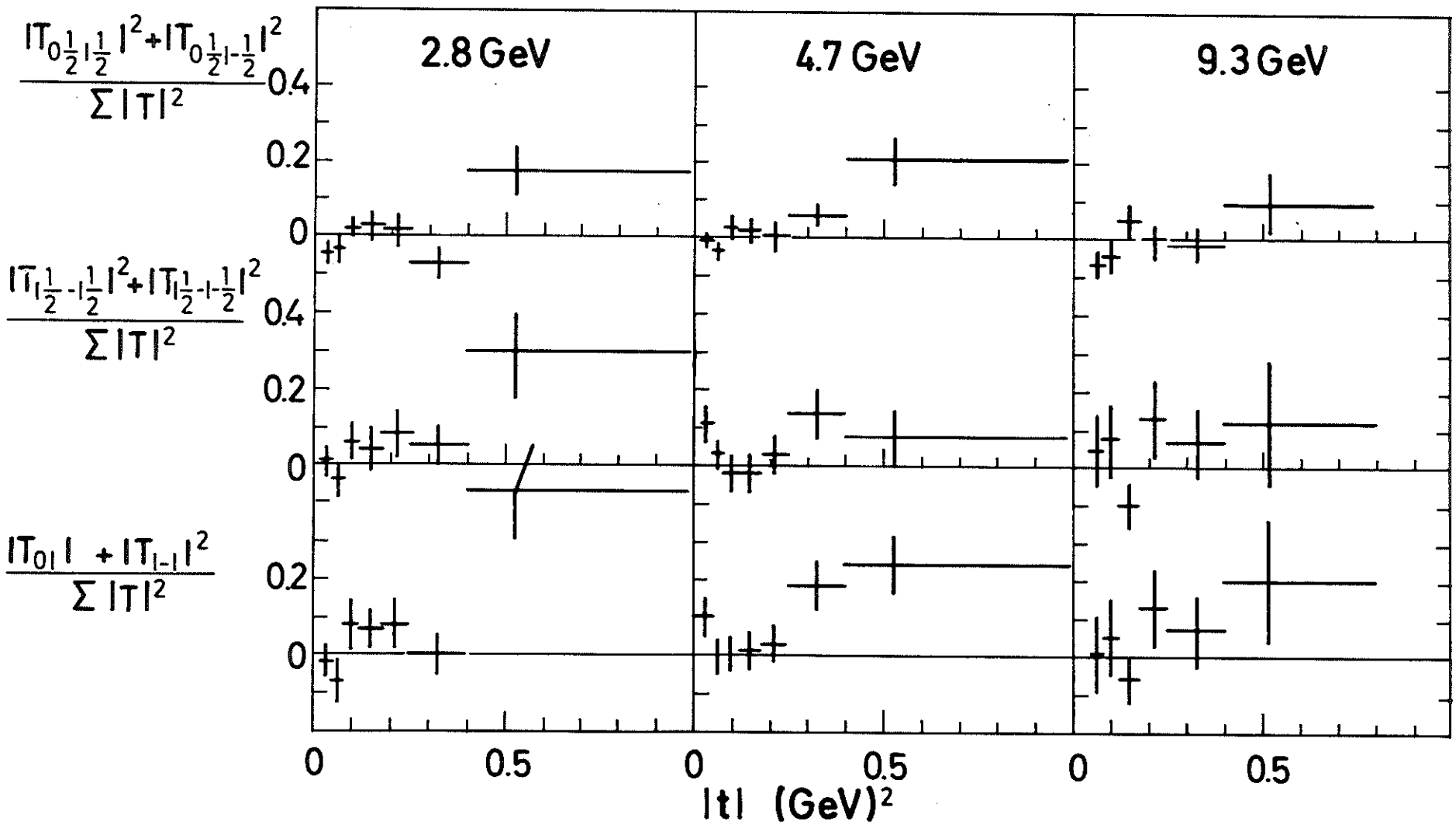
γp → ρ⁰p
HELICITY FLIP CONTRIBUTIONS
$\frac{|T_{0\frac{1}{2}1\frac{1}{2}}|^2+|T_{0\frac{1}{2}1-\frac{1}{2}}|^2}{\Sigma|T|^2}$
$\frac{|T_{1\frac{1}{2}-1\frac{1}{2}}|^2+|T_{1\frac{1}{2}-1-\frac{1}{2}}|^2}{\Sigma|T|^2}$
$\frac{|T_{01}|+|T_{1-1}|^2}{\Sigma|T|^2}$
2.8 GeV
4.7 GeV
9.3 GeV
0.4
0.2
0
0.5
|t| (GeV)²

Fig. 19

$\gamma p \longrightarrow p \pi^+ \pi^-$

SLAC - Weizmann - Tel Aviv

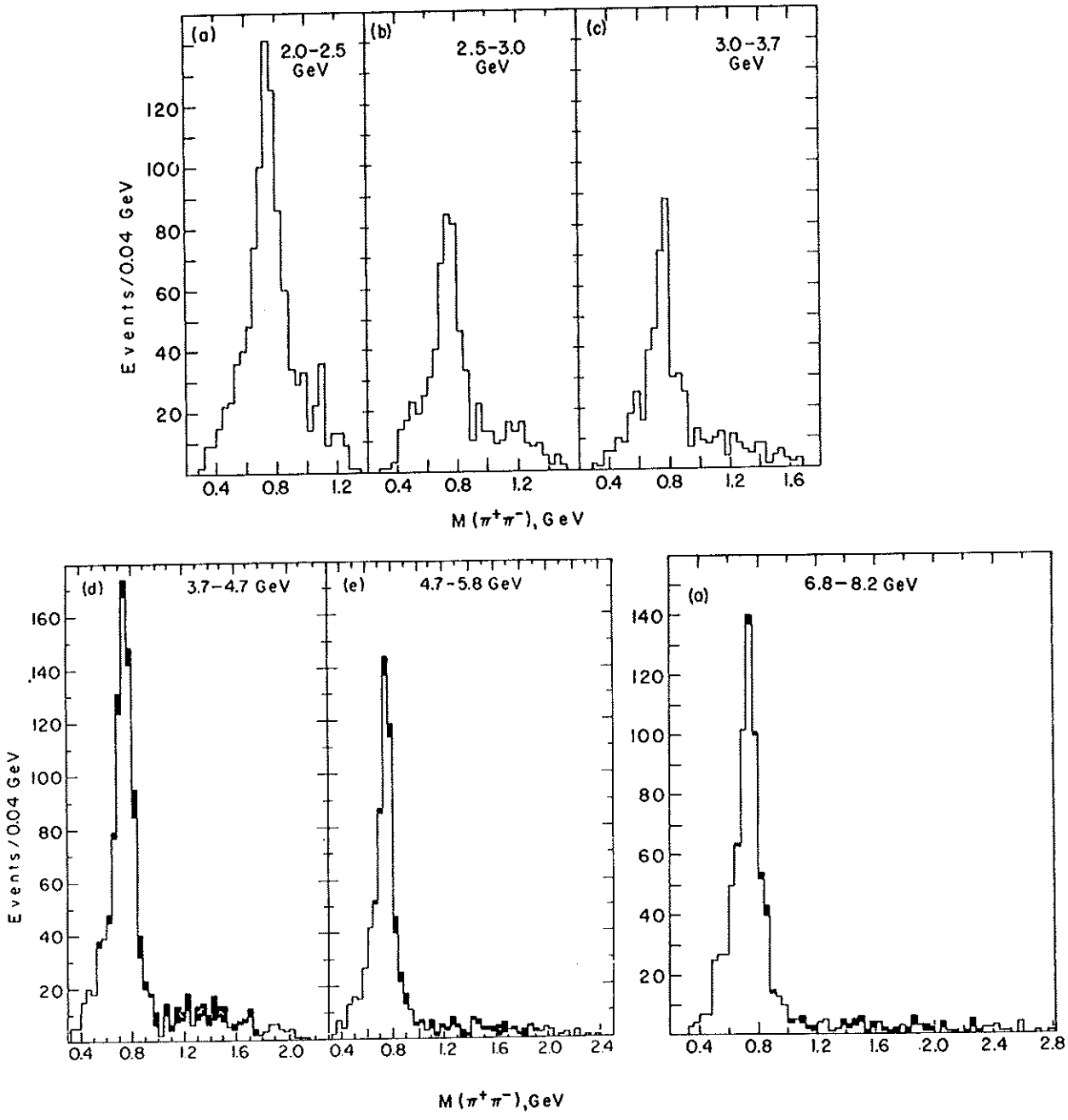

Fig. 20

$\gamma p \rightarrow p \pi^+ \pi^-$
SBT-Collaboration

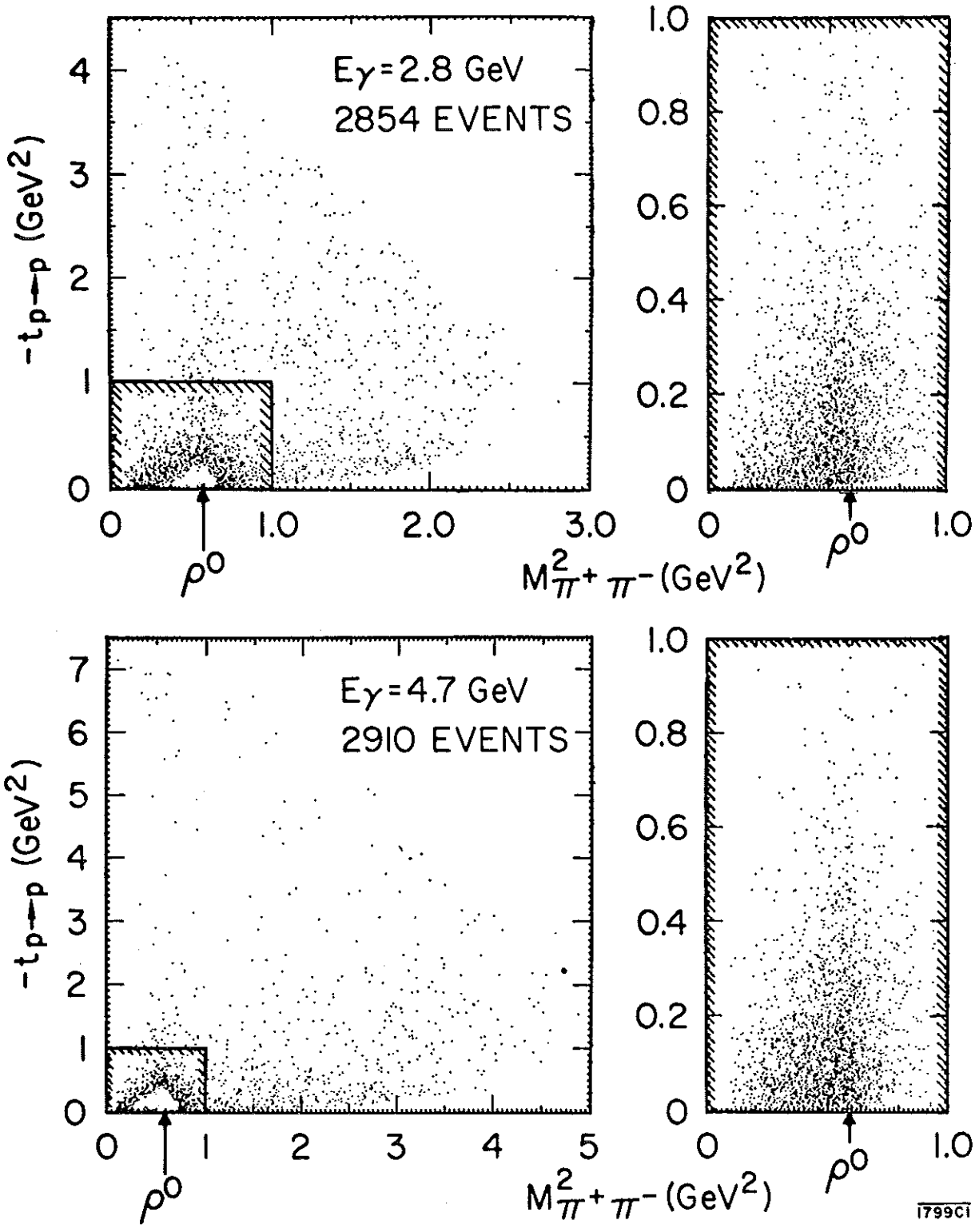

Fig. 21

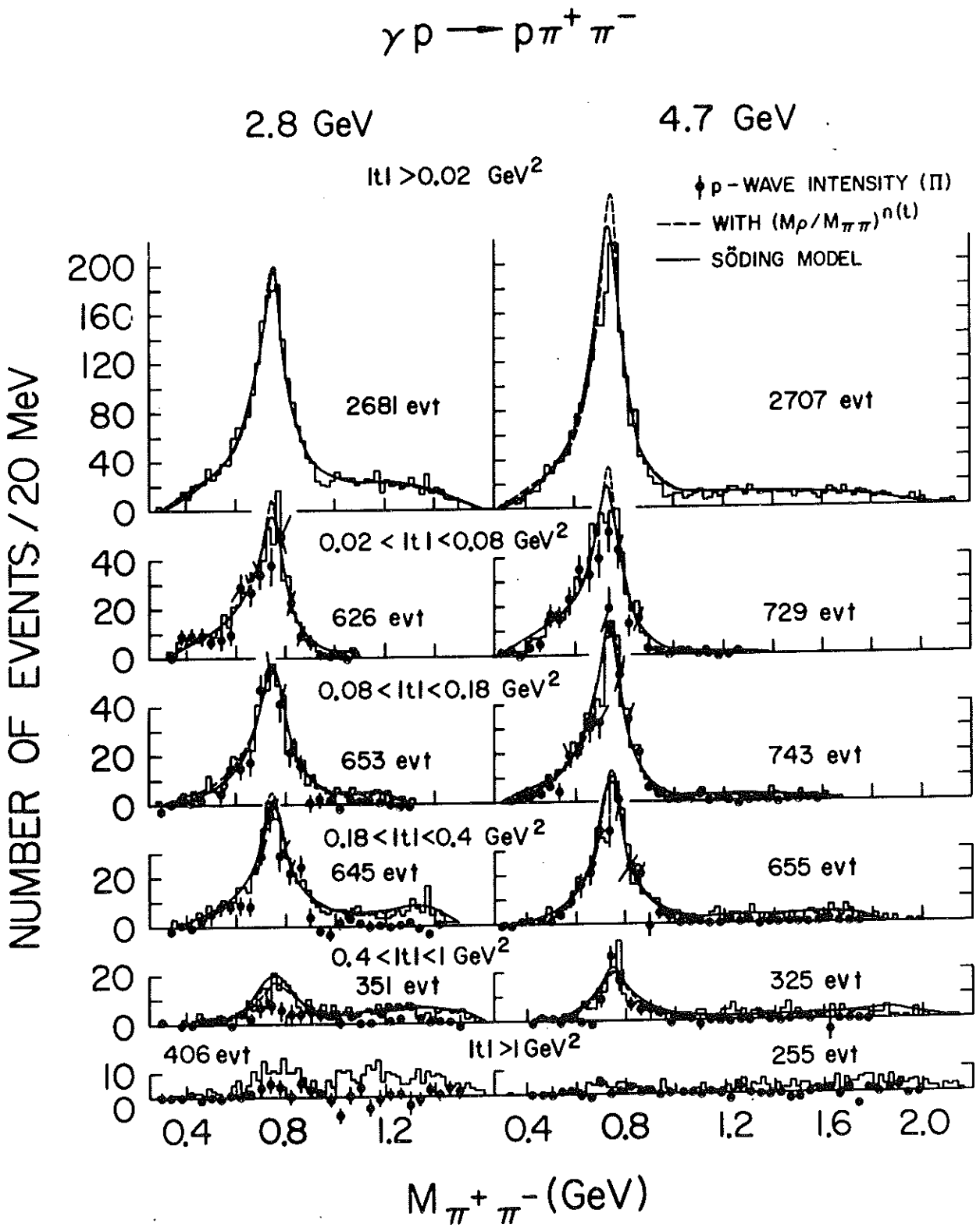
γ p → p π+ π−
2.8 GeV
4.7 GeV
|t| >0.02 GeV2
p-WAVE INTENSITY (Π)
--- WITH (Mρ/Mππ)n(t)
—— SÖDING MODEL
2681 evt
2707 evt
0.02 < |t| <0.08 GeV2
626 evt
729 evt
0.08 < |t| <0.18 GeV2
653 evt
743 evt
0.18 < |t| <0.4 GeV2
645 evt
655 evt
0.4 < |t| <1 GeV2
351 evt
325 evt
406 evt
|t| >1 GeV2
255 evt
NUMBER OF EVENTS / 20 MeV
Mπ+ π− (GeV)

Fig. 22

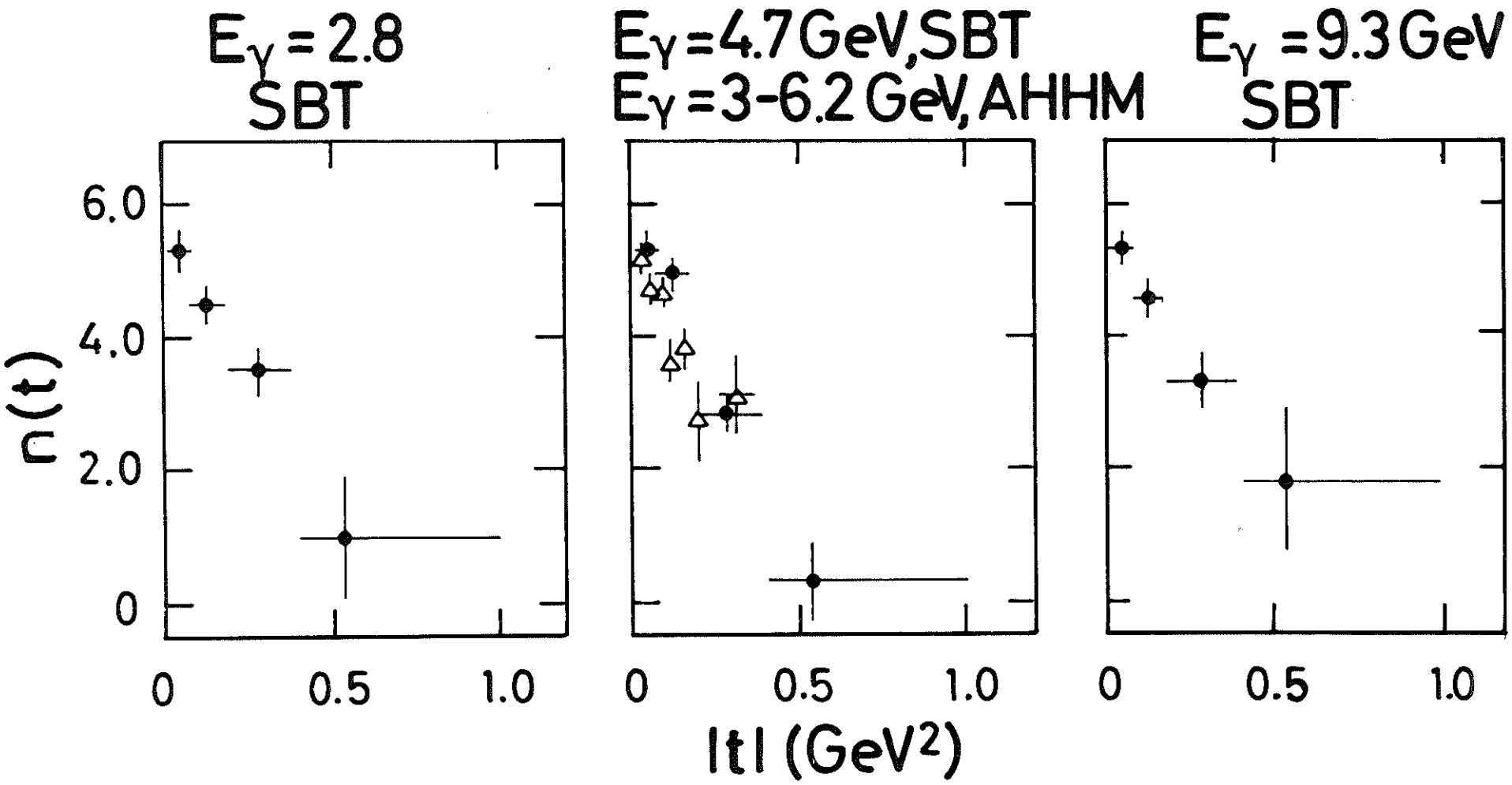
$E_\gamma = 2.8$
SBT
$E_\gamma = 4.7$ GeV, SBT
$E_\gamma = 3$-6.2 GeV, AHHM
$E_\gamma = 9.3$ GeV
SBT
n(t)
6.0
4.0
2.0
0
0
0.5
1.0
0
0.5
1.0
0
0.5
1.0
|t| (GeV²)

Fig. 23

SÖDING - MODEL

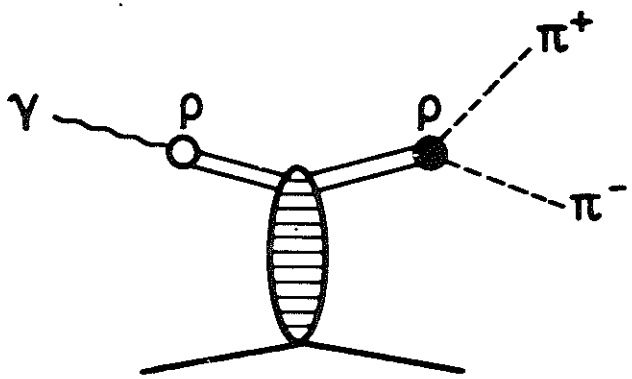

(a)

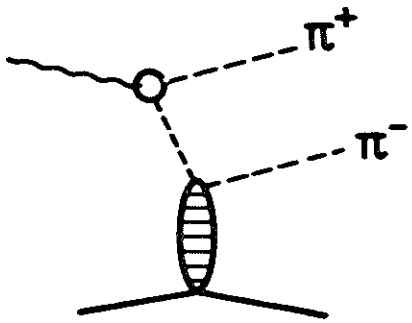

(b)

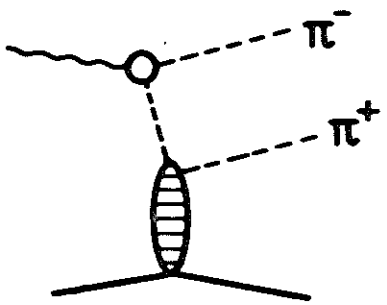

(c)

RESCATTERING TERMS

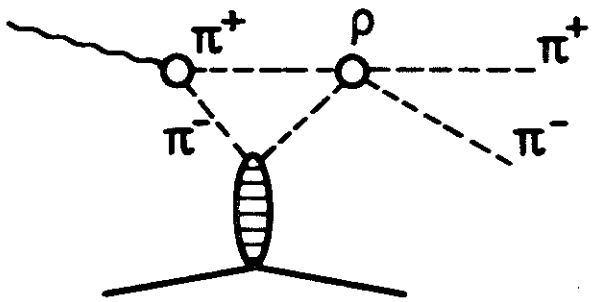

(d)

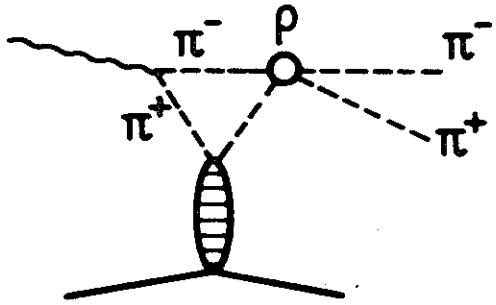

(e)

Fig. 24

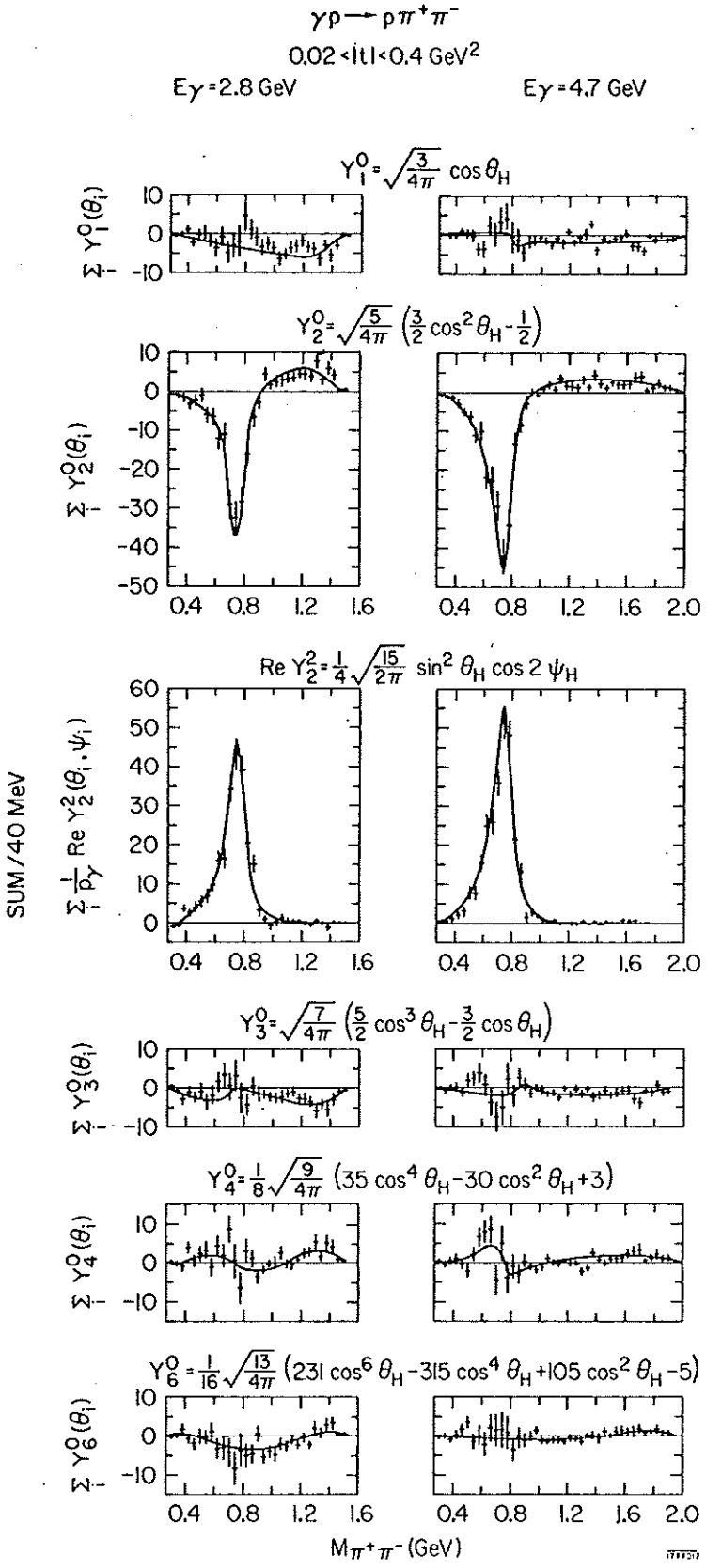
γp → pπ⁺π⁻
0.02 < |t| < 0.4 GeV²
Eγ = 2.8 GeV
Eγ = 4.7 GeV
$Y_1^0 = \sqrt{\frac{3}{4\pi}} \cos\theta_H$
$Y_2^0 = \sqrt{\frac{5}{4\pi}} \left(\frac{3}{2}\cos^2\theta_H - \frac{1}{2}\right)$
$\mathrm{Re}\, Y_2^2 = \frac{1}{4}\sqrt{\frac{15}{2\pi}} \sin^2\theta_H \cos 2\psi_H$
$Y_3^0 = \sqrt{\frac{7}{4\pi}} \left(\frac{5}{2}\cos^3\theta_H - \frac{3}{2}\cos\theta_H\right)$
$Y_4^0 = \frac{1}{8}\sqrt{\frac{9}{4\pi}} \left(35\cos^4\theta_H - 30\cos^2\theta_H + 3\right)$
$Y_6^0 = \frac{1}{16}\sqrt{\frac{13}{4\pi}} \left(231\cos^6\theta_H - 315\cos^4\theta_H + 105\cos^2\theta_H - 5\right)$
$\sum_i Y_1^0(\theta_i)$
$\sum_i Y_2^0(\theta_i)$
$\sum_i \frac{1}{\rho_\gamma} \mathrm{Re}\, Y_2^2(\theta_i, \psi_i)$
$\sum_i Y_3^0(\theta_i)$
$\sum_i Y_4^0(\theta_i)$
$\sum_i Y_6^0(\theta_i)$
SUM/40 MeV
$M_{\pi^+\pi^-}$ (GeV)

Fig. 25

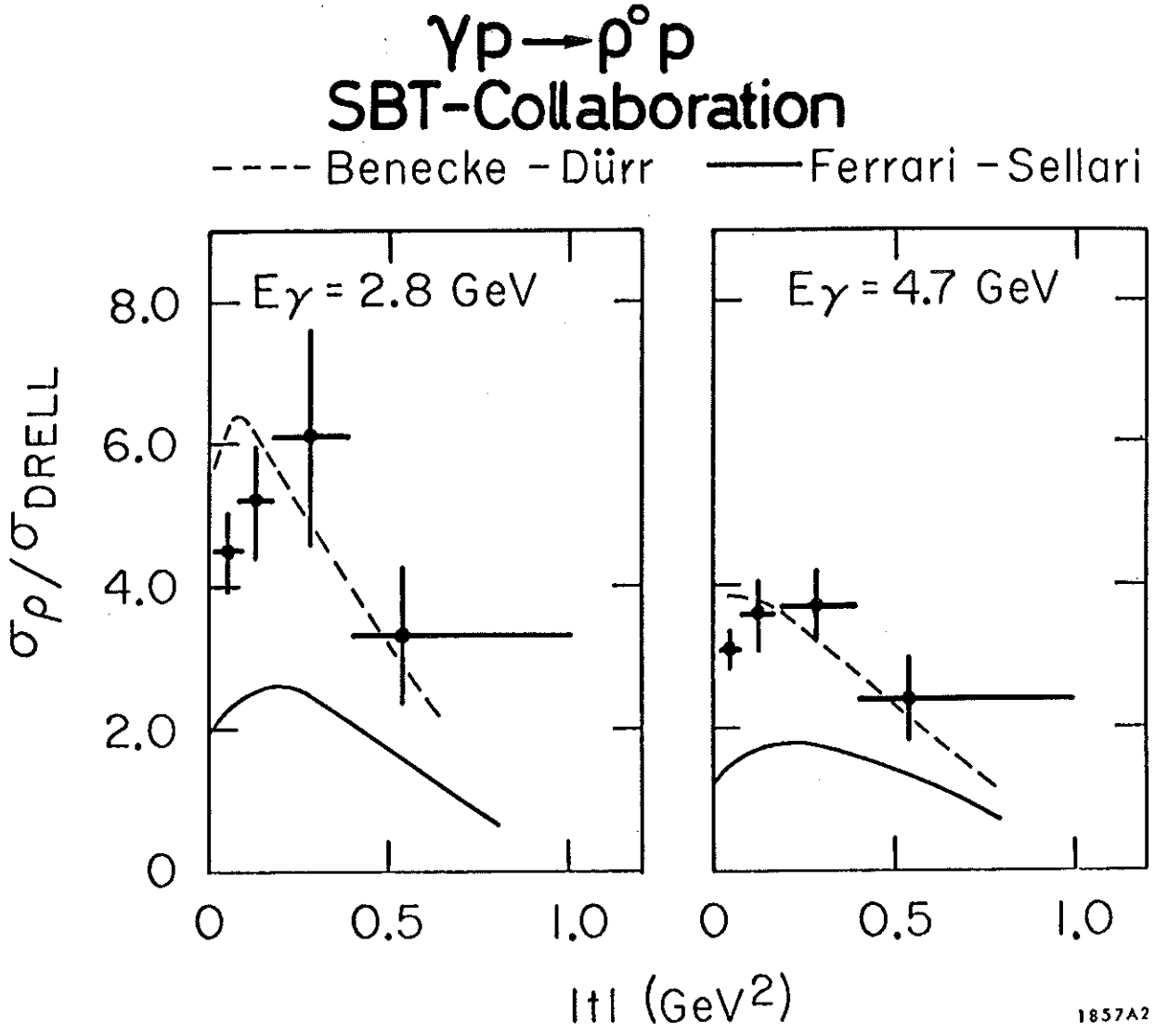
γp → ρ°p
SBT-Collaboration
---- Benecke - Dürr
—— Ferrari - Sellari
Eγ = 2.8 GeV
Eγ = 4.7 GeV
σρ/σDRELL
8.0
6.0
4.0
2.0
0
0
0.5
1.0
|t| (GeV²)
1857A2

Fig. 26

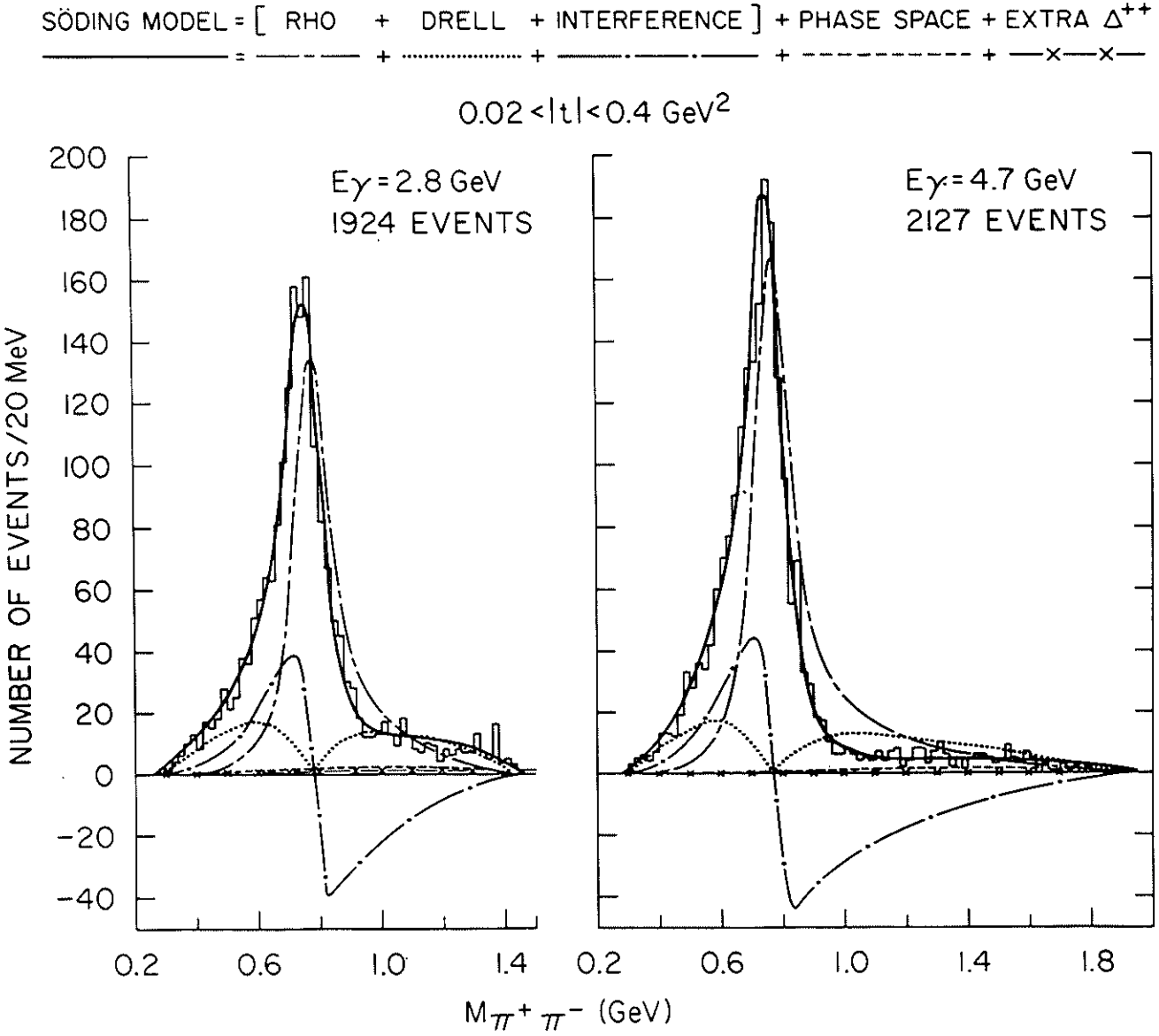
SÖDING MODEL = [RHO + DRELL + INTERFERENCE] + PHASE SPACE + EXTRA Δ++
0.02 < |t| < 0.4 GeV2
Eγ = 2.8 GeV
1924 EVENTS
Eγ = 4.7 GeV
2127 EVENTS
NUMBER OF EVENTS/20 MeV
200
180
160
140
120
100
80
60
40
20
0
-20
-40
0.2
0.6
1.0
1.4
1.8
Mπ+π− (GeV)

Fig. 27

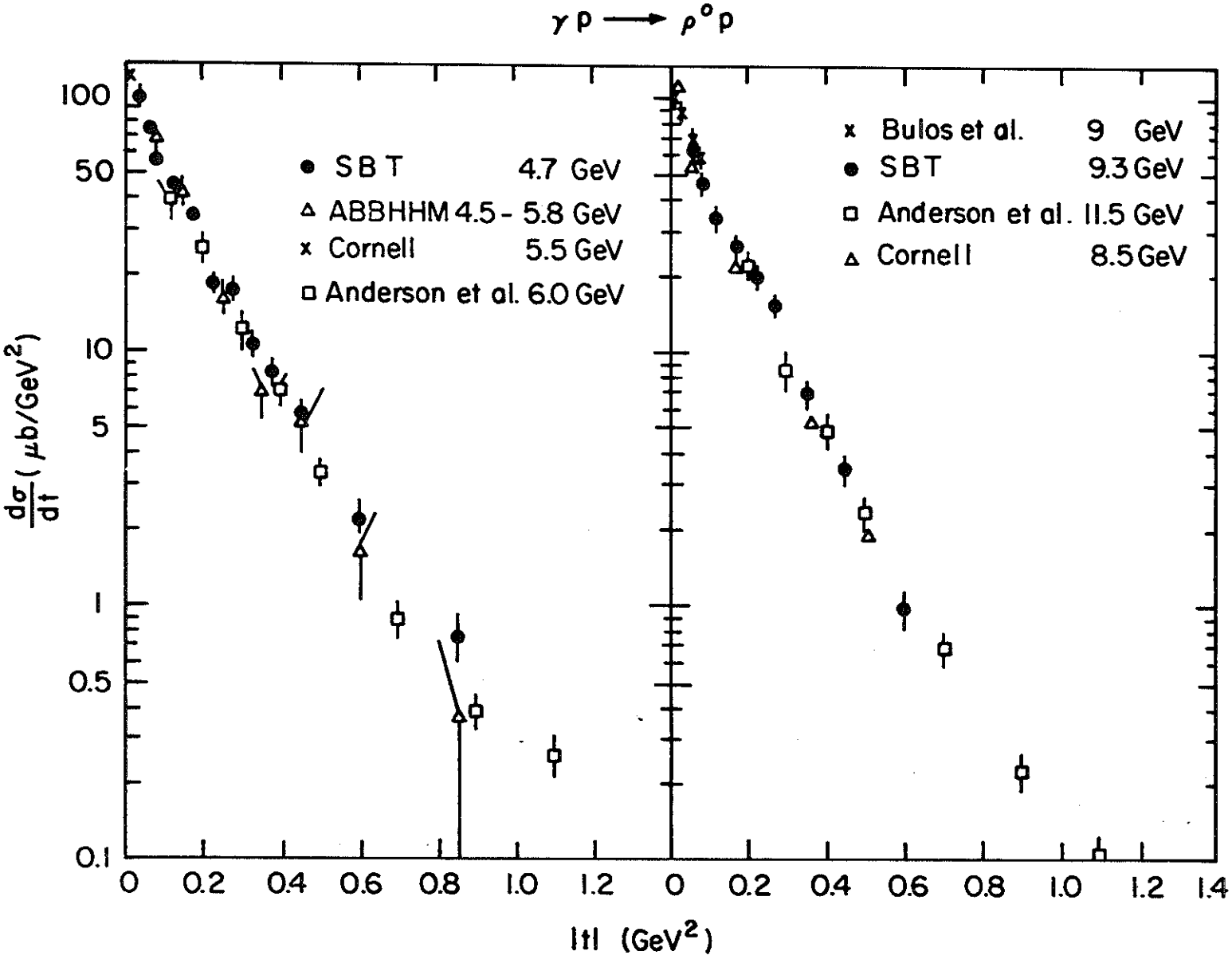
γ p ⟶ ρ° p
100
50
10
5
1
0.5
0.1
dσ/dt (μb/GeV²)
● SBT 4.7 GeV
△ ABBHHM 4.5 - 5.8 GeV
× Cornell 5.5 GeV
□ Anderson et al. 6.0 GeV
× Bulos et al. 9 GeV
● SBT 9.3 GeV
□ Anderson et al. 11.5 GeV
△ Cornell 8.5 GeV
0 0.2 0.4 0.6 0.8 1.0 1.2
0 0.2 0.4 0.6 0.8 1.0 1.2 1.4
|t| (GeV²)

Fig. 28

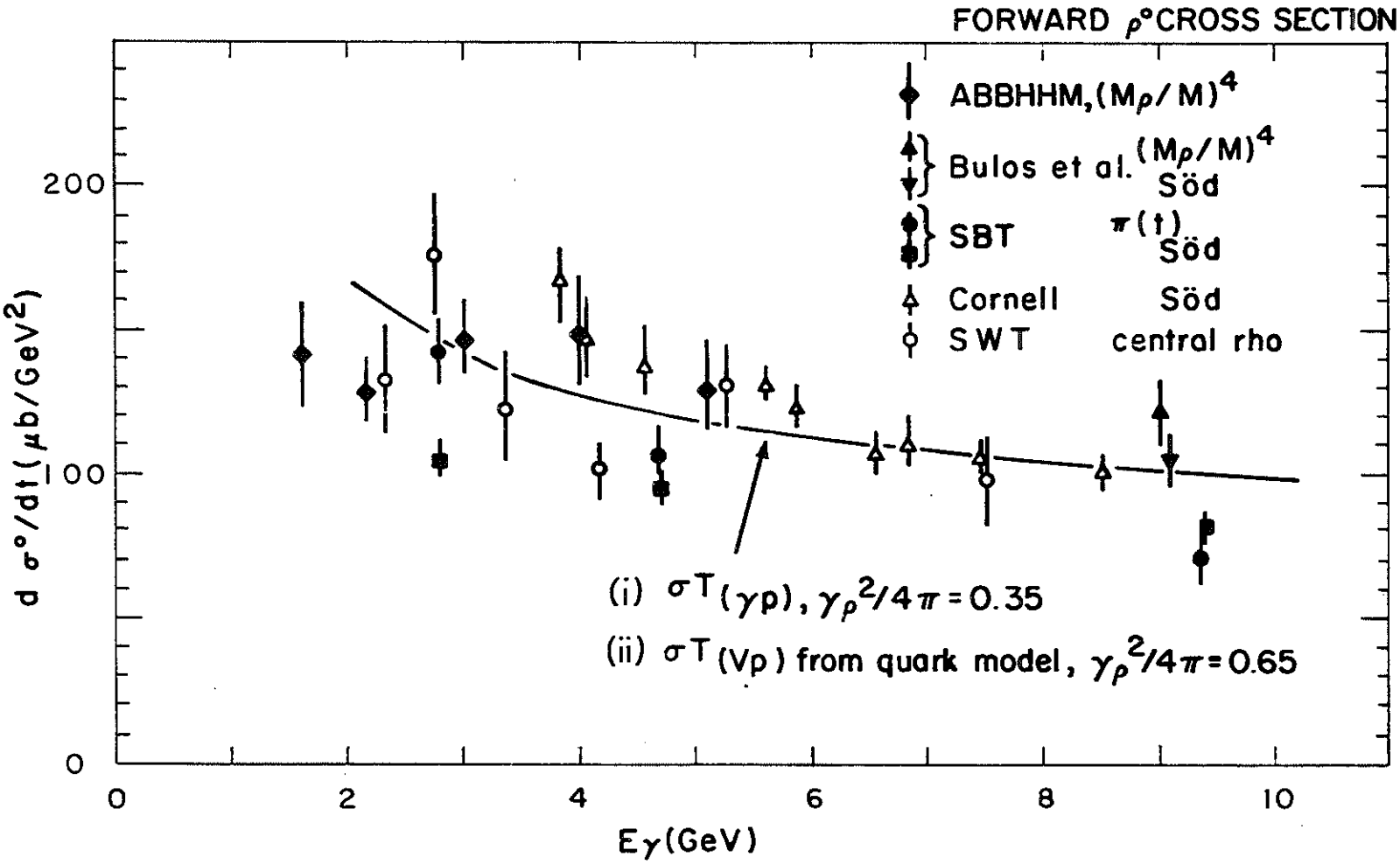
FORWARD ρ°CROSS SECTION
ABBHHM, $(M_\rho/M)^4$
Bulos et al. $(M_\rho/M)^4$ Söd
SBT $\pi(t)$ Söd
Cornell Söd
SWT central rho
(i) $\sigma_T(\gamma p)$, $\gamma_\rho^2/4\pi = 0.35$
(ii) $\sigma_T(Vp)$ from quark model, $\gamma_\rho^2/4\pi = 0.65$
$d\sigma°/dt$ (μb/GeV²)
200
100
0
0
2
4
6
8
10
Eγ(GeV)

Fig. 29

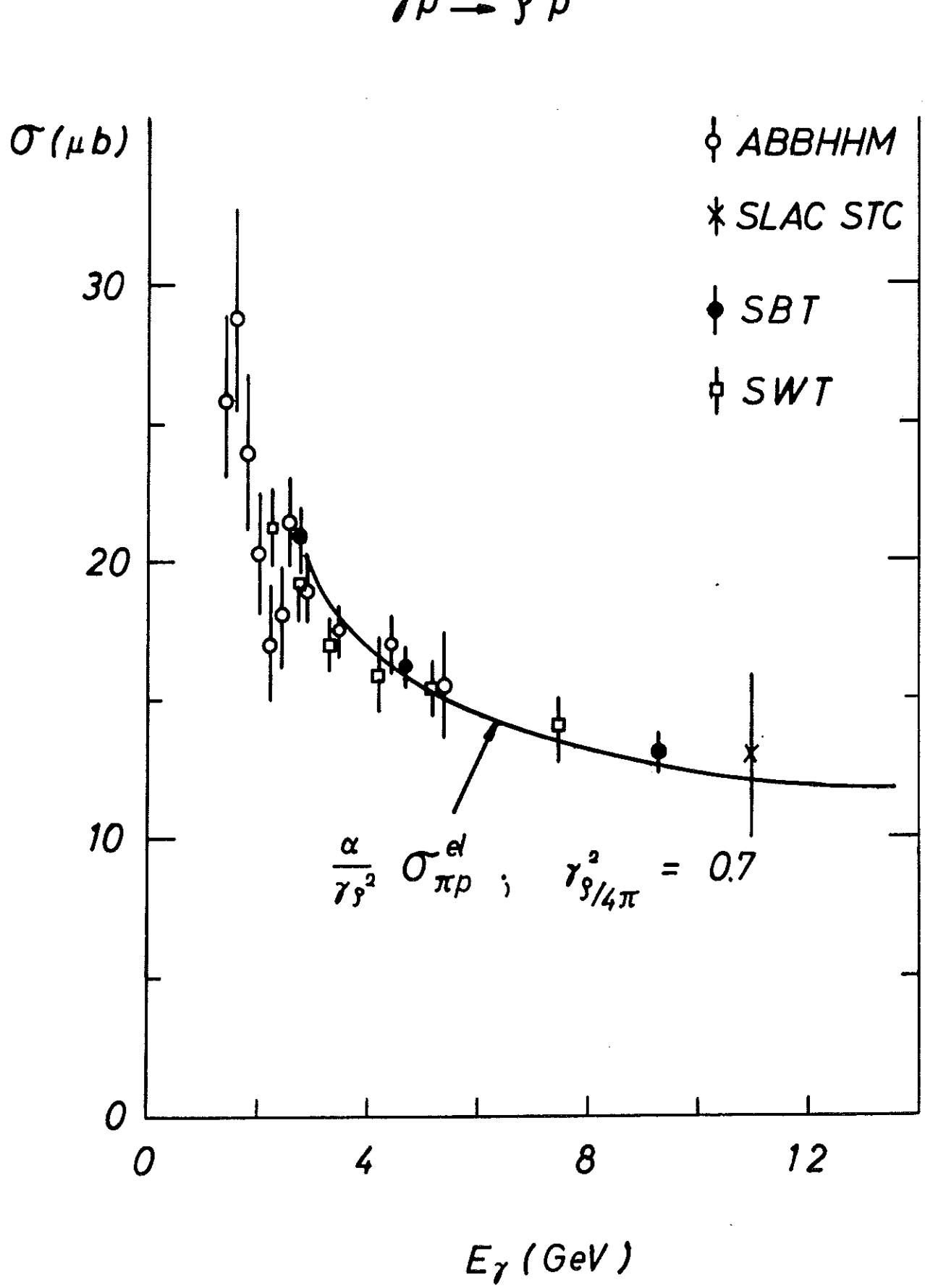
γp → ρ°p
σ (μb)
ABBHHM
SLAC STC
SBT
SWT
30
20
10
0
0
4
8
12
α/γρ² σ_πp^el ; γ²ρ/4π = 0.7
E_γ (GeV)

Fig. 30

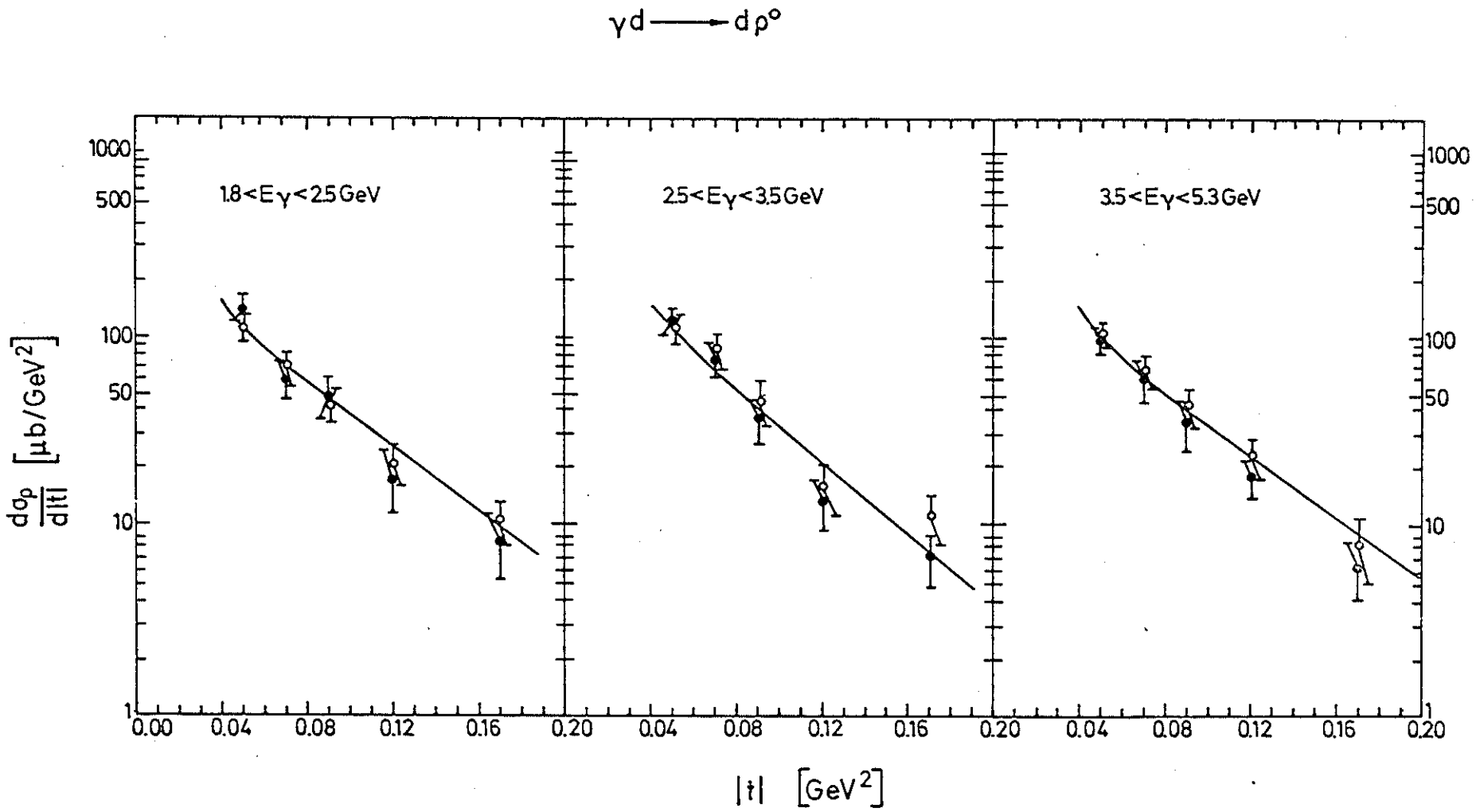
γd ⟶ dρ°
1.8<Eγ<2.5 GeV
2.5<Eγ<3.5 GeV
3.5<Eγ<5.3 GeV
dσρ/d|t| [μb/GeV²]
|t| [GeV²]
1000
500
100
50
10
1
0.00
0.04
0.08
0.12
0.16
0.20
dσρ/d|t| (γd⟶dρ°) Ross-Stodolsky-Model
dσρ/d|t| (γd⟶dρ°) Söding-Yennie-Model

Fig.31

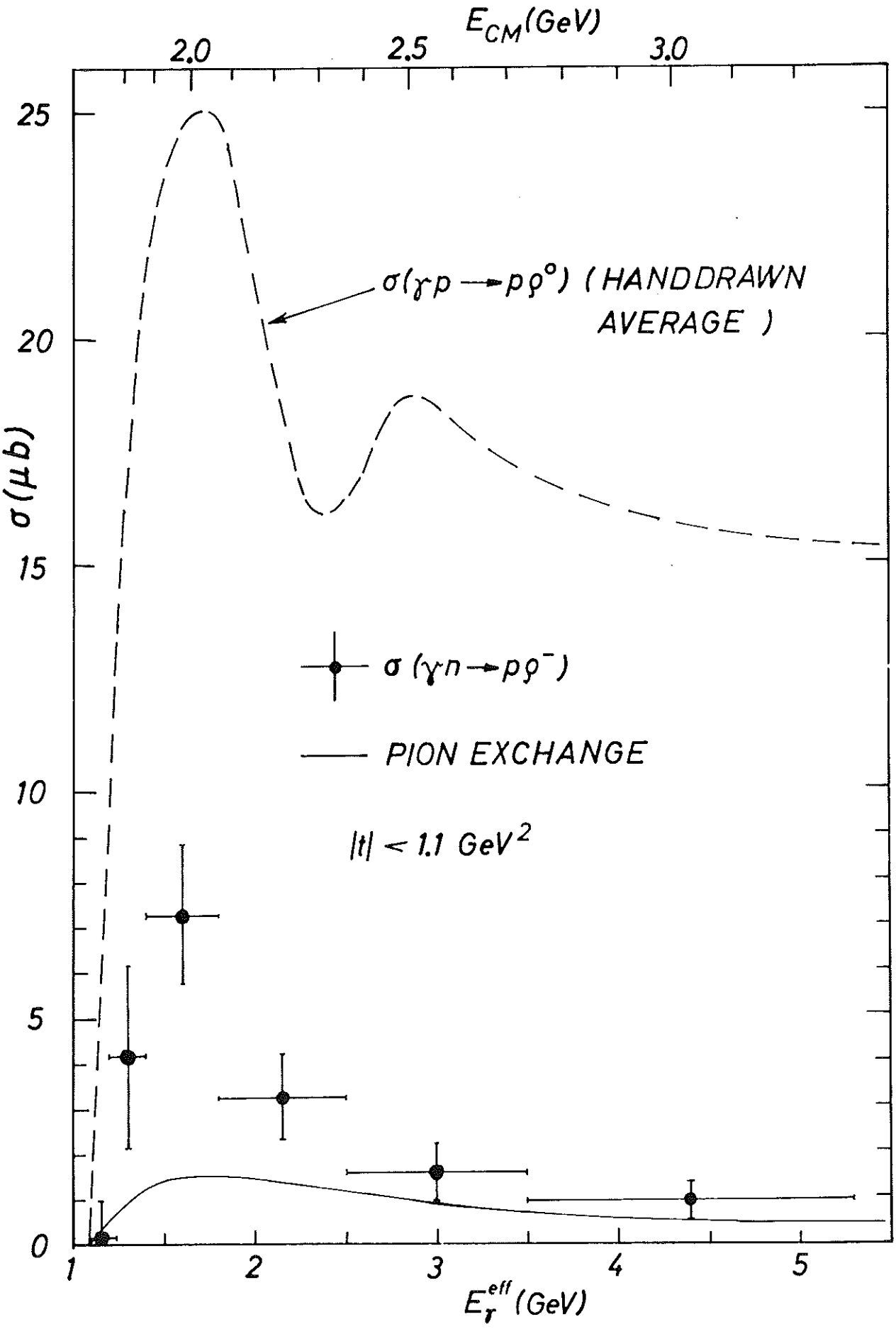
E_{CM}(GeV)
2.0
2.5
3.0
25
20
15
10
5
0
σ(μb)
σ(γp → pρ°) (HANDDRAWN AVERAGE)
σ (γn → pρ⁻)
PION EXCHANGE
|t| < 1.1 GeV²
1
2
3
4
5
E_γ^{eff} (GeV)

Fig. 32

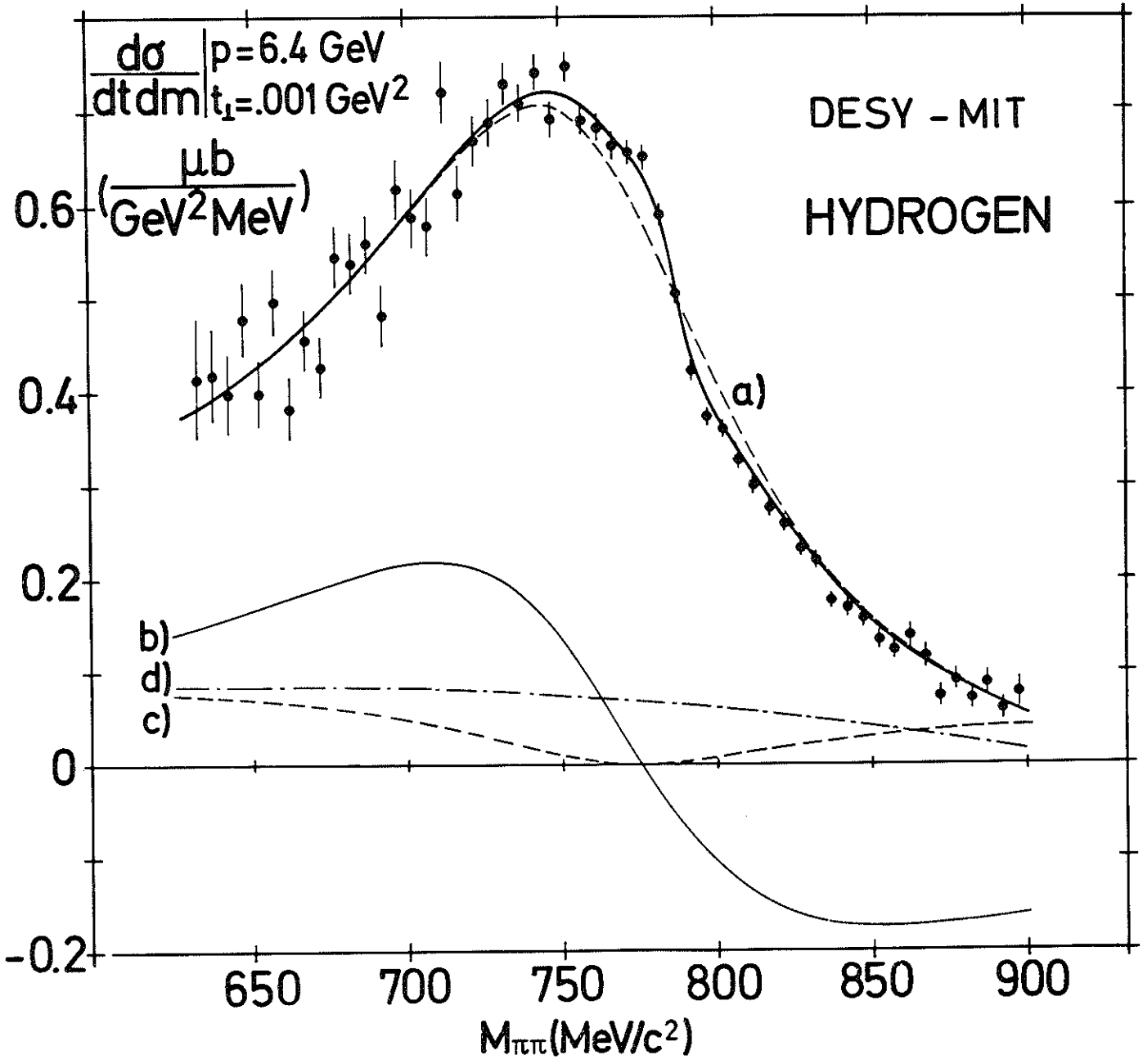
dσ/dtdm | p=6.4 GeV
t₁=.001 GeV²
μb/(GeV²MeV)
DESY - MIT
HYDROGEN
a)
b)
d)
c)
0.6
0.4
0.2
0
-0.2
650
700
750
800
850
900
Mππ(MeV/c²)

Fig. 33

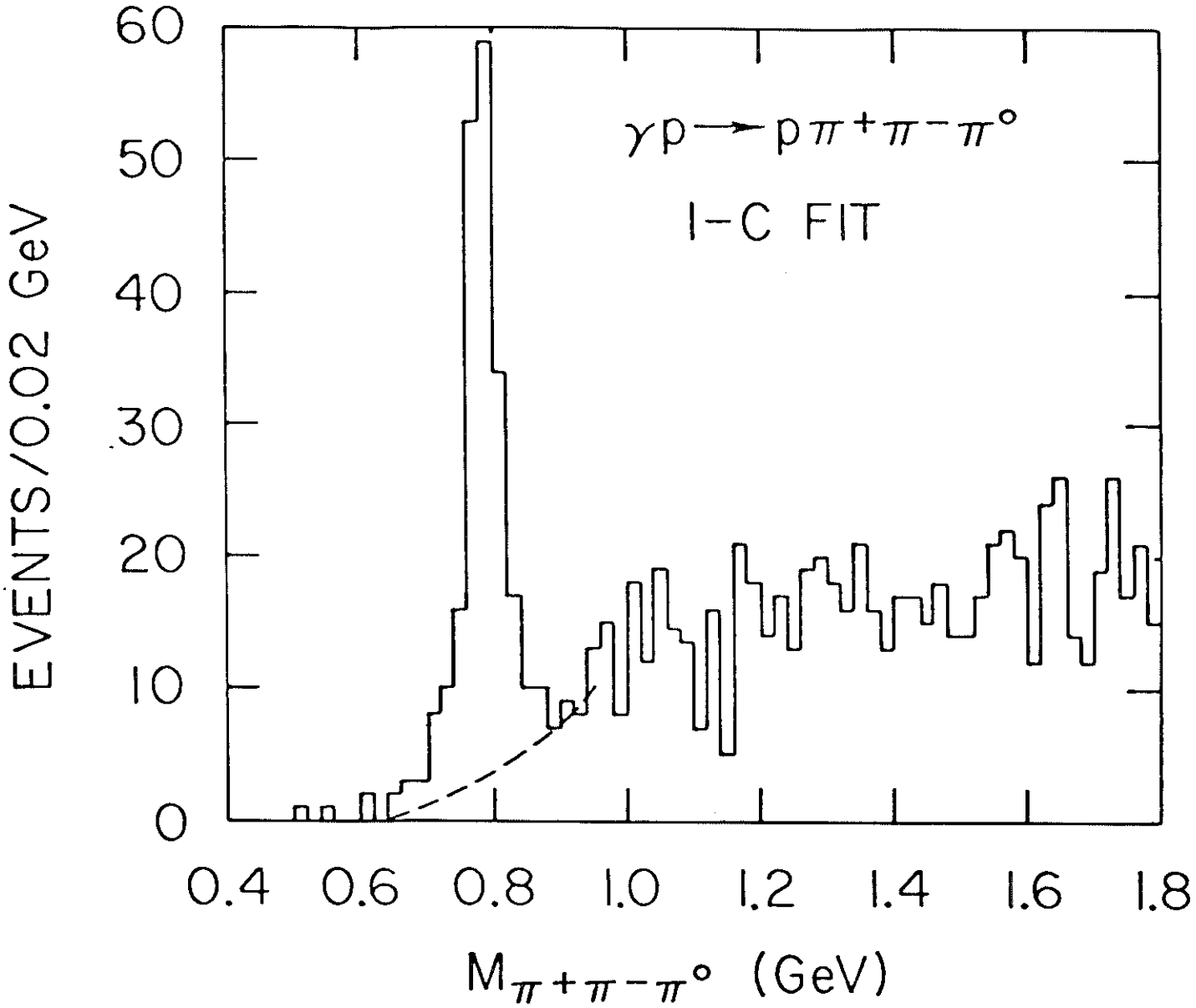
60
50
40
30
20
10
0
EVENTS/0.02 GeV
γp → pπ+π−π°
1-C FIT
0.4
0.6
0.8
1.0
1.2
1.4
1.6
1.8
Mπ+π−π° (GeV)

Fig.34

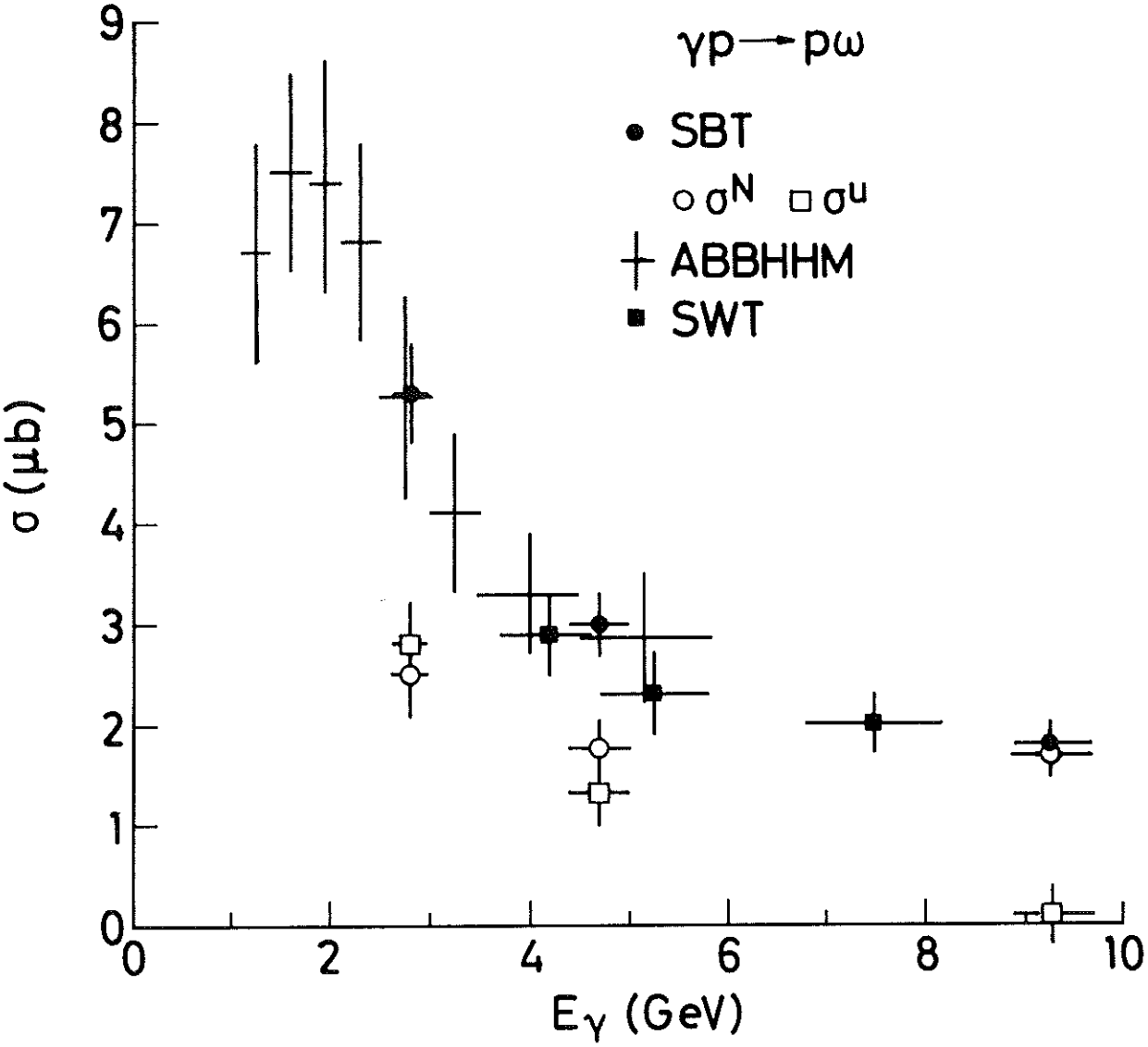

Fig. 35

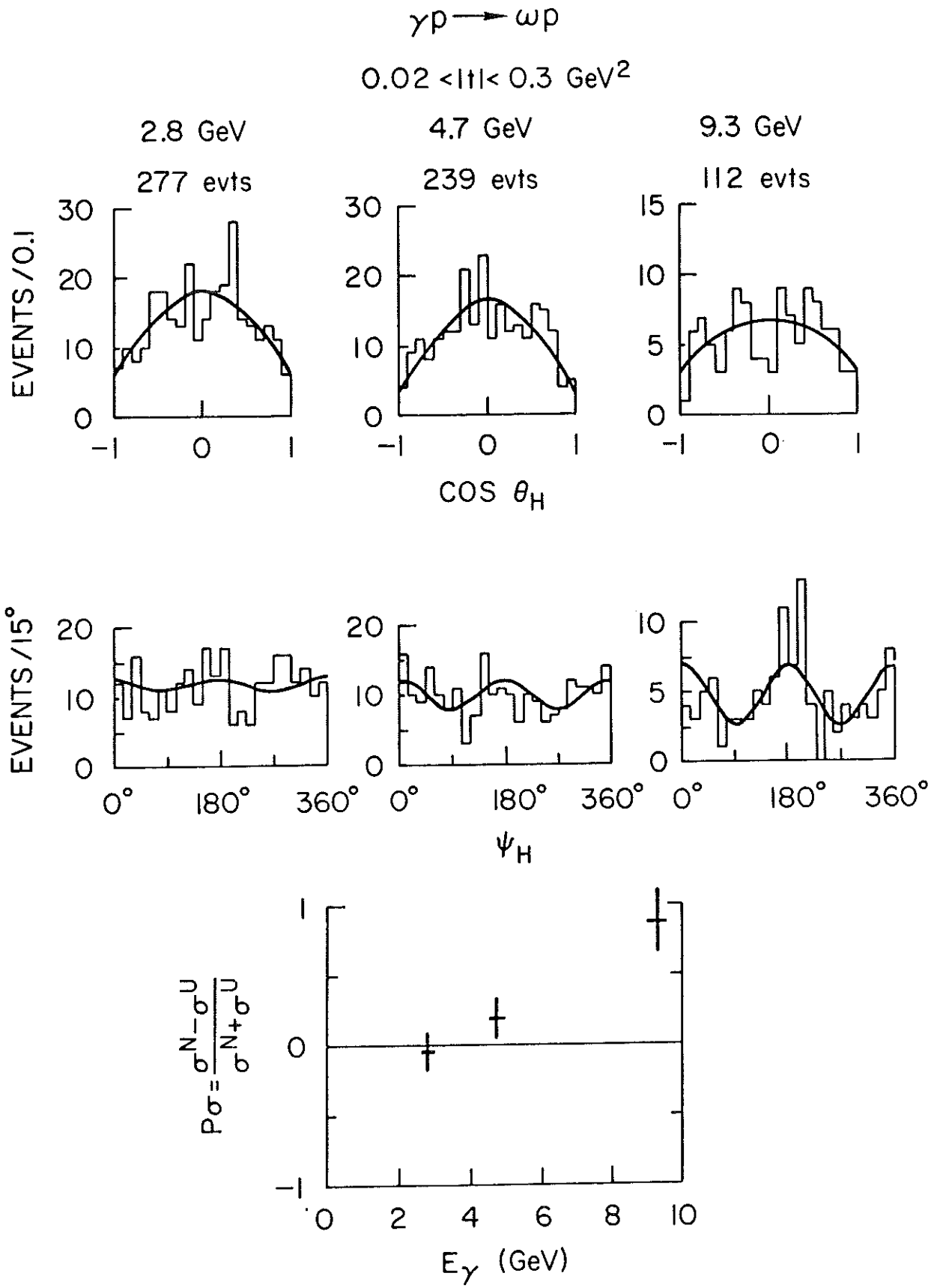
γp → ωp
0.02 <|t|< 0.3 GeV²
2.8 GeV
277 evts
4.7 GeV
239 evts
9.3 GeV
112 evts
EVENTS/0.1
COS θH
EVENTS/15°
ΨH
Pb = (N−b)/(N+b)
Eγ (GeV)

Fig. 36

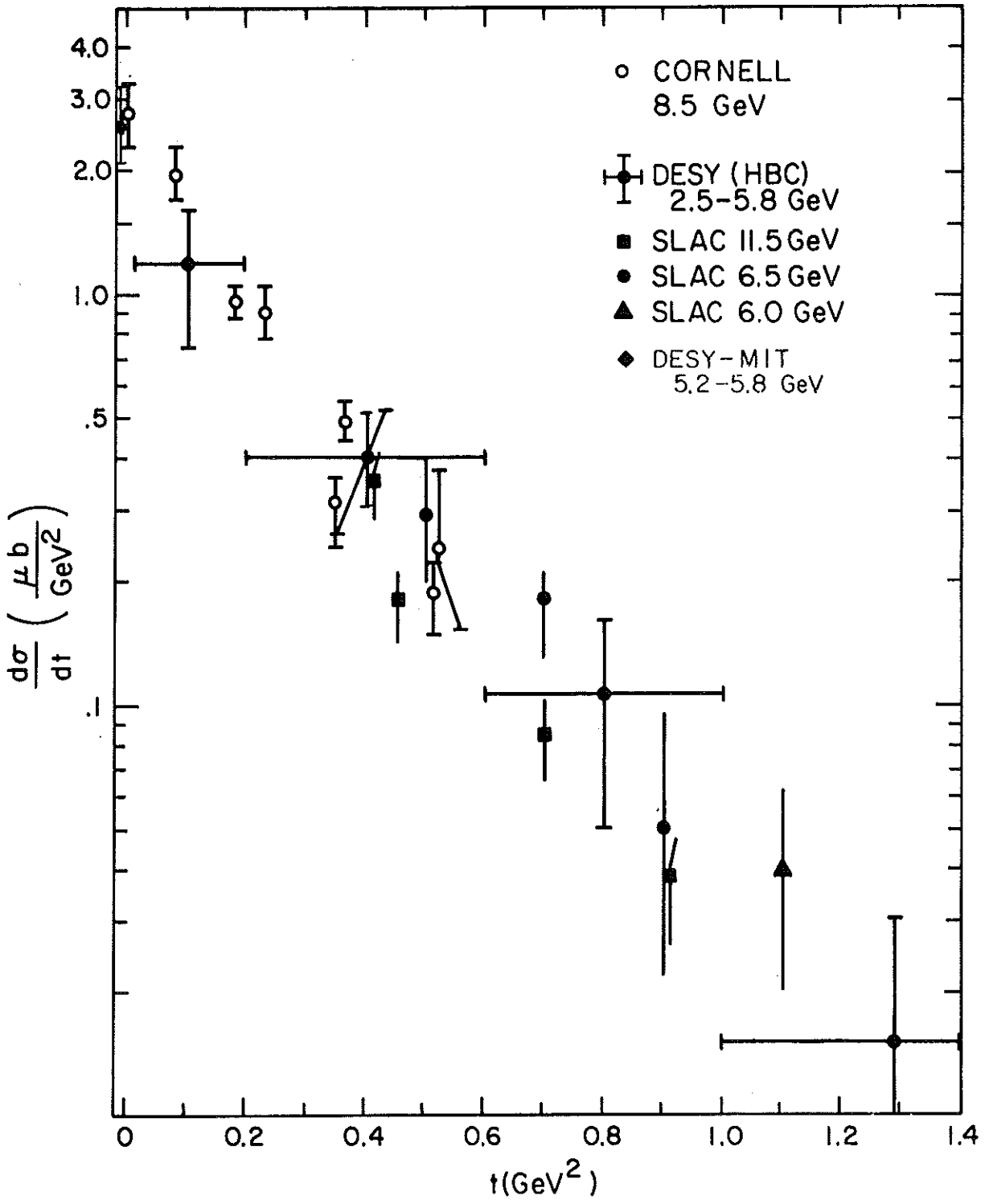
CORNELL
8.5 GeV
DESY (HBC)
2.5-5.8 GeV
SLAC 11.5 GeV
SLAC 6.5 GeV
SLAC 6.0 GeV
DESY-MIT
5.2-5.8 GeV
4.0
3.0
2.0
1.0
.5
.1
0
0.2
0.4
0.6
0.8
1.0
1.2
1.4
t(GeV²)
dσ/dt (μb/GeV²)

Fig.37

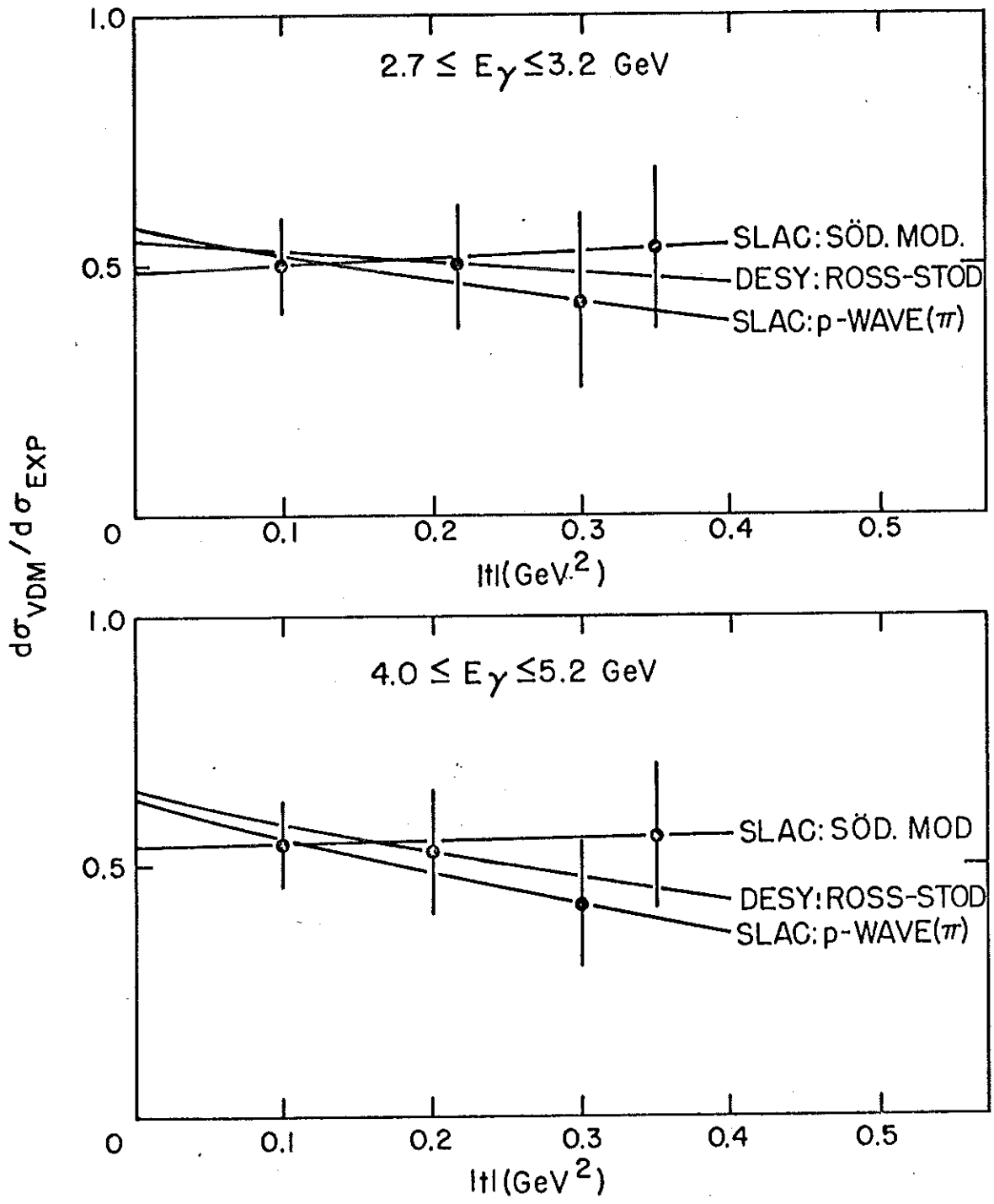
1.0
2.7 ≤ Eγ ≤3.2 GeV
0.5
SLAC: SÖD. MOD.
DESY: ROSS-STOD
SLAC: p-WAVE(π)
0
0.1
0.2
0.3
0.4
0.5
|t|(GeV.2)
dσVDM/dσEXP
1.0
4.0 ≤ Eγ ≤5.2 GeV
0.5
SLAC: SÖD. MOD
DESY: ROSS-STOD
SLAC: p-WAVE(π)
0
0.1
0.2
0.3
0.4
0.5
|t|(GeV2)

Fig.38

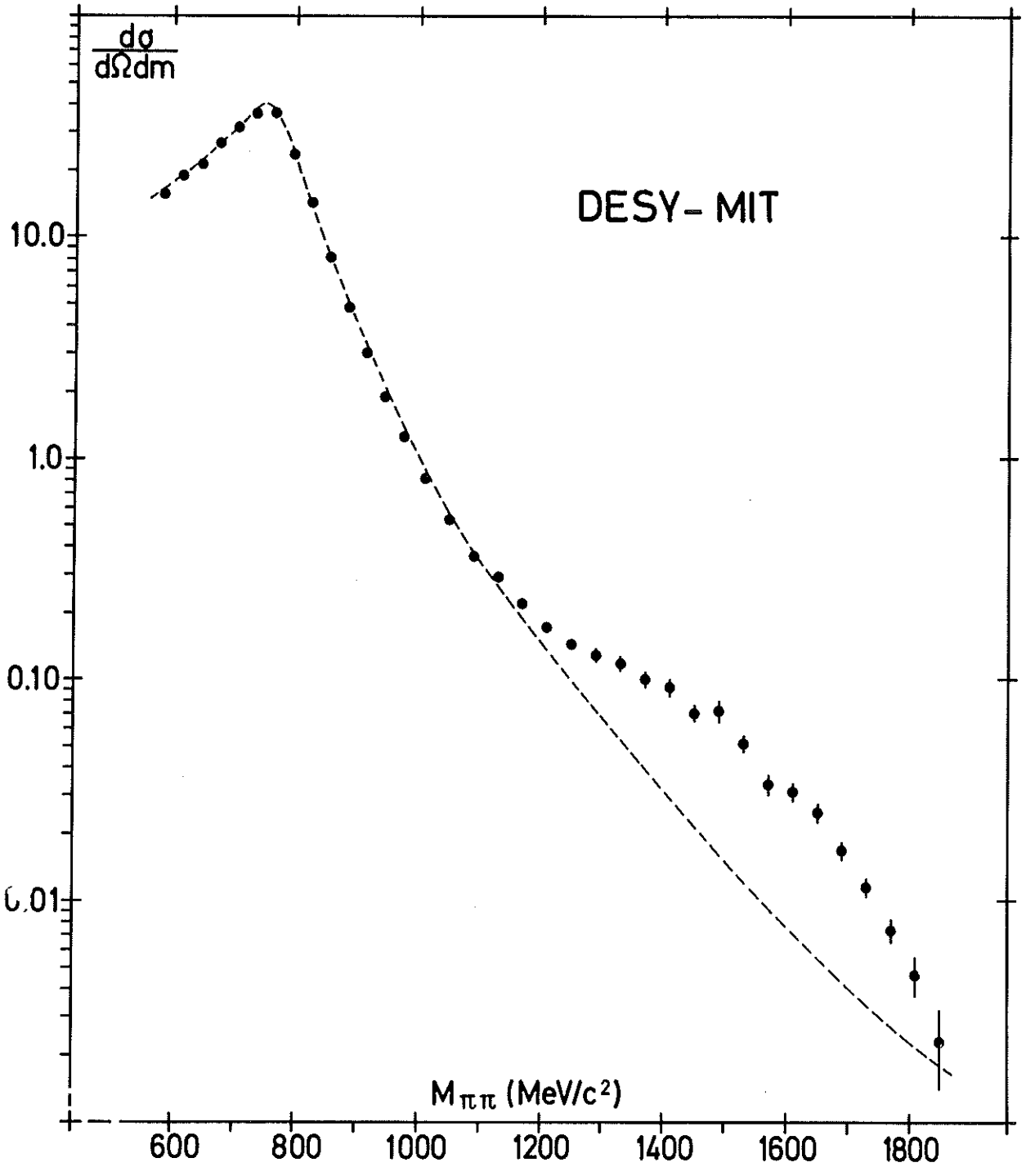
dσ/dΩdm
DESY- MIT
10.0
1.0
0.10
0.01
600
800
1000
1200
1400
1600
1800
Mππ (MeV/c²)

Fig. 39

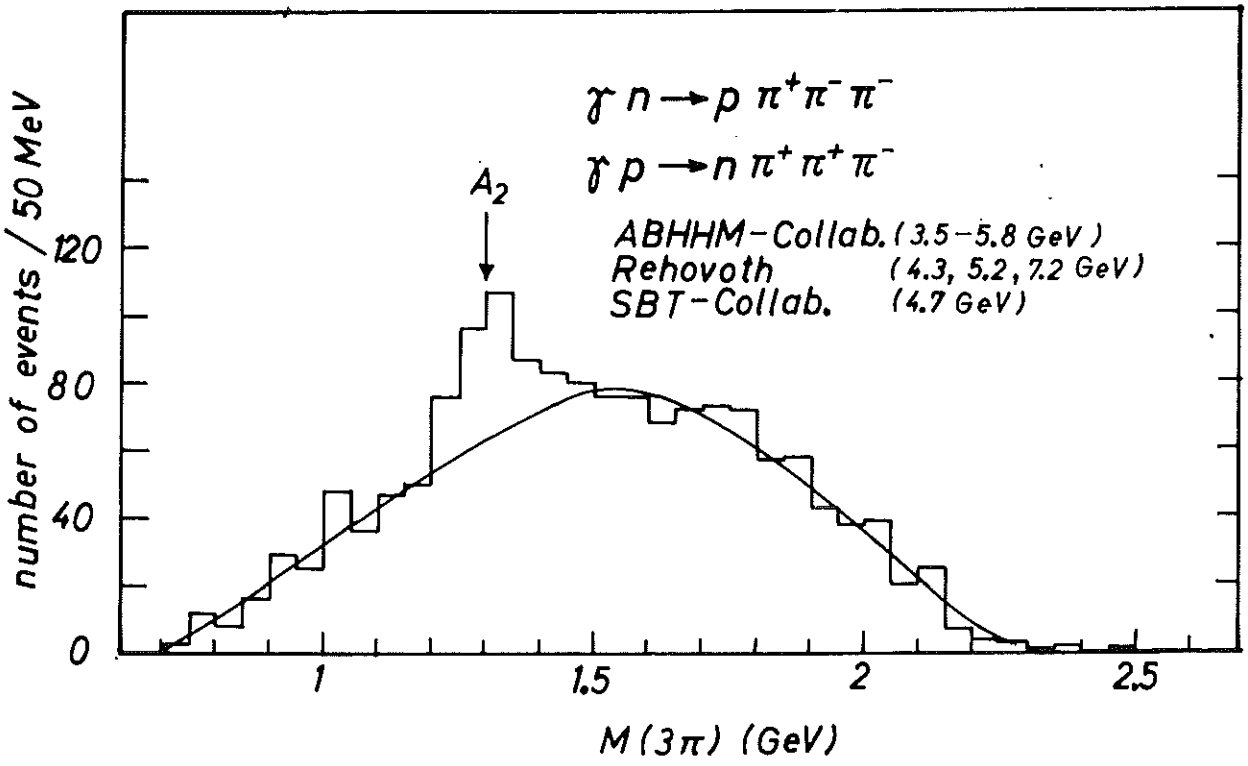
γ n → p π⁺π⁻π⁻
γ p → n π⁺π⁺π⁻
A2
ABHHM-Collab. (3.5-5.8 GeV)
Rehovoth (4.3, 5.2, 7.2 GeV)
SBT-Collab. (4.7 GeV)
number of events / 50 MeV
0
40
80
120
1
1.5
2
2.5
M(3π) (GeV)

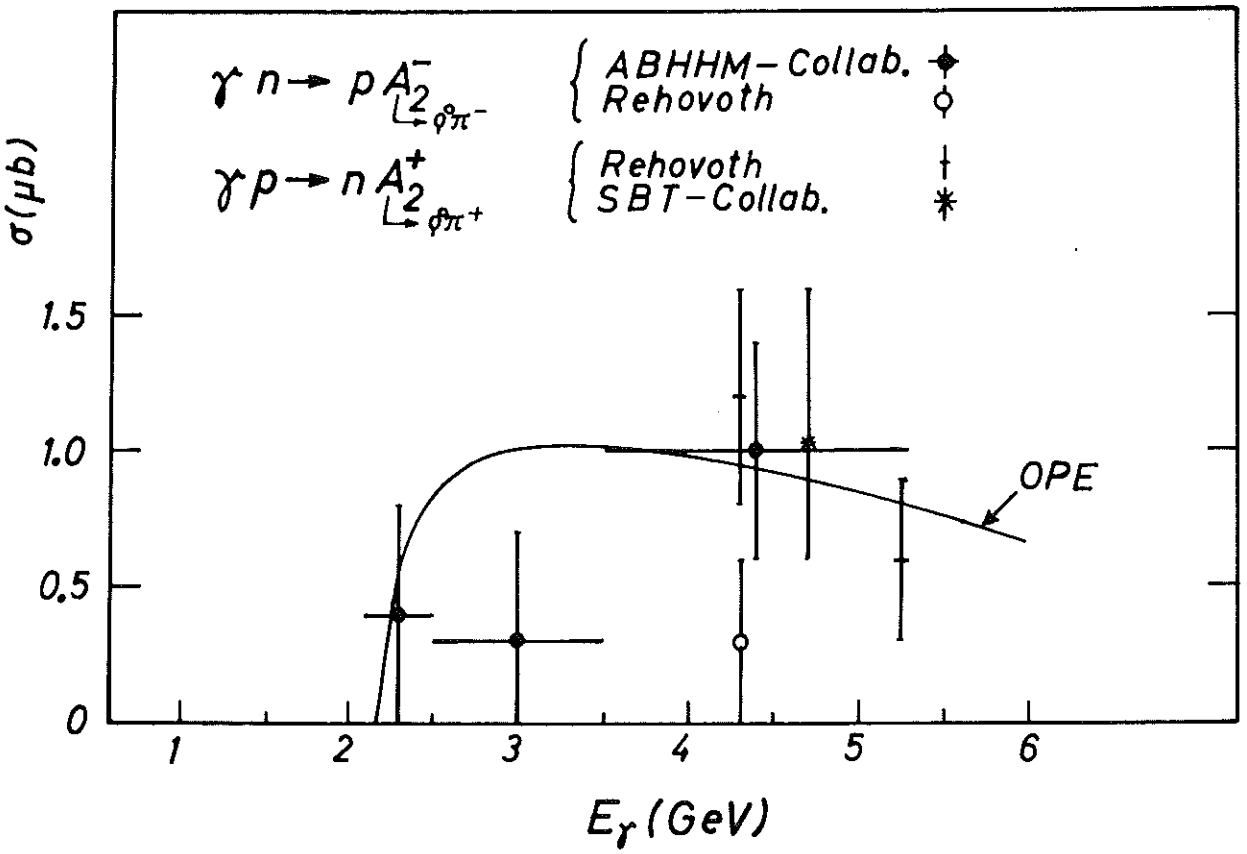
γ n → p A2⁻ → φπ⁻
γ p → n A2⁺ → φπ⁺
ABHHM-Collab.
Rehovoth
Rehovoth
SBT-Collab.
σ(μb)
0
0.5
1.0
1.5
OPE
1
2
3
4
5
6
Eγ (GeV)

Fig.40

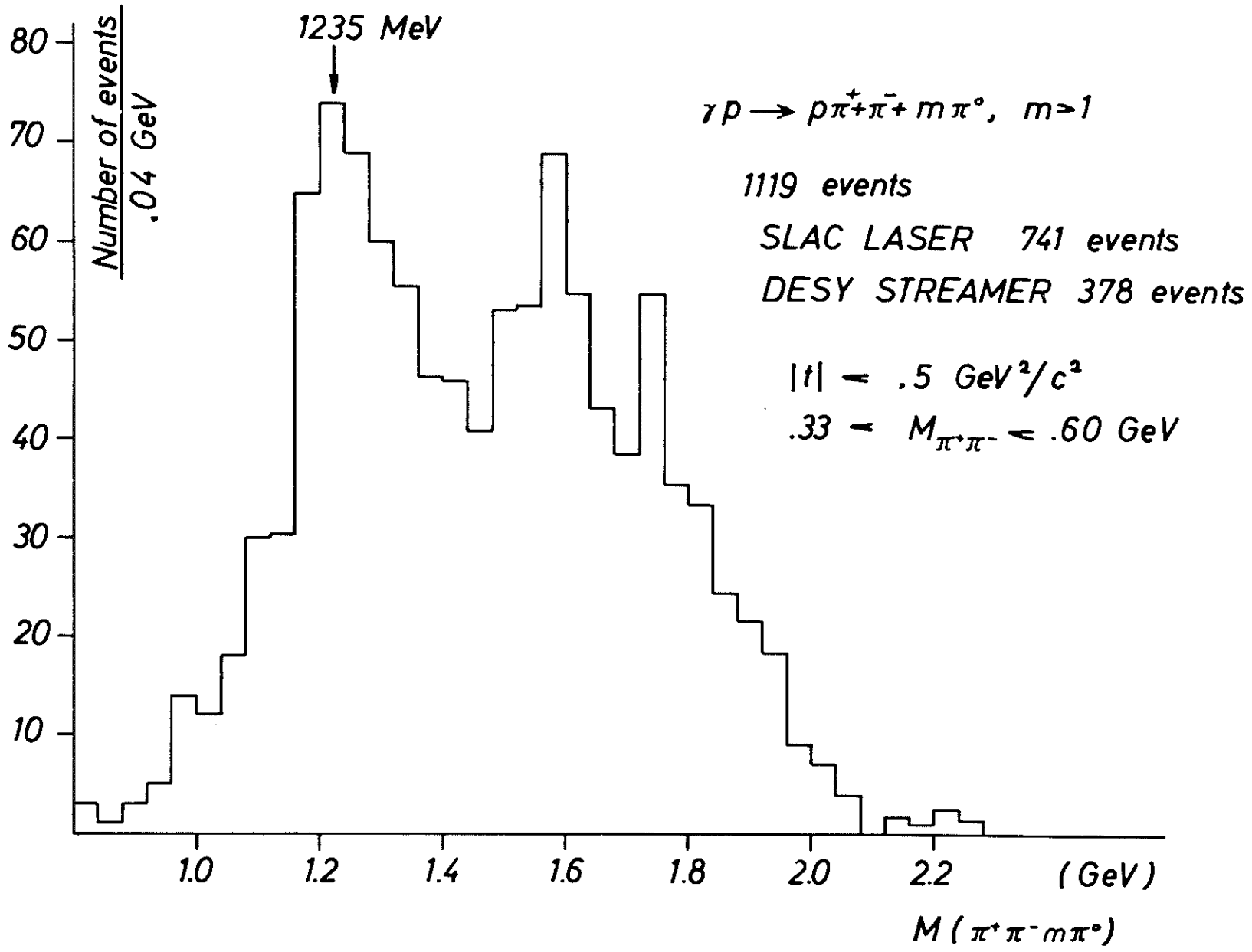
1235 MeV
Number of events
.04 GeV
80
70
60
50
40
30
20
10
1.0
1.2
1.4
1.6
1.8
2.0
2.2
(GeV)
M (π⁺π⁻mπ°)
γp → pπ⁺π⁻ + mπ°, m>1
1119 events
SLAC LASER 741 events
DESY STREAMER 378 events
|t| < .5 GeV²/c²
.33 < M_π⁺π⁻ < .60 GeV

Fig. 41

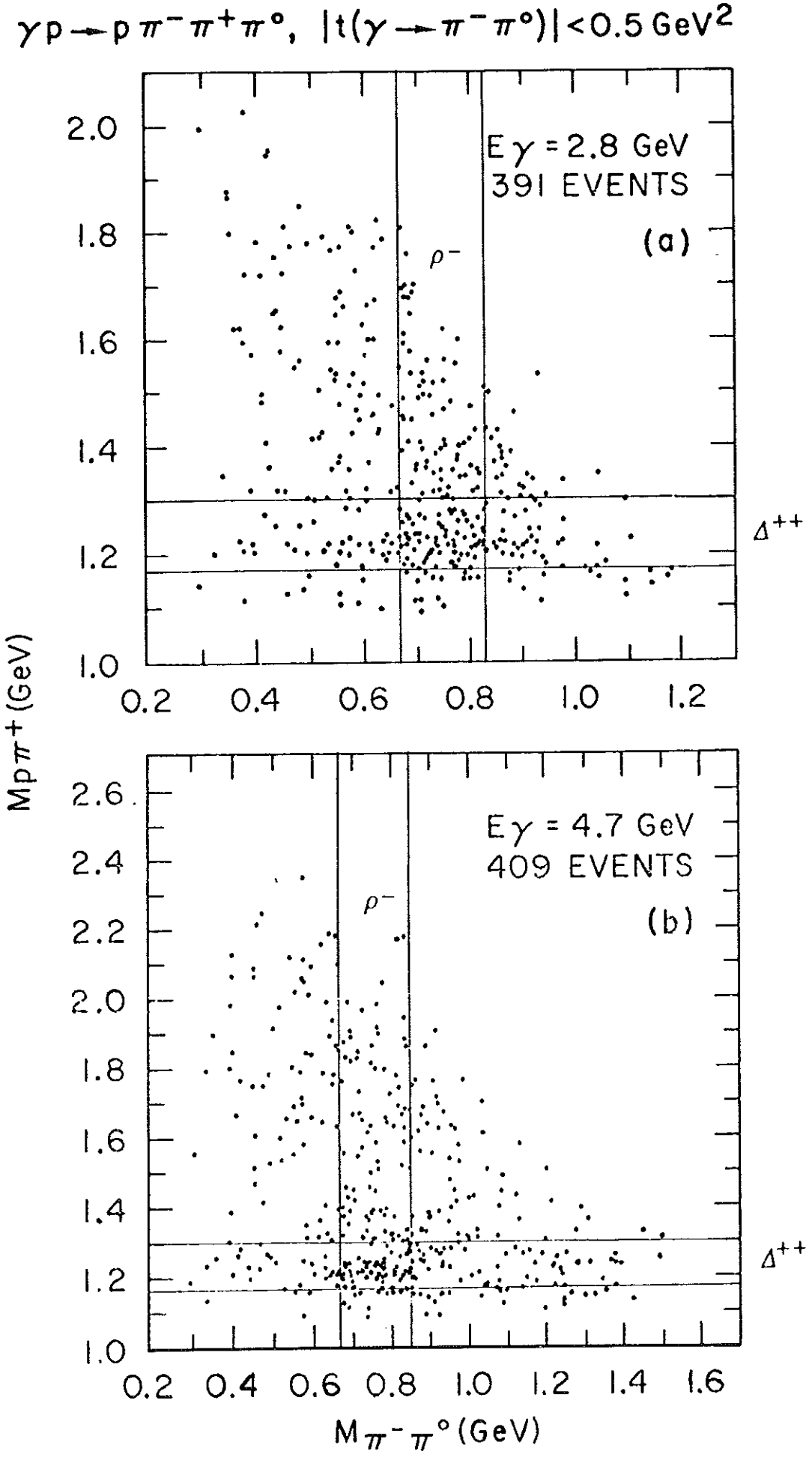
γp → pπ⁻π⁺π°, |t(γ → π⁻π°)| < 0.5 GeV²
Eγ = 2.8 GeV
391 EVENTS
(a)
ρ⁻
Δ⁺⁺
Eγ = 4.7 GeV
409 EVENTS
(b)
ρ⁻
Δ⁺⁺
Mpπ⁺ (GeV)
Mπ⁻π° (GeV)
2.0
1.8
1.6
1.4
1.2
1.0
2.6
2.4
2.2
0.2
0.4
0.6
0.8
1.0
1.2
1.4
1.6

Fig. 42

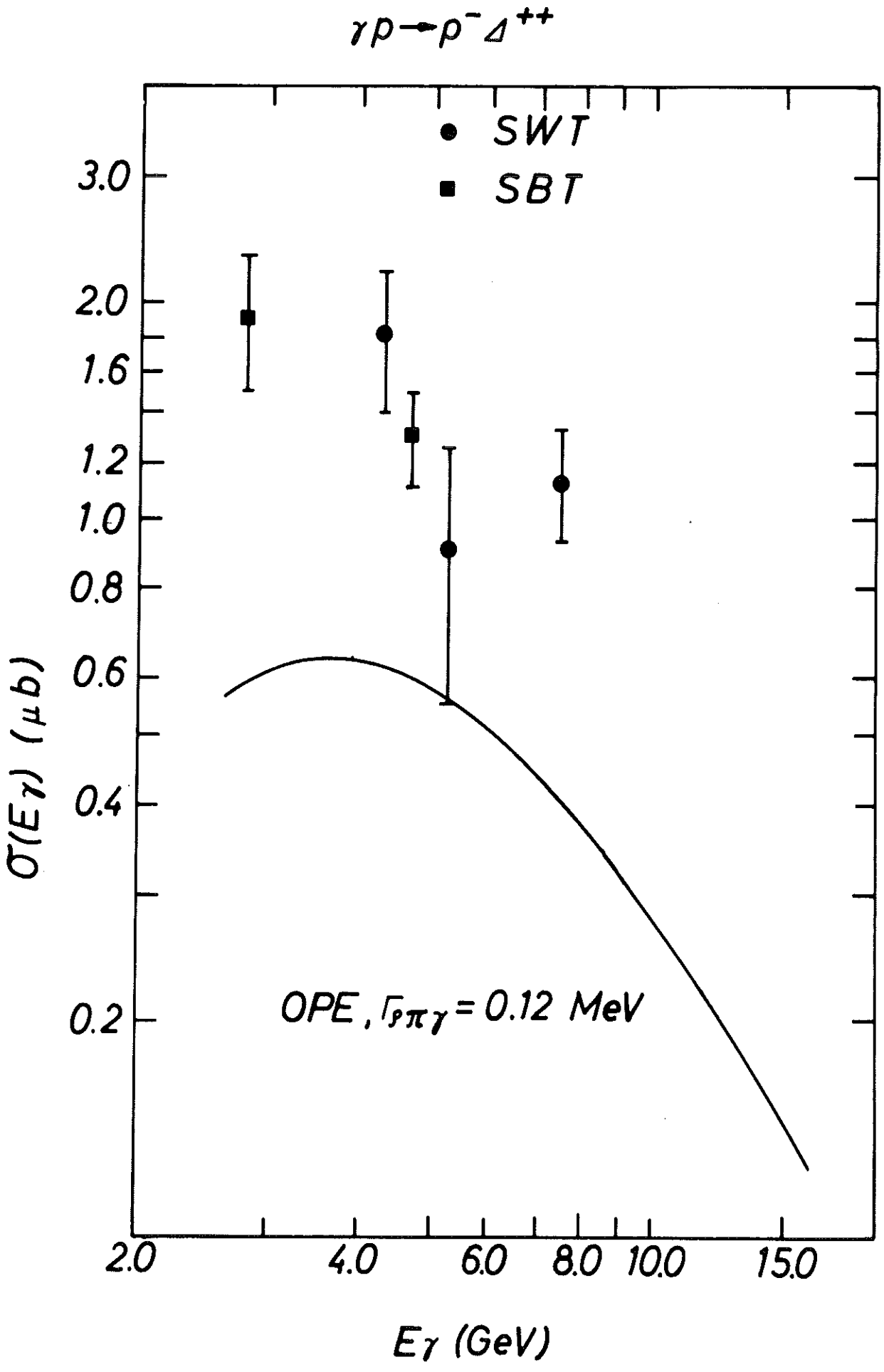
γp→ρ⁻Δ⁺⁺
SWT
SBT
3.0
2.0
1.6
1.2
1.0
0.8
0.6
0.4
0.2
σ(Eγ) (μb)
OPE, Γρπγ = 0.12 MeV
2.0
4.0
6.0
8.0
10.0
15.0
Eγ (GeV)

Fig. 43

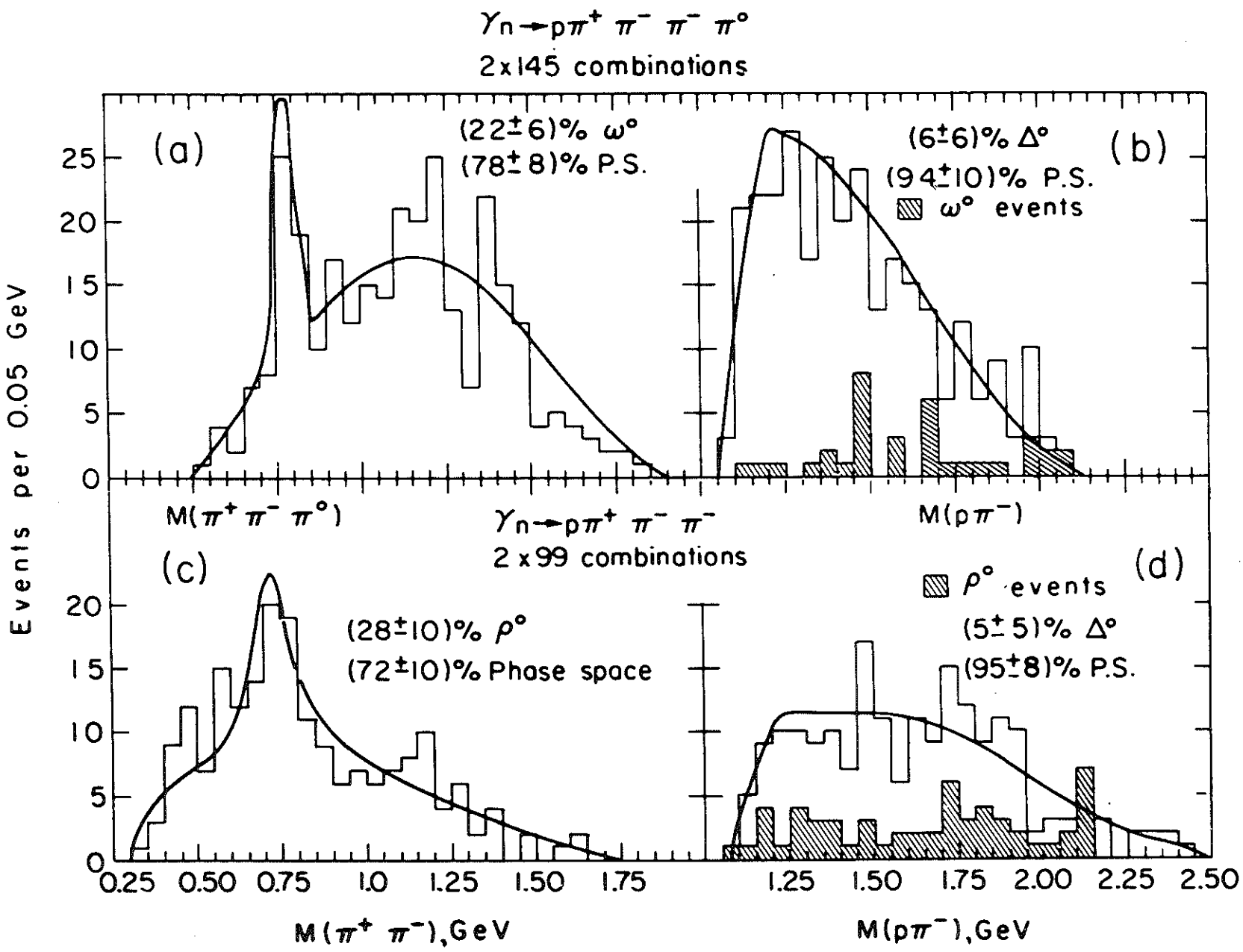
γn→pπ+ π− π− π°
2x145 combinations
(a)
(22±6)% ω°
(78±8)% P.S.
(b)
(6±6)% Δ°
(94±10)% P.S.
ω° events
Events per 0.05 GeV
M(π+ π− π°)
M(pπ−)
γn→pπ+ π− π−
2x99 combinations
(c)
(28±10)% ρ°
(72±10)% Phase space
(d)
ρ° events
(5±5)% Δ°
(95±8)% P.S.
M(π+ π−), GeV
M(pπ−), GeV

Fig. 44

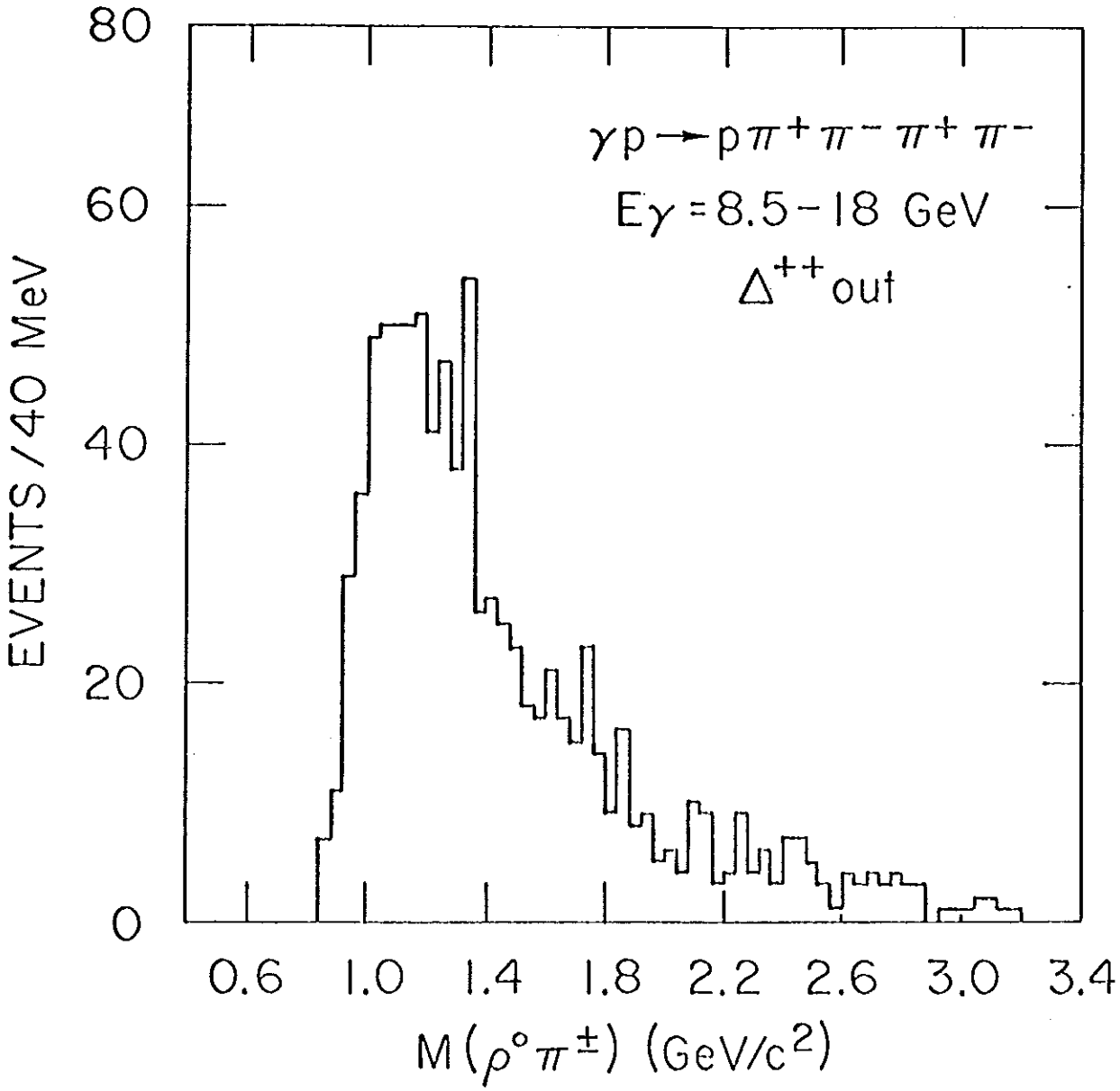
80
60
40
20
0
EVENTS / 40 MeV
γp → pπ+π−π+π−
Eγ = 8.5 − 18 GeV
Δ++ out
0.6
1.0
1.4
1.8
2.2
2.6
3.0
3.4
M(ρ°π±) (GeV/c2)

Fig. 45

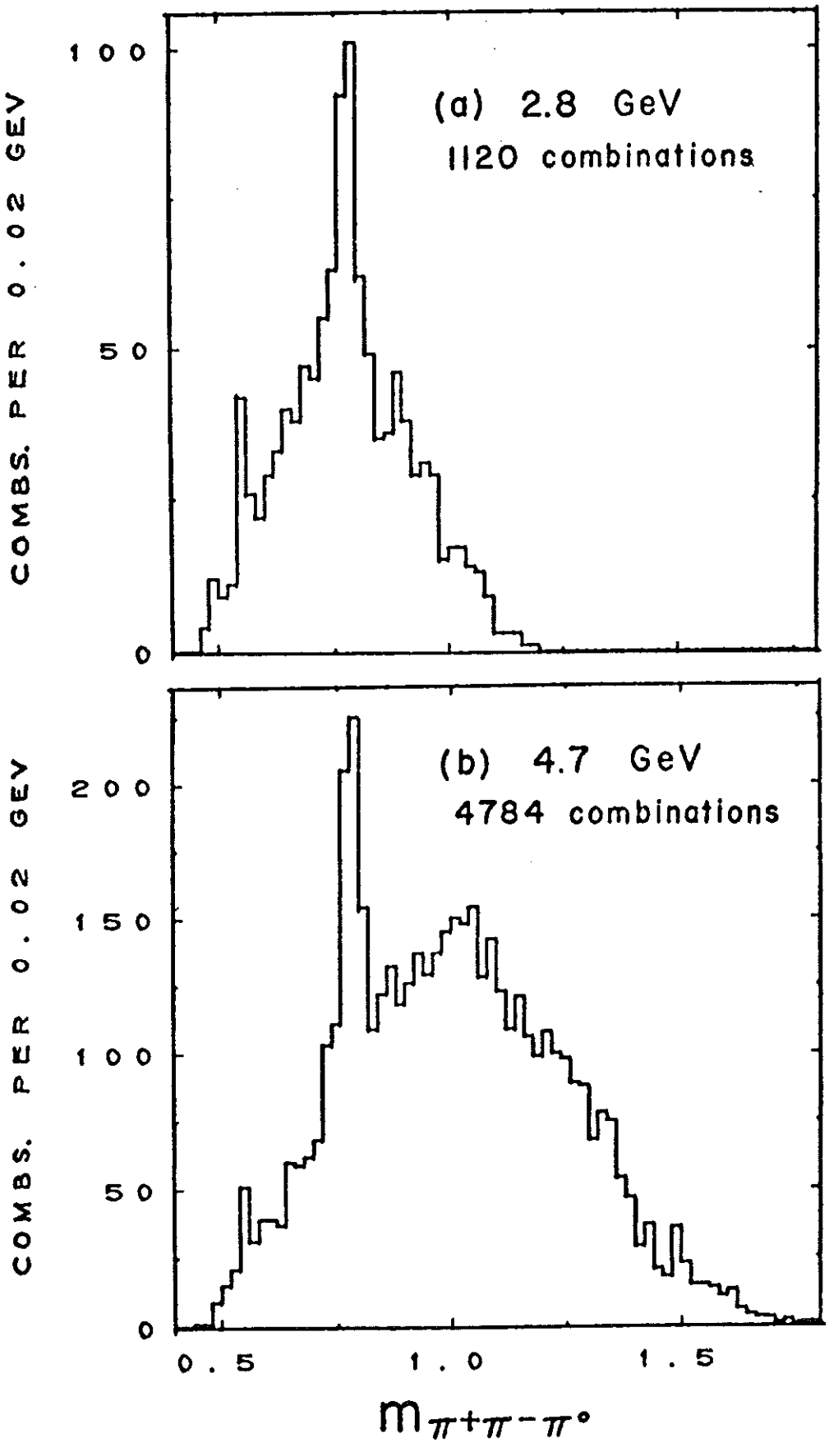

XBL 713-467

Fig.46

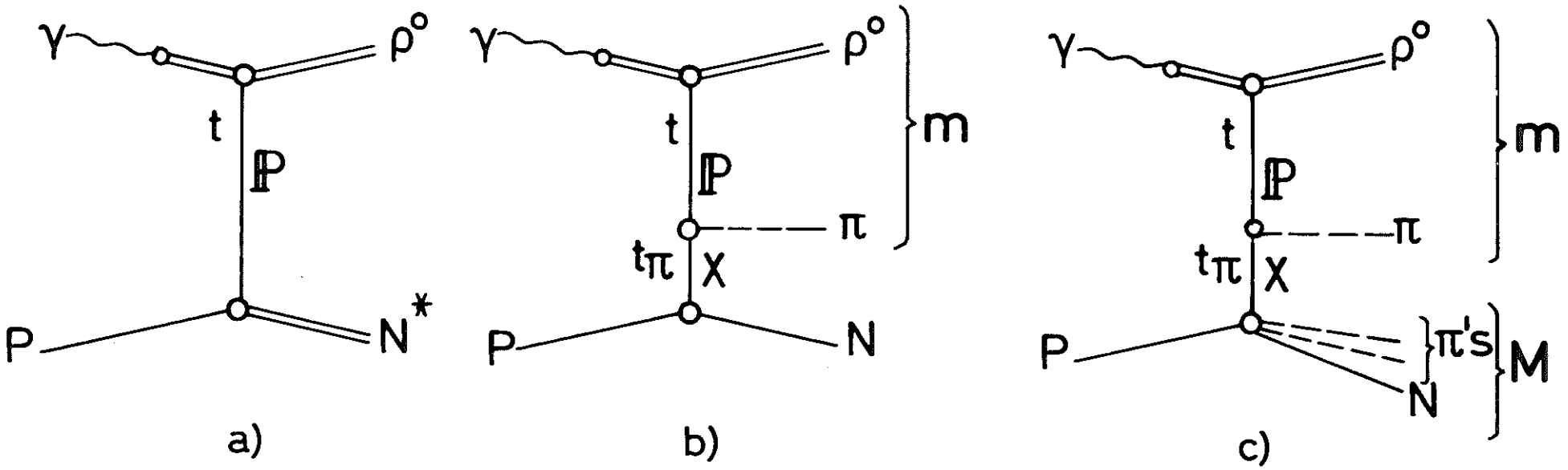

Fig. 47

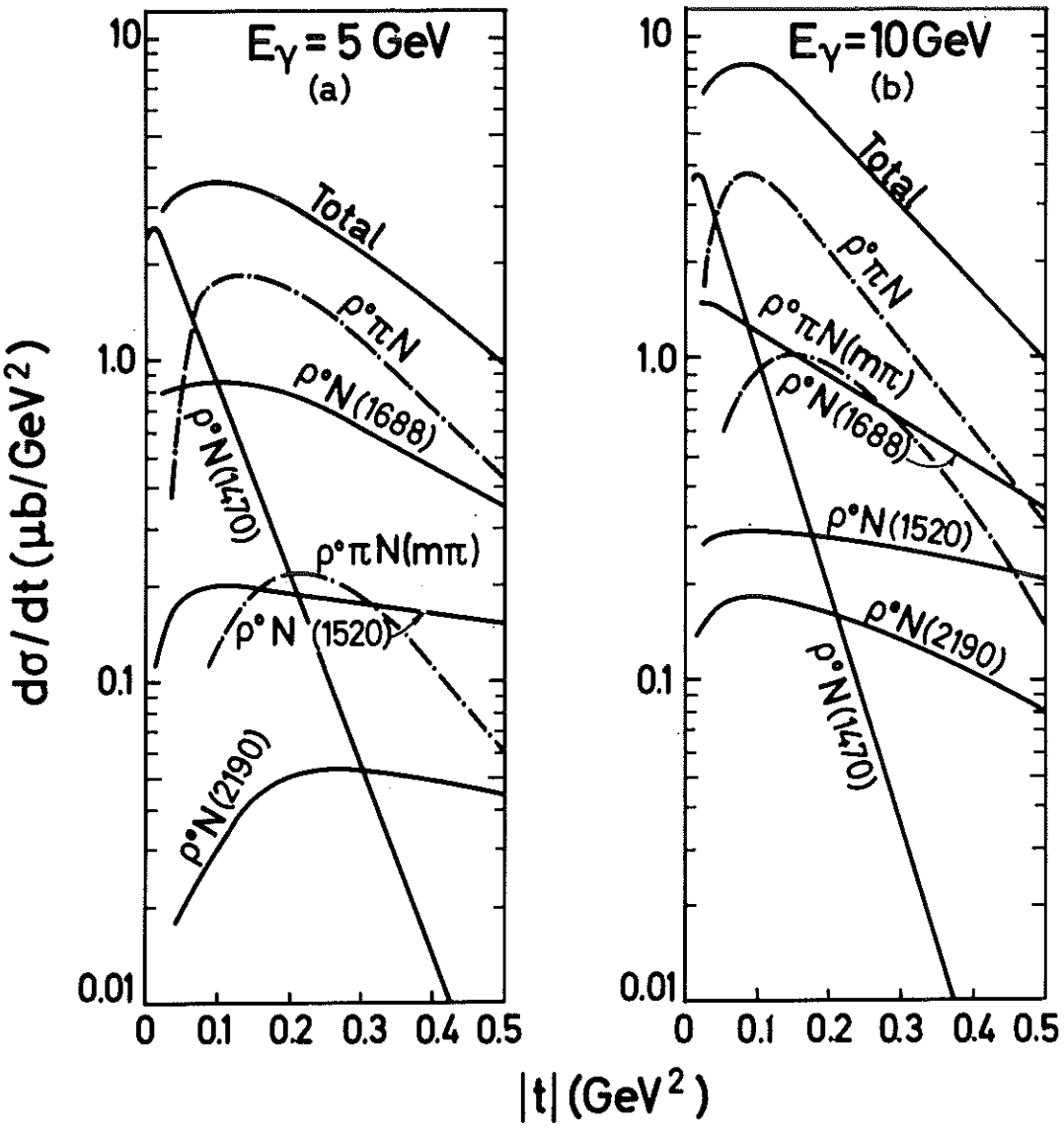
$E_\gamma = 5$ GeV
(a)
$E_\gamma = 10$ GeV
(b)
Total
$\rho^\circ\pi N$
$\rho^\circ N(1688)$
$\rho^\circ\pi N(m\pi)$
$\rho^\circ N(1520)$
$\rho^\circ N(2190)$
$\rho^\circ N(1470)$
$d\sigma/dt\ (\mu b/GeV^2)$
$|t|\ (GeV^2)$

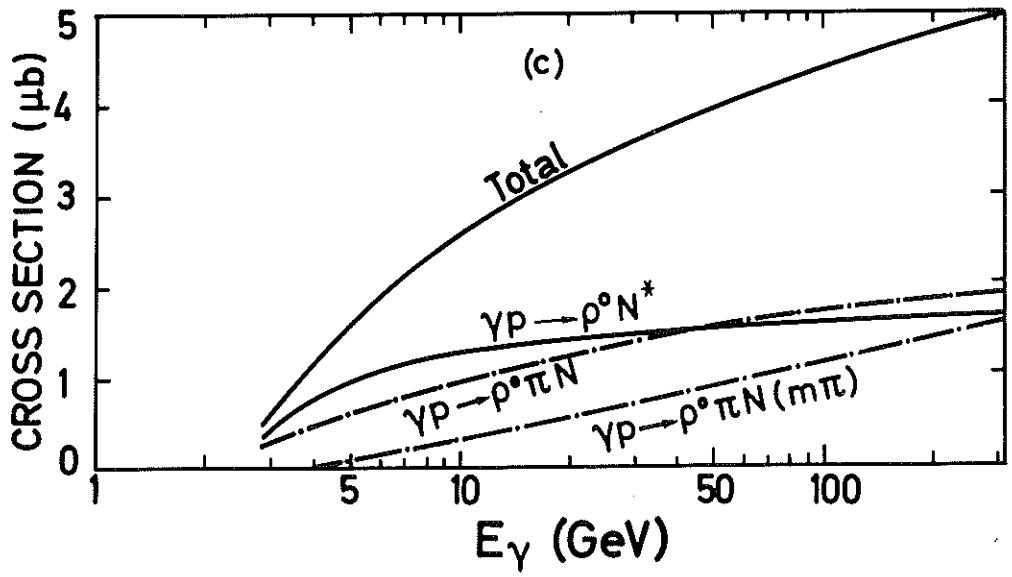
(c)
Total
$\gamma p \to \rho^\circ N^*$
$\gamma p \to \rho^\circ \pi N$
$\gamma p \to \rho^\circ \pi N(m\pi)$
CROSS SECTION (μb)
E_γ (GeV)

Fig. 48